

CHALMERS



Evaluations of Tissue Segmentation of brain MR Images

Master of Science Thesis in Biomedical Engineering

KOUSHYAR KOWKABZADEH

Department of Signals and Systems
Division of Biomedical Engineering
CHALMERS UNIVERSITY OF TECHNOLOGY
Göteborg, Sweden, 2010
Report No. EX048/2010

Abstract

Accurate brain tissue segmentation of MR (Magnetic Resonance) images has been one of the most important research areas for several years. It is important to have an accurate segmentation of different brain tissue types for various applications such as radiotherapy planning, image-guided interventions, surgical planning by using Electroencephalography (EEG) or Functional Magnetic Resonance Imaging (fMRI) information and brain disease studies such as Alzheimer and Multiple sclerosis (MS). However, all the mentioned applications are crucially dependent on the level of accuracy of brain tissue segmentation. Thus, this is important to choose the best algorithm to reach the most accurate tissue segmentation.

In this project different software packages for brain tissue segmentation were studied. We have chosen the most sophisticated ones for the evaluation and comparison. SPM8 [7], FSL [8] and FreeSurfer [9] are selected which are three most widely used brain tissue segmentation software packages. The evaluation for each software package carried out by performing tissue segmentation over 18 brain phantoms provided by Brainweb [35] with 6 different noise levels and 3 different RF inhomogeneity values. Then the resulted images for each tissue type from each software compared voxel by voxel with the ground truth images for each tissue type. To provide a volumetric voxel by voxel comparison between ground truth images and output images from software packages the 3dOverlap command line from AFNI software package [41] used together with Jimmy Shen's library in MATLAB [36].

Finally to compare the performance of these three software packages the misclassification rate were calculated for each tissue type.

Acknowledgements

I would like to thank

..My parents for their supports and kindness and providing the opportunity for me to catch my dreams.

..My advisor, Hoi-shun Lui, for his helps during the work on the project.

..My coworker on project, Antonio for all the days we have spent in the hospital helping each other.

..Medtech West and Sahlgrenska University Hospital staff especially Anders, Artur, Justin and Simon for their helps and providing a good environment to learn.

Table of contents

Chapter 1	15
1. Introduction	15
1.1. Motivation.....	15
1.2. Patient specific model development project	16
Chapter 2	19
2. Background	19
2.1. Anatomy of the brain	19
2.2. Magnetic Resonance Imaging (MRI).....	23
Chapter 3	28
3. Automated brain tissue segmentation	28
3.1. A review of different software packages for brain tissue segmentation	28
3.1.1. SPM.....	28
3.1.2. FSL.....	28
3.1.3. FreeSurfer	29
3.1.4. Bioimage suite	29
3.1.5. Brain suite	29
3.2. Tissue segmentation using SPM8	30
3.3. Tissue segmentation using FSL 4.1.5	38
3.3.1. BET	38
3.3.2. FAST.....	42
3.3.3. FLIRT	44
3.3.4. FIRST.....	45
3.4. Tissue segmentation using FreeSurfer	47
Chapter 4	53
4. Evaluation and Comparison between performances of three software packages	53
4.1. Evaluation method	53
4.1.1. Results	55
4.1.1.1. SPM8	55
4.1.1.1.1. White matter.....	55
4.1.1.1.2. Grey matter	57

4.1.1.1.3.	CSF	60
4.1.1.2.	FSL	63
4.1.1.2.1.	White matter.....	63
4.1.1.2.2.	Grey matter	65
4.1.1.2.3.	CSF	67
4.1.1.3.	FreeSurfer	70
4.1.1.3.1.	White matter.....	71
4.1.1.3.2.	Grey matter	74
4.1.1.3.3.	CSF	76
4.2.	Conclusion and discussion.....	79
5.	Terminology.....	83
6.	References.....	86

Index of figures

Figure 1, Cross section of a spherical head model for EEG dipole source localization	16
Figure 2, Cross section of a head model	17
Figure 3, Different layers of Meninges.....	19
Figure 4, Different regions of brain	20
Figure 5, Cerebral hemispheres, white and grey matter, subcortical structures, cerebral ventricles	20
Figure 6, Different regions of cerebral cortex.....	21
Figure 7, Limbic system (purple), Thalamus (orange), Hypothalamus (blue).....	22
Figure 8, Angular momentum Φ (a), magnetic dipole moment (b)	23
Figure 9, Individual nucleus in a spin system randomly oriented.....	24
Figure 10, External static magnetic field B and resulted nuclear magnetization vector M	24
Figure 11, Magnetization vector and its components	25
Figure 12, Precession of magnetization vector, free induction decay due to transverse relaxation.....	25
Figure 13, Transverse relaxation and $T2^*$ decay (a), longitudinal relaxation (b).....	26
Figure 14, Sagittal view of a $T2$ weighted image and transverse relaxation time for different tissues	26
Figure 15, Sagittal view of a $T1$ weighted image and longitudinal relaxation time for different tissues ...	27
Figure 16, SPM8 start up menu	30
Figure 17, SPM8 fMRI menu	30
Figure 18, Brain extracted $T1$ weighted input image results in an odd output in SPM8 (left), $T2$ weighted input image results in an odd output in SPM8 (right) both are in transverse view	31
Figure 19, SPM8 coregister estimate menu	32
Figure 20, SPM8 coregister reslice menu	33
Figure 21, Bias field correction in transverse view of a $T1$ weighted image.....	34
Figure 22, Segmented in Native Space: GM (left), WM (middle), CSF (right)	35
Figure 23, Unmodulated normalized Segmented: GM (left), WM (middle), CSF (right).....	35
Figure 24, Modulated normalized Segmented: GM (left), WM (middle), CSF (right)	36
Figure 25, ICBM tissue probability maps: GM (left), WM (middle), CSF (right)	36
Figure 26, SPM8 segment menu.....	38
Figure 27, FSL 4.1.5 graphical user interface for BET (Brain Extraction Tool).....	39
Figure 28, Left column: shows the extracted brain for	40
Figure 29, A comparison between the results of “-R” and “-c” for brain extraction	40
Figure 30, A comparison between the results of “-A” and “-A2” options.....	41
Figure 31, FSL 4.1.5 graphical user interface for FAST (FMRIB’s Automated Segmentation Tool)	42
Figure 32, Segmentation results from FAST, $T1$ weighted image (left), $T2$ weighted image (right).....	43
Figure 33, FSL 4.1.5 graphical user interface for FLIRT (FMRIB’s Linear Image Registration Tool).....	44
Figure 34, Volumes of different subcortical structures.....	46
Figure 35, Surface meshes of different subcortical structures	46
Figure 36, Different extracted tissues and structures in “aseg.mgz”	48
Figure 37, White matter and pial surfaces	49
Figure 38, White matter in “wm.mgz” (left), grey matter in “aparc.a2009s+aseg.mgz” (right).....	49

Figure 39, White and grey matter in “ribbon.mgz”	50
Figure 40, Screen snapshot: MRICron user interface	52
Figure 41, Screen snapshot from ITKsnap user interface	52
Figure 42, Sensitivity of segmentation for white matter in SPM8	55
Figure 43, Specificity of segmentation for white matter in SPM8	56
Figure 44, Misclassification rate of segmentation for white matter in SPM8.....	57
Figure 45, Segmented white matter using SPM8 (red), Brainweb phantom ground truth (green)	57
Figure 46, Sensitivity of segmentation for grey matter in SPM8	58
Figure 47, Specificity of segmentation for grey matter in SPM8	58
Figure 48, Misclassification rate of segmentation for grey matter in SPM8	59
Figure 49, Segmented grey matter using SPM8 (red), Brainweb phantom ground truth (green)	59
Figure 50, Sensitivity of segmentation for CSF in SPM8.....	60
Figure 51, Specificity of segmentation for CSF in SPM8	61
Figure 52, Misclassification rate of segmentation for CSF in SPM8	61
Figure 53, Segmented CSF using SPM8 (red), Brainweb phantom ground truth (green)	62
Figure 54, Overall evaluation of tissue segmentation using SPM8	62
Figure 55, Sensitivity of segmentation for white matter in FSL	63
Figure 56, Specificity of segmentation for white matter in FSL.....	64
Figure 57, Misclassification rate of segmentation for white matter in FSL.....	64
Figure 58, Segmented white matter using FSL (red), Brainweb phantom ground truth (green)	65
Figure 59, Sensitivity of segmentation for grey matter in FSL.....	65
Figure 60, Specificity of segmentation for grey matter in FSL	66
Figure 61, Misclassification rate of segmentation for grey matter in FSL	67
Figure 62, Segmented grey matter using FSL (red), Brainweb phantom ground truth (green)	67
Figure 63, Sensitivity of segmentation for CSF in FSL.....	68
Figure 64, Specificity of segmentation for CSF in FSL.....	68
Figure 65, Misclassification rate of segmentation for CSF in FSL.....	69
Figure 66, Segmented CSF using FSL (red), Brainweb phantom ground truth (green)	69
Figure 67, Overall evaluation of tissue segmentation using FSL	70
Figure 68, Sensitivity of segmentation for white matter in FreeSurfer.....	72
Figure 69, Specificity of segmentation for white matter in FreeSurfer	72
Figure 70, Misclassification rate of segmentation for white matter in FreeSurfer	73
Figure 71, Segmented white matter using FreeSurfer (red), Brainweb phantom ground truth (green)	73
Figure 72, Sensitivity of segmentation for grey matter in FreeSurfer	74
Figure 73 , Specificity of segmentation for grey matter in FreeSurfer	75
Figure 74, Misclassification rate of segmentation for grey matter in FreeSurfer	75
Figure 75, Segmented grey matter using FreeSurfer (red), Brainweb phantom ground truth (green).....	76
Figure 76, Sensitivity of segmentation for CSF in FreeSurfer.....	76
Figure 77, Specificity of segmentation for CSF in FreeSurfer	77
Figure 78, Misclassification rate of segmentation for CSF in FreeSurfer	78
Figure 79, Segmented CSF using FreeSurfer (red), Brainweb phantom ground truth (green)	78
Figure 80, Overall evaluation of tissue segmentation using FreeSurfer	79

Figure 81, Comparison of misclassification rates between three software packages	80
Figure 82, Segmented tissues by SPM8 together with extracted skull and scalp by FSL.....	81
Figure 83, Segmented tissues and extracted skull and scalp by FSL, planes: sagittal (left).....	81

Index of Tables

Table 1, Elapsing time for different tissues	26
Table 2, Recovery time for different tissues	27
Table 3, Summary of capabilities of five different brain tissue segmentation software packages	30
Table 4, SPM8 Coregister tool option descriptions summary	34
Table 5, SPM8 Coregister tool option descriptions summary	37
Table 6, Commands for generating images in figure28	40
Table 7, Commands for generating images in figure29	40
Table 8, Commands for generating images in figure30	41
Table 9, FSL BET option descriptions summary	42
Table 10, Commands for generating images in figure32	43
Table 11, FSL FAST option descriptions summary	44
Table 12, Name codes for different possible subcortical structures in FIRST	45
Table 13, Command for generating images in FIRST	46
Table 14, FSL FIRST option descriptions summary	47
Table 15, Command for generating registration and brain extraction in FreeSurfer	47
Table 16, Command for generating “aseg.mgz”	48
Table 17, Name codes and intensities for different possible extracted structures using FreeSurfer	48
Table 18, Different stages of tissue segmentation in FreeSurfer	50
Table 19, Different possible image formats conversion using FreeSurfer	51
Table 20, Definition of true and false classification	54
Table 21, Sensitivity of segmentation for white matter in SPM8	55
Table 22, Specificity of segmentation for white matter in SPM8	56
Table 23, Misclassification rate of segmentation for white matter in SPM8	56
Table 24, Sensitivity of segmentation for grey matter in SPM8	57
Table 25, Specificity of segmentation for grey matter in SPM8	58
Table 26, Misclassification rate of segmentation for grey matter in SPM8	59
Table 27, Sensitivity of segmentation for CSF in SPM8	60
Table 28, Specificity of segmentation for CSF in SPM8	60
Table 29, Misclassification rate of segmentation for CSF in SPM8	61
Table 30, Overall evaluation of tissue segmentation using SPM8	62
Table 31, Sensitivity of segmentation for white matter in FSL	63
Table 32, Specificity of segmentation for white matter in FSL	63
Table 33, Misclassification rate of segmentation for white matter in FSL	64
Table 34, Sensitivity of segmentation for grey matter in FSL	65
Table 35, Specificity of segmentation for grey matter in FSL	66
Table 36, Misclassification rate of segmentation for grey matter in FSL	66
Table 37, Sensitivity of segmentation for CSF in FSL	67
Table 38, Specificity of segmentation for CSF in FSL	68
Table 39, Misclassification rate of segmentation for CSF in FSL	69

Table 40, Overall evaluation of tissue segmentation using FSL.....	70
Table 41, Different possible extracted structures using FreeSurfer.....	71
Table 42, Sensitivity of segmentation for white matter in FreeSurfer.....	71
Table 43, Specificity of segmentation for white matter in FreeSurfer.....	72
Table 44, Misclassification rate of segmentation for white matter in FreeSurfer.....	73
Table 45, Sensitivity of segmentation for grey matter in FreeSurfer.....	74
Table 46, Specificity of segmentation for grey matter in FreeSurfer.....	74
Table 47, Misclassification rate of segmentation for grey matter in FreeSurfer.....	75
Table 48, Sensitivity of segmentation for CSF in FreeSurfer.....	76
Table 49, Specificity of segmentation for CSF in FreeSurfer.....	77
Table 50, Misclassification rate of segmentation for CSF in FreeSurfer.....	77
Table 51, Overall evaluation of tissue segmentation using FreeSurfer.....	78
Table 52, Comparison of misclassification rates between three software packages.....	80

Chapter 1

1. Introduction

This chapter summarizes the necessity and importance of accurate brain tissue segmentation and explains the motivation of this project.

1.1. Motivation

Accurate brain tissue segmentation of MR images has been one of the most important research areas for several years. It is important to have an accurate segmentation of different brain tissue types for various applications such as radiotherapy planning, image-guided interventions, surgical planning by using EEG or fMRI information and brain disease studies such as Alzheimer and MS. [1]

For instance a study on Alzheimer disease carried out on department of radiology in university of California at San Francisco medical center [2] to compare volume of brain tissues in patients with Alzheimer¹ disease and control subjects. They extracted white matter (WM), Grey matter (GM) and Cerebrospinal fluid (CSF) volumes using quantitative tissue segmentation techniques. Their results showed significant decrease in GM and an increase in the ventricular and sulcal CSF for Alzheimer patients which shows the importance of having an accurate brain tissue segmentation for this study.

On the other hand, combining the functional information from hemodynamic approaches (ex. fMRI, PET) or electromagnetic approaches (ex. EEG, MEG) with anatomical MR images can play a significant role for neurosurgical planning. For instance in fMRI, it is possible to avoid losing different abilities for the patients by using BOLD² response information. Motor, sensory, memory and language mapping can be done by using a combination of functional data with anatomical images. In electromagnetic approaches like EEG, source localization of abnormal

signals is important for surgical planning. Again both of mentioned approaches need accurate tissue segmentation over anatomical brain MR images.

These explicit examples show the importance of having accurate tissue segmentation of brain tissues. There are number of different software packages using different image analysis and processing techniques and algorithms to perform tissue segmentation in brain MR images. However, the accuracy of the results of these techniques and algorithms is crucial for subsequent use and yet it has not been well studied. Thus, it is important to have an evaluation of these software packages to choose practical ones.

1.2. Patient specific model development project

In Sahlgrenska University Hospital, Medtech West research group is developing a new method for providing patient specific accurate head models for EEG dipole source localization to replace them with the regular spherical models which are already used in hospital for EEG dipole source localization.

Spherical head models normally have a homogeneous layer for scalp following by a sphere shaped shell representing the skull. The third layer is normally CSF and finally the innermost layer representing the cortex. Each of these layers has a specific conductivity and thickness. It is possible to add more layers to the model such as dura and even some inhomogeneous parts to make the model more accurate. However, a normal spherical head model which illustrated in figure 1 is mainly useful for extracting general information. [3]

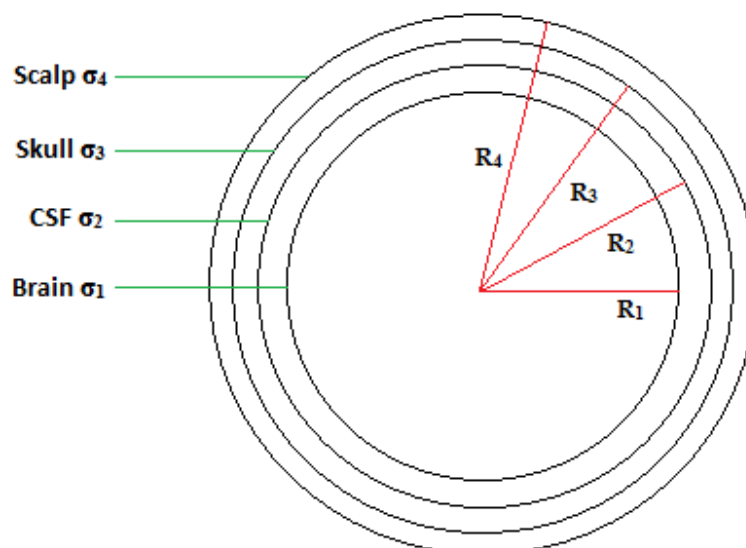


Figure 1, Cross section of a spherical head model for EEG dipole source localization, different tissues with different conductivities and radiuses are depicted in the figure.

Signals are always perpendicular to the surface of cortex. It means for a flat surface of cortex such as a gyrus, the signal will be detected in the right place (figure 2a). But, if the origin of the signal is located in a sulcus, then the measured signal will be appear in both sides of the head due to the fact that the signal propagates perpendicular to the cortex surface (figure 2b). Thus, by using a spherical head model accurate detection of these signals will be impossible. This problem of source localization can be solved by constructing a more accurate head model. The first step to develop this new head model is to extract different head and brain structures and tissues precisely. The main idea is to extract this information from the anatomical MR images and the first step is to perform accurate tissue segmentation on head MR images. The motivation of this project is basically reaching this goal and besides that it tries to find the best possible way to obtain the most accurate brain tissue segmentation considering the state of art.

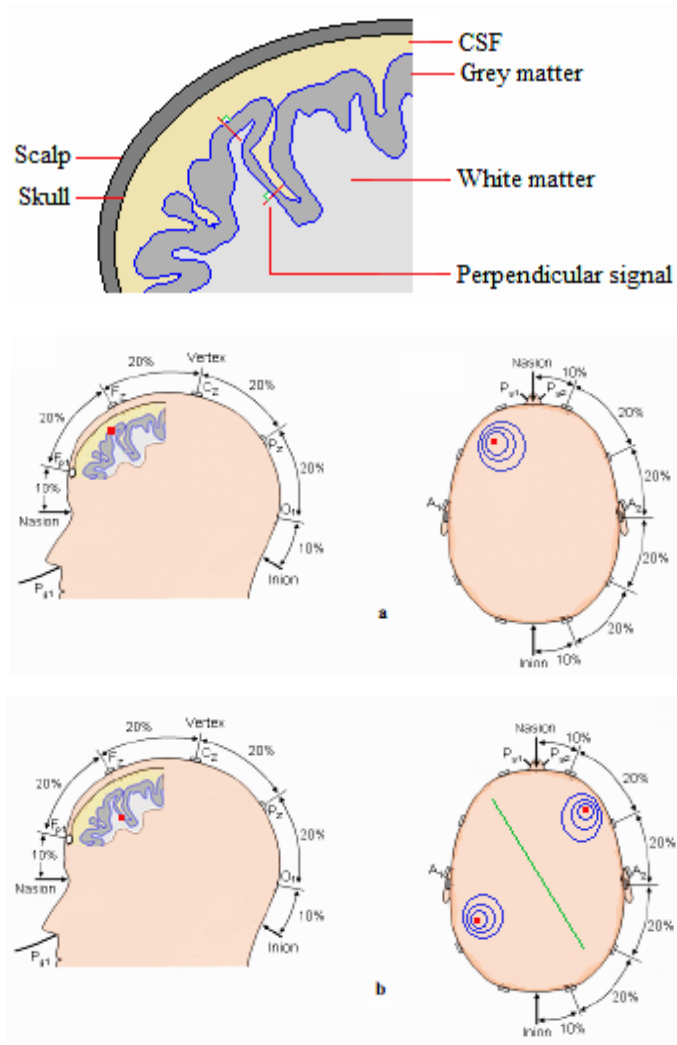


Figure 2, Cross section of a head model, (a) Signal detection from gyrus, (b) Signal detection from a sulcus

In this project different software packages for brain tissue segmentation were studied to pick the most sophisticated ones for the evaluation and comparison. SPM8 [7], FSL [8] and FreeSurfer [9] are selected which are three most widely used brain tissue segmentation software packages. The evaluation for each software package was carried out by performing tissue segmentation over 18 brain phantoms provided by Brainweb [35] with 6 different noise levels and 3 different RF inhomogeneity values. Then the resulted images for each tissue type from each software compared voxel by voxel with the ground truth images for each tissue type. To provide a volumetric voxel by voxel comparison between ground truth images and output images from software packages the 3dOverlap command line from AFNI software package [41] used together with Jimmy Shen's library in MATLAB [36].

Finally to compare the performance of these three software packages the misclassification rate were calculated for each tissue type.

Chapter 2

2. Background

This chapter explains the anatomy of brain and its different structures. In the second part, some background of magnetic resonance imaging will be given.

2.1. Anatomy of the brain [4]

Central nervous system (CNS) is a long tube which consists of spinal cord and brain. CNS is covered by a system of membranes called Meninges which consists of three layers: Dura matter³, Arachnoid matter⁴ and the Pia matter⁵ which illustrated in figure 3.

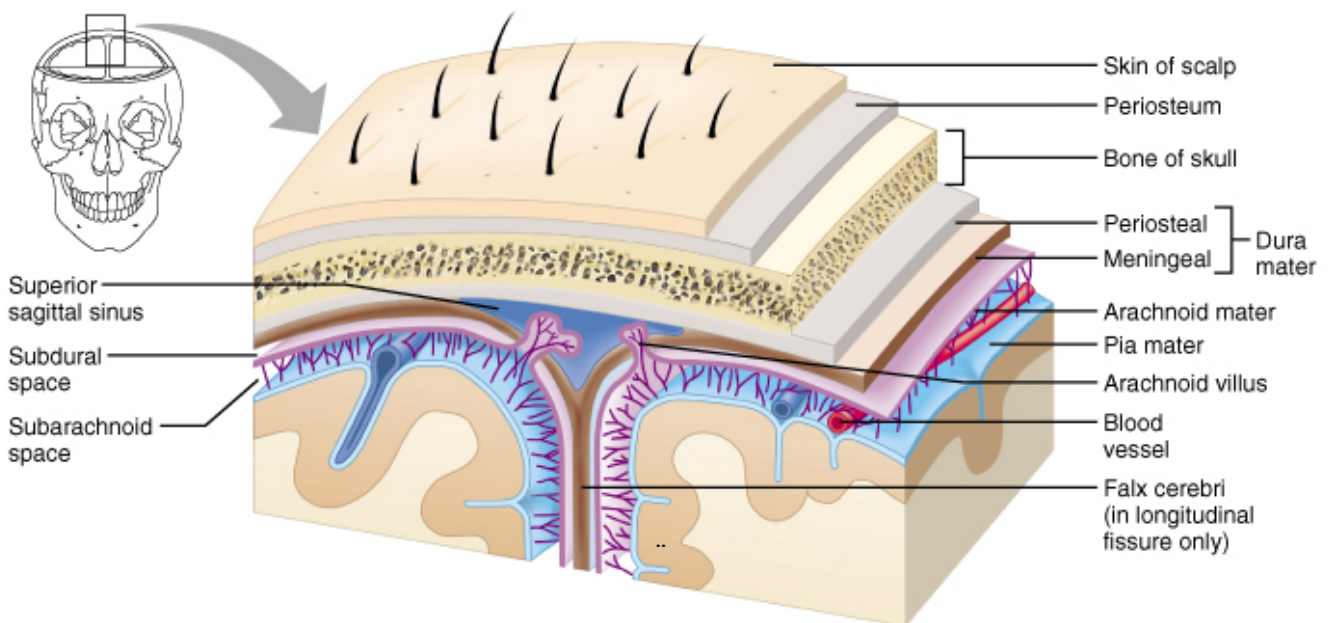


Figure 3, Different layers of Meninges [5]

Brain itself is a folded structure placed inside the skull consisting of four different regions: Cerebrum, Diencephalon, Cerebellum and Brainstem.

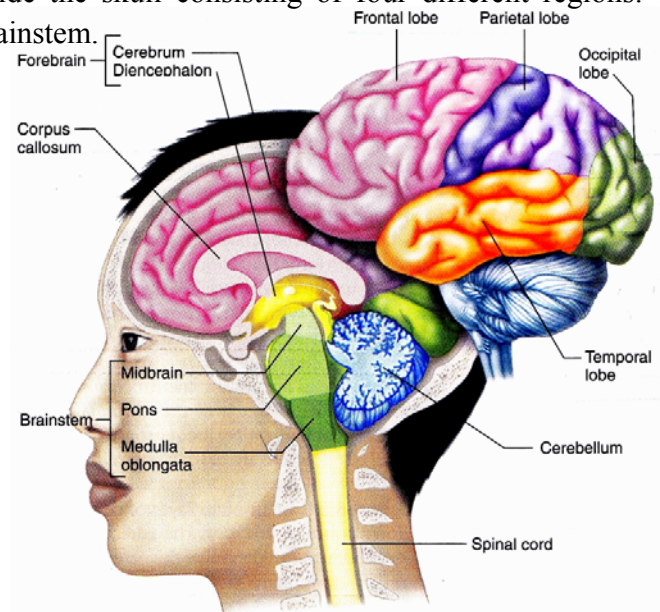


Figure 4, Different regions of brain [4]

Subsequently as illustrated in figure 4, cerebrum and Diencephalon together are forming forebrain. Midbrain, Pons and Medulla oblongata together are forming Brainstem in the bottom. As it is illustrated in figure 5, cerebral ventricles are four interconnected cavities in the brain which filled with CSF.

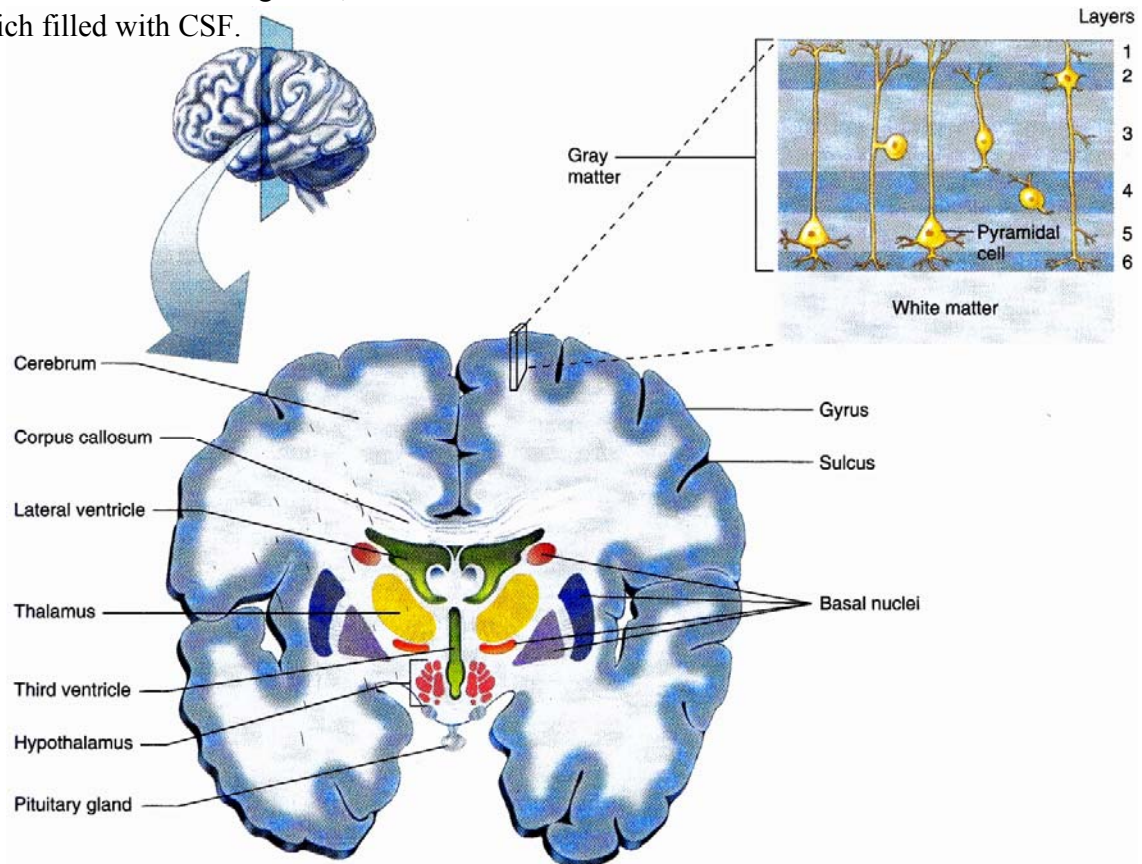


Figure 5, Cerebral hemispheres, white and grey matter, subcortical structures, cerebral ventricles [4]

As it mentioned before cerebrum and diencephalon are two subdivisions of forebrain. Brain consists of two hemispheres, left and right. As a result, all structures in the brain have two hemispheres. The hemispheres of cerebrum are called cerebral hemispheres which connected together by a group of nerve fibers known as corpus callosum. Each cerebral hemisphere consists of cerebral cortex which is a layer of neural tissue. The folded ridges on cerebral cortex are called gyri and between each gyrus (singular) there is a sulcus. The outer layer of cerebral cortex is made of grey matter (GM) which contains the cell bodies of neurons and because of that it has a grey color. It forms only 3 mm of the brain cortex in average. There are two different types of cortical neurons, pyramidal cells and non-pyramidal cells. The processing of information and controlling the systems are carried out in the cerebral cortex. It consists of four lobes: frontal, parietal, occipital and temporal. Occipital lobe contains the visual cortex which controls the vision. The auditory cortex is in the temporal lobe. The olfactory cortex is in the frontal lobe and the somatosensory cortex is located in the parietal lobe. Different lobes and primary sensory areas are illustrated in figure 6.

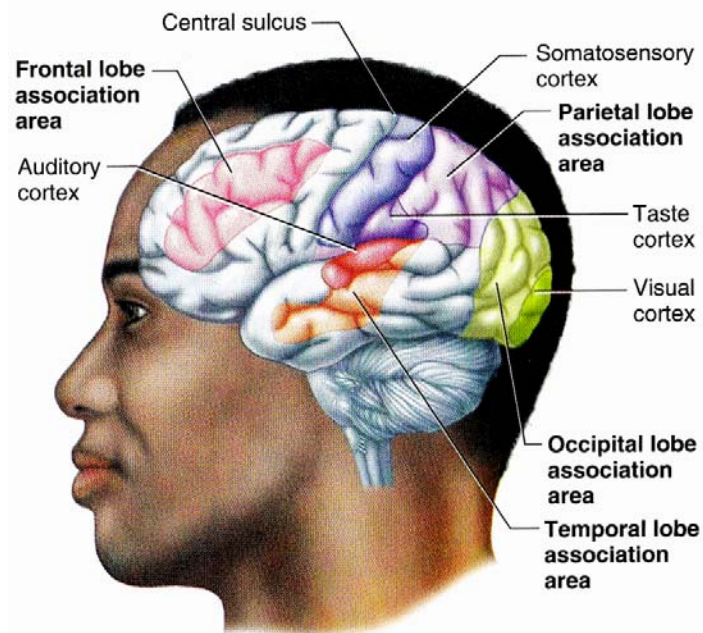


Figure 6, Different regions of cerebral cortex [4]

On the other hand, the inner layer of cerebral cortex is made of white matter (WM) which contains myelinated fiber tracts and has a brighter look. Each fiber tract has several nerve fibers and their function is to transfer information inside the hemisphere.

Another part of the brain is subcortical nuclei that contain number of structures made of grey matter and located inside of the cerebral hemispheres. A group of these subcortical structures (striatum⁶, pallidum⁷, substantia nigra⁸ and subthalamic nucleus⁹) together form basal nuclei (basal ganglia) which are responsible for controlling movement and posture and behaviors such

as reactions in response to rewarding stimuli. Basal nuclei and its structures are illustrated in figure 5.

As mentioned before forebrain consists of two parts: cerebrum and diencephalon. Diencephalon itself is a subcortical structure which is made up of two parts: thalamus and hypothalamus. The thalamus, as shown in figures 5 and 7, is located between cerebral cortex and midbrain and it is made up of several large nuclei. It plays a significant role in relaying the sensing signals in synapses heading to the cerebral cortex. Thalamus is also responsible for regulating consciousness, sleep, general arousal and focused attention. The hypothalamus is a tiny structure (less than 1% of brain weight) and consists of several small nuclei situated under thalamus (figures 5 and 7). It has many different functions such as controlling behaviors like eating, drinking and reproduction. However, its most important function is coordinating the connection between nervous system and endocrine system through pituitary gland¹⁰ (hypophysis).

Hippocampus¹¹, amygdala¹², anterior thalamic nuclei¹³ and limbic cortex¹⁴ together form a functional structure called limbic system. Limbic system is responsible for number of functions such as learning, emotional, behavior, long term memory, olfaction and several visceral and endocrine functions. The limbic system is illustrated in figure 7.

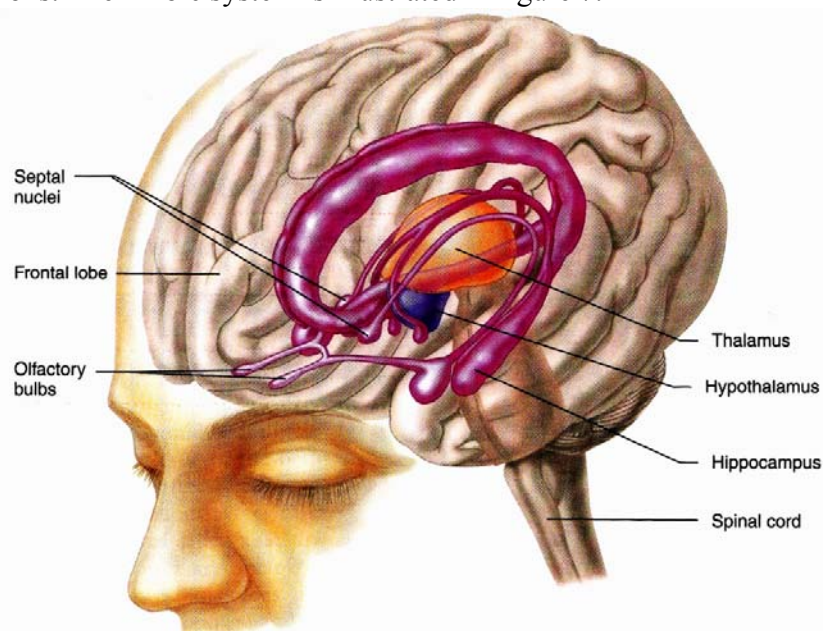


Figure 7, Limbic system (purple), Thalamus (orange), Hypothalamus (blue) [4]

Another region of the brain is cerebellum which situated at the back of the brain. Its surface called cerebellar cortex which made of grey matter while its inside is made of white matter. Cerebellum has a lot of functions. It is mostly responsible for coordinating the motor control (movement, posture and balance) and connected to different parts of the brain which are responsible for movement as well as different parts of the body like ears, eyes, viscera, joints and muscles. Although, cerebellum controls the movements in the body but it cannot initiate any

voluntary movement. Cerebellum also has other functions such as regulating fear and pleasure (emotional functions), controlling attention and language (cognitive functions).

The forth region of the brain is brainstem. It is situated at the bottom of the brain and is the starting part of spinal cord. Brainstem contains nerve fibers which carrying signals between spinal cord, cerebellum and forebrain. As it is illustrated in figure 4, brainstem comprises three parts: Midbrain¹⁵, Pons¹⁶ and Medulla oblongata¹⁷. This part of brain contains “reticular formation” which is situated in the core of Pons and considered an essential region for controlling many basic functions. All signals from different parts of central nervous system will enter to reticular formation at first place and the neural information processing will take place in this structure. It is responsible for sleep and wakefulness cycles, respiratory and cardiovascular systems and motor functions.

After this brief review of human brain anatomy, this is also good to have a basic knowledge about magnetic resonance imaging.

2.2. Magnetic Resonance Imaging (MRI) [6]

Magnetic resonance imaging generates tomographic images with high spatial resolution and contrast. Although the image generation method in MRI is totally different from CT (Computed Tomography), both modalities generate tomographic images. However, what makes it more interesting is being a risk-free imaging modality. Unlike computed tomography, MRI doesn't use ionizing radiation. It is based on a physical phenomenon known as nuclear magnetic resonance (NMR) which is defined as the ability of magnetic nuclei to absorb energy from an electromagnetic pulse and radiating this energy back.

Nucleus of atoms contains protons and neutrons which are considered positive charges. They have two important properties: angular momentum¹⁸ (spin) and magnetic dipole moment¹⁹ (figure 8). A nucleus of an atom with an odd atomic number or an odd mass number such as ¹H, ¹³C, ¹⁹F and ³¹P has these two properties and as a result can provide NMR signal. However, in MR imaging the ¹H atoms are important simply because of high water content of human body.

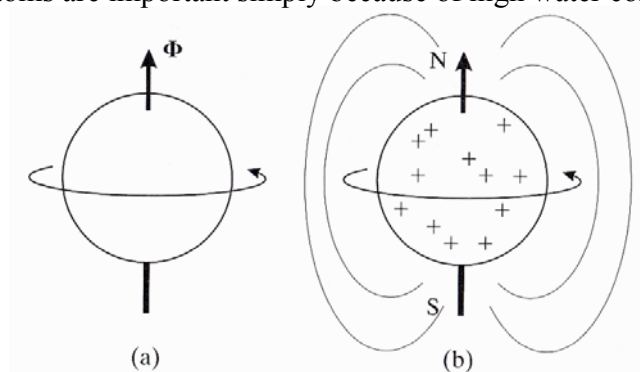


Figure 8, Angular momentum Φ (a), magnetic dipole moment (b) [6]

Now consider a group of nuclei of the same atom in a medium, they are called nuclear spin system. This spin system in a molecular environment in absence of an external magnetic field has no macroscopic magnetic field because the orientation of each nucleus in a spin system is randomized (They influenced by molecular thermal motion) and as a result they cancel each other's nuclear magnetic moment vector microscopically (figure 9).



Figure 9, Individual nucleus in a spin system randomly oriented and there is no macroscopic magnetic field [60]

Nuclear magnetic moment vector is the magnetic field of each nucleus and can be calculated by:

$$\mu = \gamma \cdot \Phi \quad (2.1)$$

Where Φ is the angular momentum of the nucleus and γ is known as the gyromagnetic ratio which has different values for different atoms.

By applying an external static magnetic field the magnetic moments of nuclei in the spin system will align to the external static magnetic field and as a result the spin system will become macroscopically magnetized which known as nuclear magnetization which essentially is the summation of nuclear magnetic moments in the spin system (figure 10).

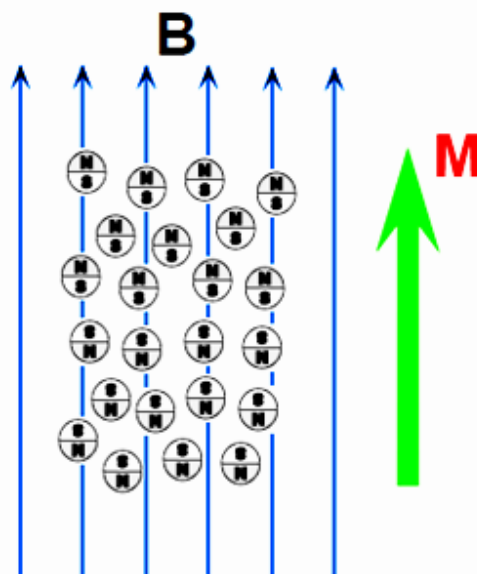


Figure 10, External static magnetic field B and resulted nuclear magnetization vector M [60]

In MR imaging the magnetization vector is brought out of alignment with the external static magnetic field using a radio frequency pulse. The gyromagnetic property of ^1H nuclei will cause a precession²⁰ of magnetization vector to come back in alignment with the external static magnetic field and reaching thermal equilibrium (relaxation). The frequency of this precession is known as Larmor frequency ω_0 which given by:

$$\omega_0 = \gamma \cdot B \quad (2.2)$$

The magnetization vector as it is shown in figure 11 has two components: Longitudinal and Transversal. As it mentioned before an RF pulse is used to manipulate the magnetization vector and take it out of equilibrium, which means bring it out of alignment with the external static magnetic field vector. By using the right RF pulse the magnetization vector can totally pushed toward the transverse plane. It means the magnetization vector will change its position 90° degrees. The angle of perturbation is called tip angle and the excitation pulse that used for creating this perturbation is called a $\pi/2$ pulse. As a result of a $\pi/2$ pulse the only remained component of magnetization vector will be transversal component. However, there is another common excitation pulse called a π pulse or inversion pulse that changes the direction of magnetization vector 180° degrees.

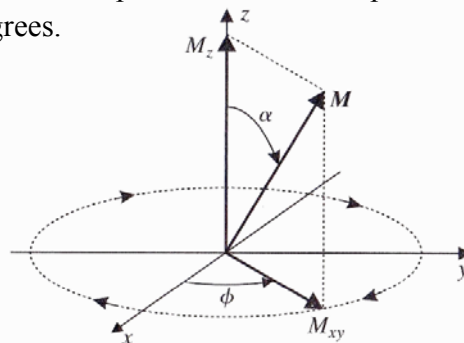


Figure 11, Magnetization vector and its components [6]

When the magnetization vector is brought out of equilibrium using a $\pi/2$ pulse, it will start the precession in a spiral form (figure 12a) to come back in alignment with the external static magnetic field. This precession (transverse relaxation or spin-spin relaxation) produces an RF pulse from the spin system which is known as Free Induction Decay (FID) with a time constant called transverse relaxation time T_2 (figure 12b). This signal then received by antennas around the spin system to produce images.

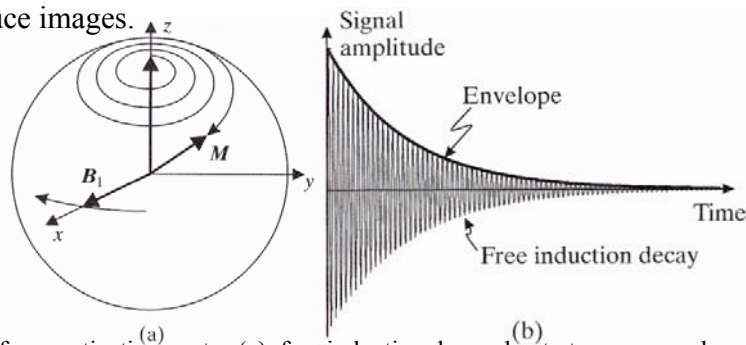


Figure 12, Precession of magnetization vector (a), free induction decay due to transverse relaxation (b) [6]

However, the signal which received by antennas will decay faster than T_2 due to local perturbations in the external static magnetic field. This shorter time constant is called T_2^* and illustrated in figure 13a.

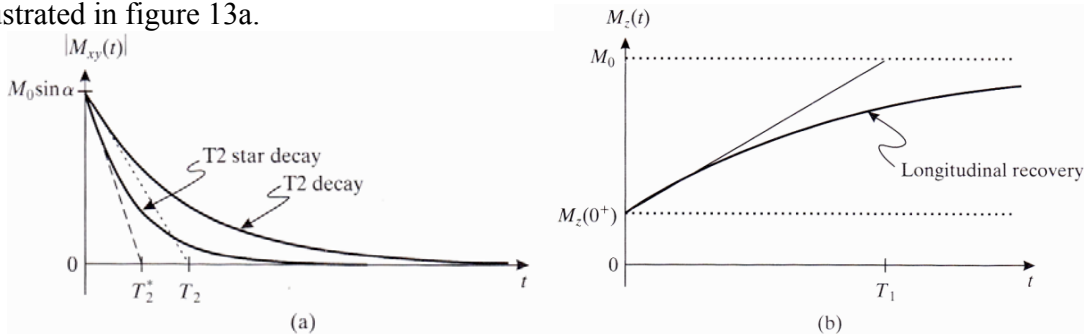


Figure 13, Transverse relaxation and T2* decay (a), longitudinal relaxation (b) [6]

Different tissues have various T_2 decay time. Thus, by choosing a good sampling time it is possible to capture an image with a good contrast between different tissues. Figure 14 shows a T_2 image and transverse relaxation time for different tissues. The sampling time of the image specified in the figure. Table 1 gives the relative elapsing time for various tissues.

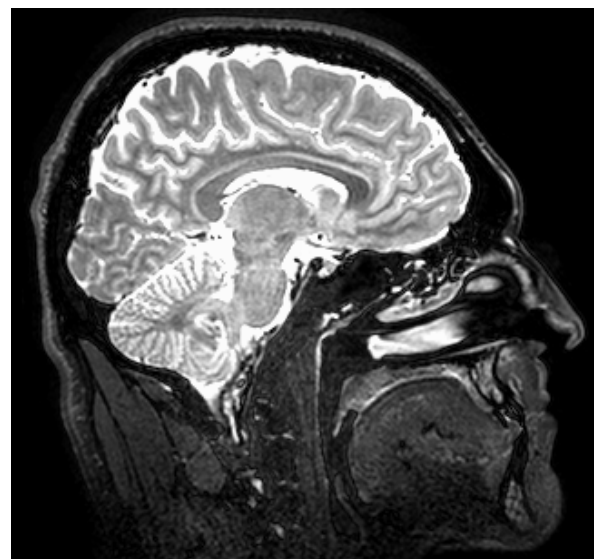
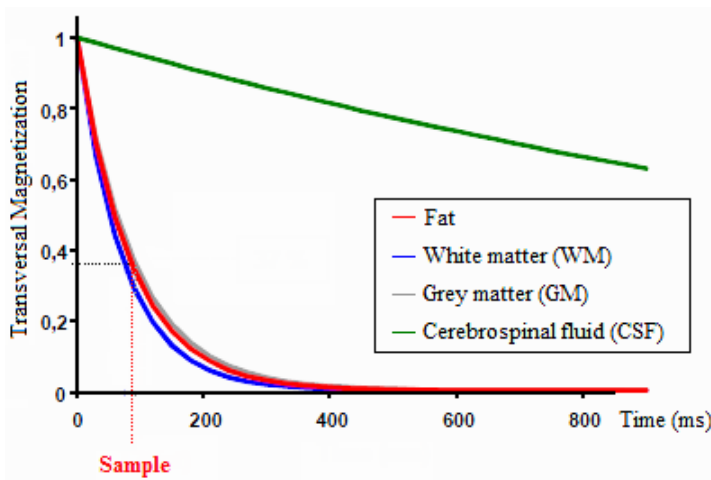


Figure 14, Sagittal view of a T_2 weighted image and transverse relaxation time for different tissues [60]

Tissue	T_2 (ms)
Fat	84
WM	73
GM	90
CSF	>2000

Table 1, Elapsing time for different tissues [60]

If instead of observing transversal component decay, we focus on recovery of longitudinal component of magnetization vector to its equilibrium, it is possible to measure another relaxation time known as longitudinal relaxation time T_1 (figure 13b). This relaxation mechanism unlike

transverse relaxation is an increasing exponential. However, in both mechanisms the produced NMR signal from spin system will decay. This process is known as longitudinal relaxation or spin/lattice relaxation and like transverse relaxation has different recovery time for different tissues. As a result, with a good choice in sampling time we can capture images with good contrast between various tissues. Figure 15, shows the recovery time for different tissues and the sampling time to capture a T_1 weighted image and Table 2 shows the relative recovery time for various tissues. T_1 normally ranges between $250\text{ms} < T_1 < 2500\text{ms}$, T_2 is much shorter and ranges between $25\text{ms} < T_2 < 250\text{ms}$.

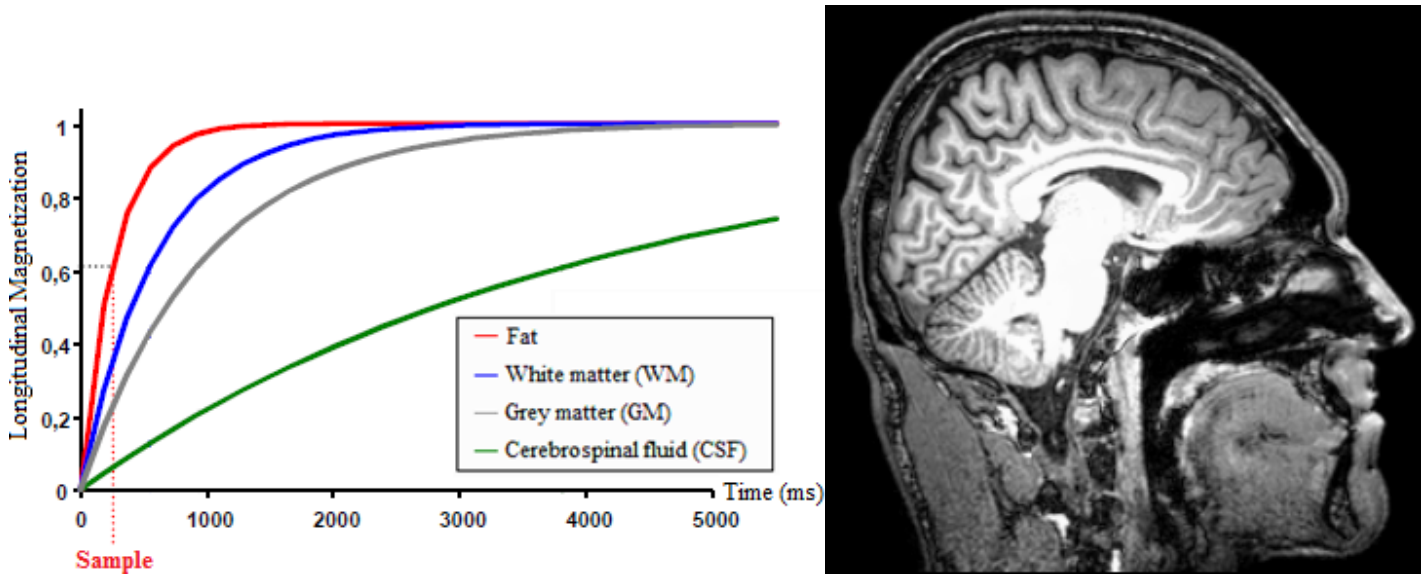


Figure 15, Sagittal view of a T_1 weighted image and longitudinal relaxation time for different tissues [60]

Tissue	T_1 (ms)
Fat	260
WM	582
GM	982
CSF	>4000

Table 2, Recovery time for different tissues [60]

Chapter 3

3. Automated brain tissue segmentation

This chapter starts by giving a brief review of different software packages for brain tissue segmentation and then continues with more in details explanation and instructions for performing tissue segmentation on some of the most used ones.

3.1. A review of different software packages for brain tissue segmentation

There are number of software packages available for brain tissue segmentation which are using different algorithms and image processing techniques to perform brain tissue segmentation and sometimes overlap in capabilities. It is useful to have a brief review and understanding about number of widely used software packages for brain tissue segmentation. The software packages for this review are: SPM [7], FSL [8], FreeSurfer [9], Bioimage suite [10] and Brain suite [11]. The mentioned software packages have different usages. However, this review only aimed to give a brief summary of capabilities of these software packages in brain tissue segmentation.

3.1.1. SPM [7]

Statistical Parametric Mapping (SPM) is an open source software which developed in MATLAB [12] environment. The software basis is a voxel-based approach for tissue segmentation using modified versions of the ICBM Tissue Probabilistic Atlases [13]. The user is able to use a graphical user interface to segment white matter (WM), grey matter (GM) and cerebrospinal fluid (CSF) from T1 images which are roughly aligned to probability maps. However, subcortical segmentation cannot be done using SPM. Another important issue for SPM is that multi spectral segmentation has not implemented in this software yet (During writing this thesis the latest available version was SPM8). This means it is not possible to use registered T1 and T2 images to segment skull and scalp. Nevertheless, image registration, bias field correction, spatially normalizing images and smoothing can be done using this software package.

3.1.2. FSL [8]

FSL is an open source software package which developed in FMRIB, Oxford, UK. FSL uses MNI probability atlases (Montreal Neurological Institute) [14] for tissue segmentation in a voxel-based algorithm. It has a graphical user interface but it can be more useful by using command line. FSL is able to segment white matter (WM), grey matter (GM), cerebrospinal fluid (CSF) and subcortical structures. It is possible to perform multi spectral segmentation and as a result extracting skull and scalp. Moreover, bias field correction and also image registration can be done by FSL.

3.1.3. FreeSurfer [9]

FreeSurfer is an open source software package developed at the Martinos Center for Biomedical Imaging [15]. Like SPM and FSL, FreeSurfer segmentation method is based on voxel intensities and Talairach anatomical atlases [16]. It has a graphical user interface which mostly used for visualization purposes. However, for performing segmentation using command line is recommended. It is possible to segment white matter (WM), grey matter (GM), cerebrospinal fluid (CSF) and subcortical structures using T1 images in FreeSurfer but multi spectral segmentation is not an option for this software package. As a result it cannot extract skull and scalp using T2 images. Bias field correction and spatially normalization can be done by FreeSurfer.

3.1.4. Bioimage suite [10]

Bioimage suite is an open source software package developed at Yale University. It has developed in C++ environment and Tcl (Tool Command Language) has been used for constructing its user interface. Bioimage suite uses FSL options for brain tissue segmentation. Therefore, the output is the same as FSL which reviewed earlier. Manual image registration can be done by Bioimage suite.

3.1.5. Brain suite [11]

Brain suite is an open source software which written in C++ [11]. This software package uses a volume based algorithm to create a likelihood model for tissue classification. It is possible to segment white matter (WM), grey matter (GM) and cerebrospinal fluid (CSF) using this software package. Although, it cannot perform subcortical segmentation but it is possible to extract skull and scalp using brain suite.

By comparing the capabilities of these five software packages, it can be seen that FSL, FreeSurfer and SPM are considered more reliable software packages for brain tissue segmentation considering their broad usage. Therefore, this project will focus on using these three software packages and giving step by step instructions of tissue segmentation for each of them. A summary of this overview is available in table 3.

Software package	Segmentation					Visualization
	WM	GM	CSF	Sub-cortical	Skull and Scalp	
SPM	✓	✓	✓	×	×	✓
FSL	✓	✓	✓	✓	✓	✓
FreeSurfer	✓	✓	✓	✓	×	✓
Bioimage Suite	✓	✓	✓	×	✓	✓
Brain Suite	✓	✓	✓	×	✓	✓

Table 3, Summary of capabilities of five different brain tissue segmentation software packages

3.2. Tissue segmentation using SPM8 [37]

By running SPM8 in MATLAB, a menu will appear which comprises three options to choose (figure3.1).

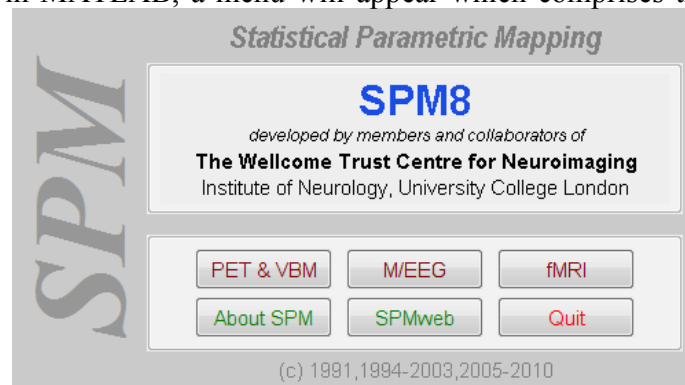


Figure 16, SPM8 start up menu

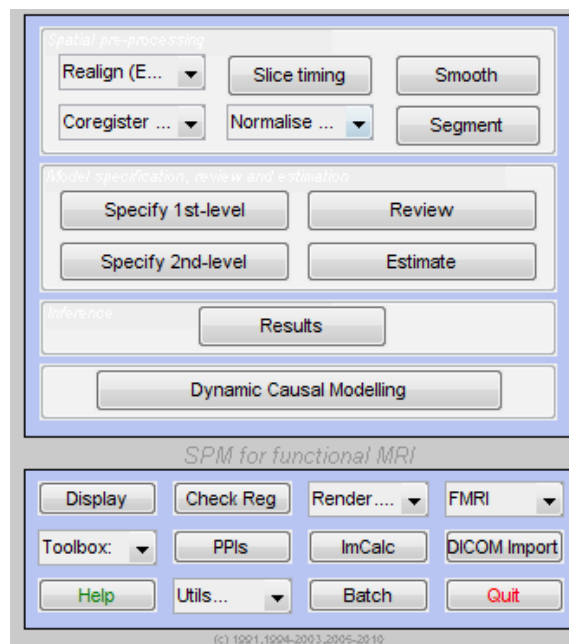


Figure 17, SPM8 fMRI menu

For tissue segmentation fMRI option must be chosen. In the fMRI window (figure 17) there are different options which will be discussed in details. The first thing to know for tissue segmentation in SPM is that, original T_1 weighted images, which are roughly aligned with the probability maps, must be used. Using T_1 images which are not aligned with the probability maps, brain extracted T_1 images or using T_2 weighted images will give strange results in the output (figure 18).

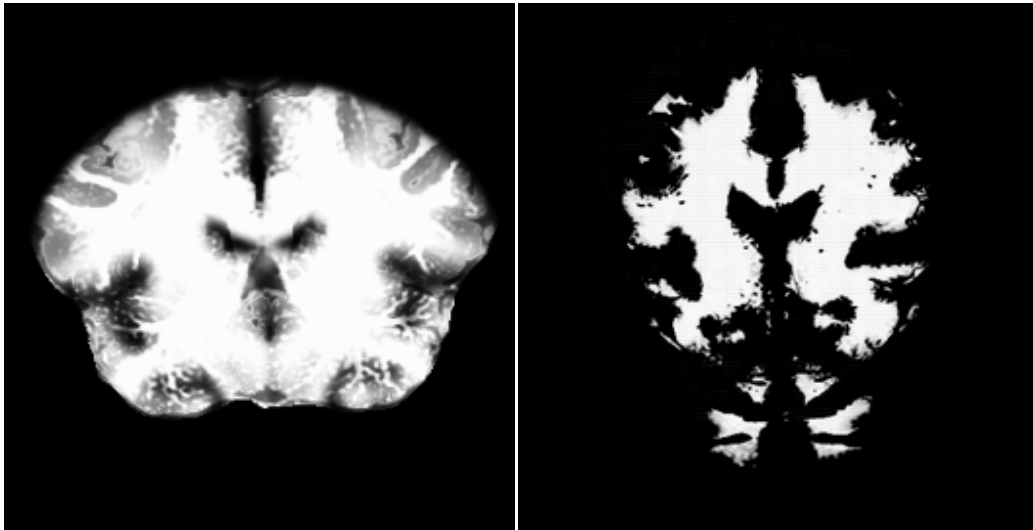


Figure 18, Brain extracted T_1 weighted input image results in an odd output in SPM8 (left), T_2 weighted input image results in an odd output in SPM8 (right) both are in transverse view

This problem has been anticipated in SPM8. To overcome this problem the coregister option can be used to realign the images with the probability maps. There is another option called realign but it is mainly designed to use for aligning PET and fMRI data sessions on anatomical images.

Coregister option has three choices: Estimate, Reslice and Est & Res. By clicking on coregister (Estimate) option a window will open (figure 19). The estimate option uses Collignon et al [17] method. First task is to select a reference image. It is better to choose an image from ICBM Tissue Probabilistic Atlases as reference image because the segmentation tool uses the same probability maps for tissue classification. After specifying the reference, the source image should be selected which is the image that will align with reference. There is another option named other images that make it possible to select as many images as desired to align with the source image. Afterwards, the estimation options can be manipulated to reach an optimized registration. The first option is “Objective Function” which is a real-valued function used in every optimization problem to be minimized or maximized. While in this project we are interested in tissue segmentation, thus, only T_1 weighted anatomical images are of our interest. As a result, three options of objective function may be used that are mutual information [17, 18], normalized mutual information [19] or entropy correlation coefficient [20]. The default choice is normally give the best estimate. The normalized Cross Correlation option is useful for image registration between different modalities.

Next estimation option is “Separation” which is a 1-by-x array in millimeters to specify the average distance between sampled points.

The other estimation option is “Tolerances” which is a 1-by-12 array to define the value of difference between two consecutive iterations. If the difference is more than the tolerance the iteration will continue otherwise it will stop.

Finally the last option is “Histogram Smoothing” which is a Gaussian smoothing filter. There is a default value for the filter however it is possible to choose any combination of a 1-by-2 array.

The “Coregister Estimate” window is illustrated in figure 19:

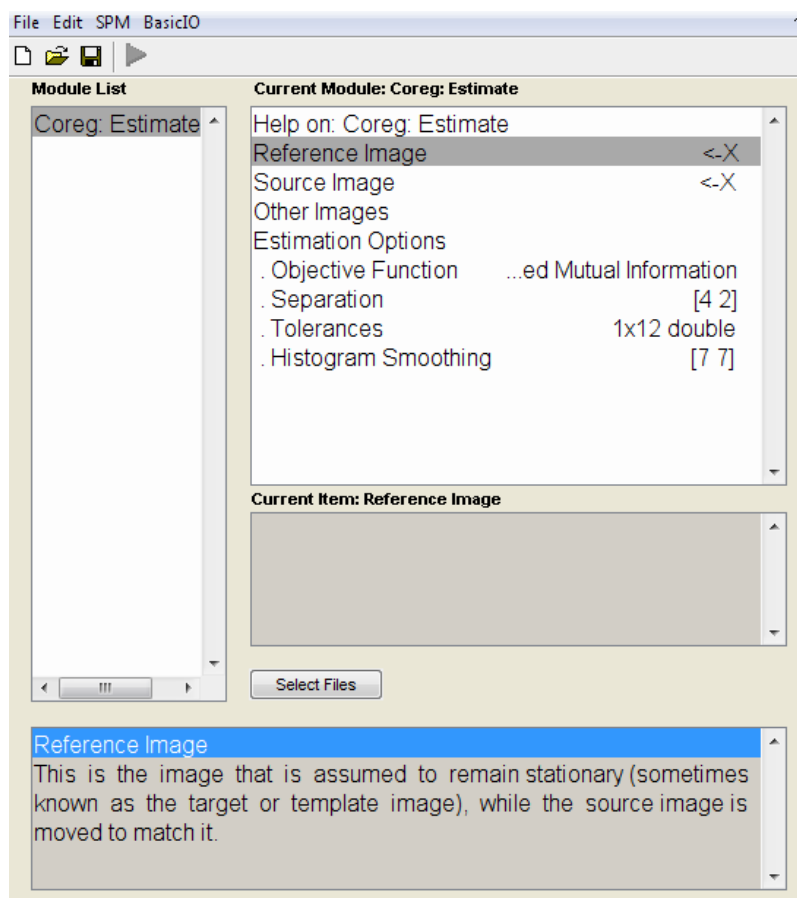


Figure 19, SPM8 coregister estimate menu

The second registration option is reslice. This option will reslice the input image to match the reference image. It means the voxel sizes, dimensions and orientations will be changed to match the reference image. In the menu of “Registration Reslice” (figure 20), instead of reference image you will find image defining space. The second step is to choose images that we want to be registered to the reference. It can be found in the third line “Images to Reslice”. After choosing the images, for optimizing the results we need to manipulate the “Reslice Options”. The first option is “Interpolation”. There are three choices: Nearest neighbor, Trilinear and B-spline.

The nearest neighbor option is very fast but the results won't be as good as the others. It can be useful to re-orient the images while they keeping their original voxel intensities. The other two options both will give good results however for high motion artifact higher degrees of B-spline option is recommended. The drawback is it will take much longer to perform the registration because it will use more neighbors.

The second option is "Wrapping". This option makes it possible to wrap the images in X, Y and Z directions. However, normally no wrapping is needed.

Motion artifact highly influences the MR images. Therefore, during sampling some of the voxels cannot save any data. "Masking" option will using the data from time series to refill these voxels.

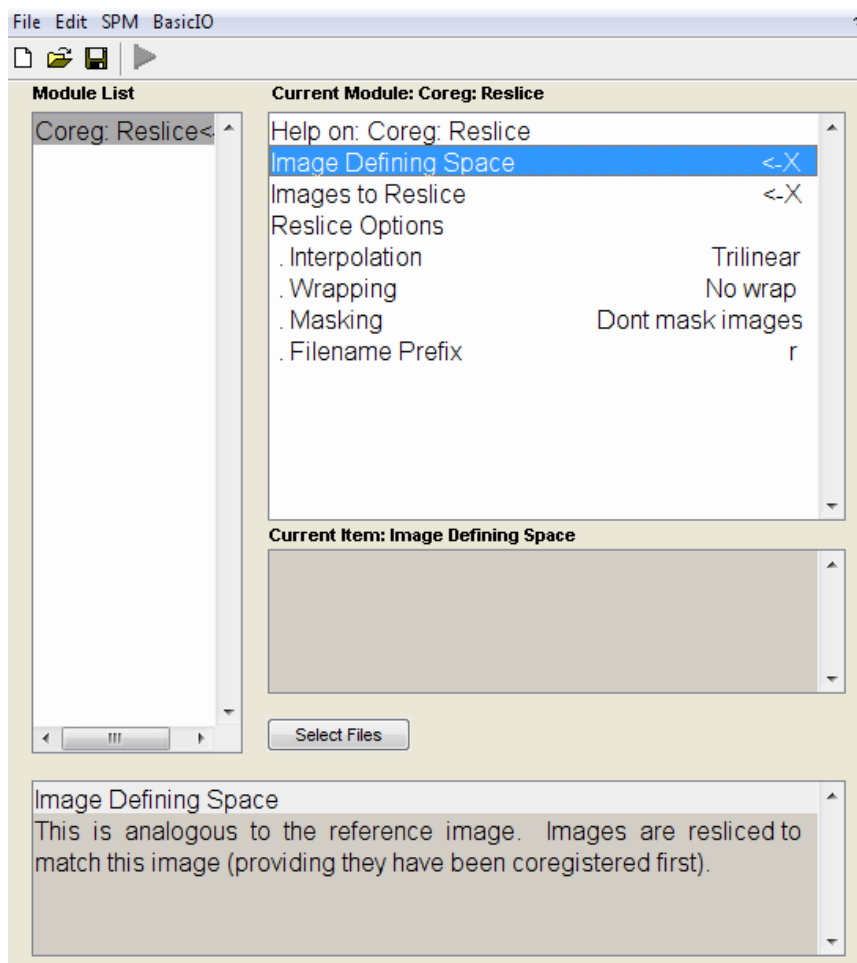


Figure 20, SPM8 coregister reslice menu

The "Coregister: Est & Res" is simply doing both options at the same time and giving the files in the output. Resliced files have the "r" filename prefix to be distinguished. Table 4 gives a summary of different options in "Coregister: Estimate" and "Coregister: Reslice".

Coregister : Estimate	
Reference image	The image that other images are supposed to be aligned to
Source image	The image that will align with reference
Other images	Select as many images as desired to align with the source image
Objective function	A real-valued function used in optimization problem
Separation	Specifies the average distance between sampled points
Tolerances	Defines the value of difference between two consecutive iterations
Histogram smoothing	Possibility to choose any combination for a Gaussian smoothing filter
Coregister : Reslice	
Image defining space	The image that other images are supposed to be aligned to
Images to Reslice	Select as many images as desired to align with the reference image
Interpolation	Choosing the method that images have been sampled
Wrapping	Wrap the images in X, Y and Z directions
Masking	Refilling the blank voxels
Filename prefix	Changing the filename prefix, default is "r"

Table 4, SPM8 Coregister tool option descriptions summary [31]

Now the images are aligned with the probability maps and ready for segmentation by choosing "Segment". The aligned T₁ weighted image should be selected in "Data". The SPM segment tool will automatically perform the bias field correction²¹ over the image. However, it is arbitrary to save the bias corrected image or not.

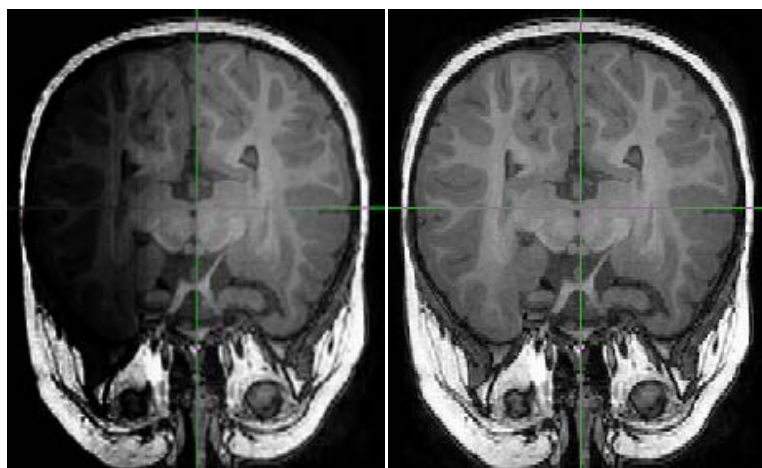


Figure 21, Bias field correction in transverse view of a T₁ weighted image, left image is the original image with inhomogeneous pattern and right image is the bias field corrected version

There is also an option for optimizing the brain extraction called "Clean up any partitions". It is off by default however there are choices to have light or through clean up. The problem with clean up tool is sometimes it will totally cut off some parts of the brain. Thus, it is recommended to keep the default configuration in this option.

There are three classes for tissue segmentation GM, WM and CSF and three optional choices: Native Space, Unmodulated normalized and Modulated normalized. The “Native Space” option will classify three tissue classes in images which are aligned with the original T₁ weighted image. Figure 22 illustrated the results of segmentation for “Native Space” option with the default custom options.

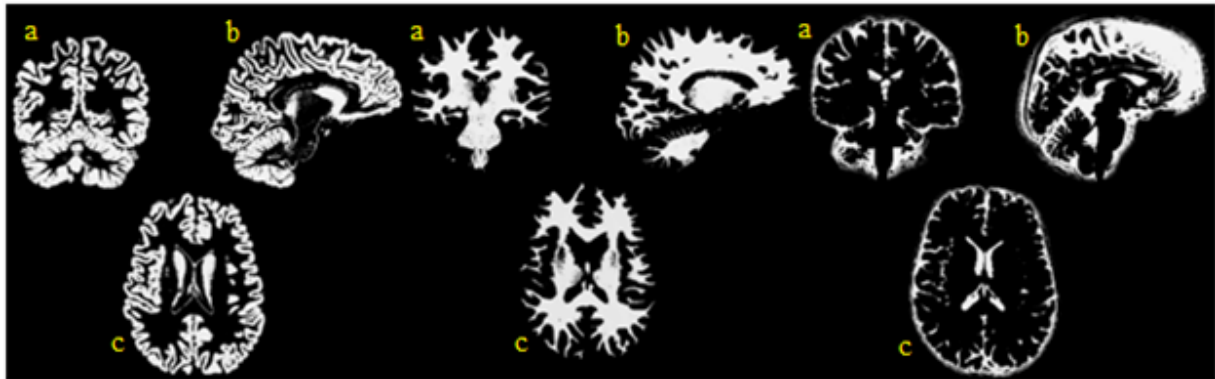


Figure 22, Segmented in Native Space: GM (left), WM (middle), CSF (right), coronal (a), sagittal (b) and transverse view (c)

The second option for tissue segmentation is “Unmodulated Normalized”. There are two differences between the resulted images from this option comparing to native space. First of all, the images will be spatially normalized and second, they will be aligned to the probability maps instead of original images. Thus, the orientation and voxel sizes will be changed. Results of “Unmodulated Normalized” with the default custom options are illustrated in figure 23.

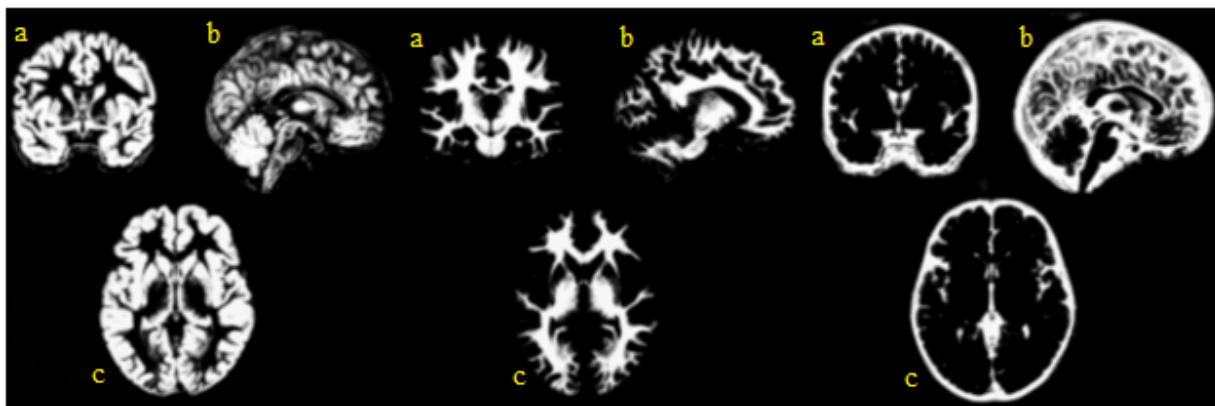


Figure 23, Unmodulated normalized Segmented: GM (left), WM (middle), CSF (right), coronal (a), sagittal (b) and transverse view (c)

As mentioned, normalization will realign the images to the probability maps and change the orientation and voxel sizes. Therefore, the volumes will change in the segmented images. To overcome this problem we can use the “Modulated Normalized” option. The segmentation results using this option are shown in figure 24.

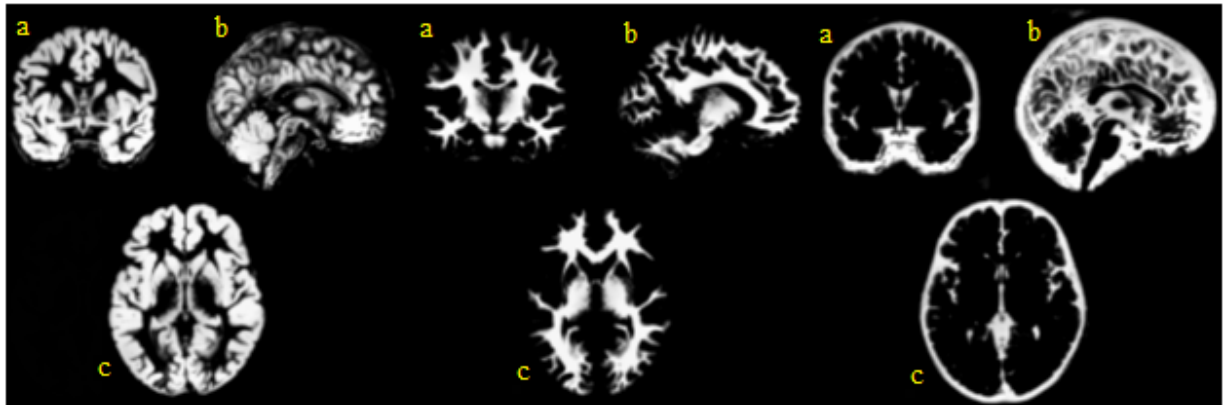


Figure 24, Modulated normalized Segmented: GM (left), WM (middle), CSF (right), coronal (a), sagittal (b) and transverse view (c)

For optimizing these results we may use the “Custom” options. The first option in the list is “Tissue probability maps” and as it mentioned before SPM uses modified versions of the ICBM Tissue Probabilistic Atlases which comprises GM, WM and CSF with 2mm resolution (figure 25). The second option for improving segmentation performance is the ability to change the number of Gaussians per class. It means that it is better to use more than one Gaussian for representing the intensity distribution for each tissue class. The reason is, normally each voxel in the image contains intensity information from more than just one tissue class. Therefore, theoretically assigning only one Gaussian per class should decrease the accuracy of the segmentation. The default values for Gaussian for each tissue type are two for GM, two for WM, two for CSF and four for everything else which has not fit into these three classes.

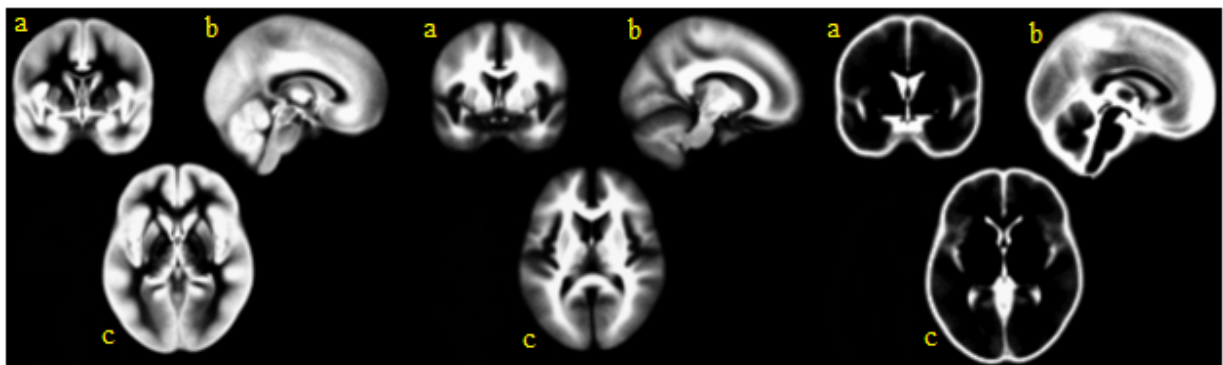


Figure 25, ICBM tissue probability maps: GM (left), WM (middle), CSF (right), coronal (a), sagittal (b) and transverse view (c)

“Affine Regularization” option will lead to a more robust segmentation due to an affine registration of images to tissue probability maps. However, this option may be turned off if the images are already registered to tissue probability maps.

Next option is “Warping Regularization”. It regulates the registration procedure when the images being aligned with the tissue probability maps. The default value is 1 however in the case of having distorted normalized images increasing the amount of warping regularization will give

smoother deformation in the registration process. Decreasing the “Warp Frequency Cutoff” will lead to more detailed deformation in the images. However, this is a trade off as long as it will increase the processing time.

“Bias Regularization” option makes it possible to change the intensity of bias field estimation procedure. It is recommended to increase the bias regularization for highly bias field corrupted images. If the intensities in the image are very smooth, the segmentation tool needs a high cutoff for FWHM of Gaussian smoothness of bias. It means despite low variations in intensity levels for different tissue types, the algorithm will be able to classify them.

“Sampling Distance” is a 1-by-1 array which specifies the relative distance between two consecutive sampled voxels. It is obvious that by choosing smaller sampling distance more data points will be used in the segmentation process.

The segment tool in SPM8 has the option to use a “Masking Image” to mask the segmentation and avoiding the blank voxels without any data in the output. However, it is important to use an image with the same orientation and voxel sizes as the images to be segmented. Figure 26 shows the “Segment” menu of SPM8. And Table 5 summarizes different tools and options in this tool.

Segment	
Data	A T ₁ weighted image roughly aligned to tissue probability maps
Grey matter	The output tissue class can be choose to be one of three options or none
White matter	The output tissue class can be choose to be one of three options or none
Cerebrospinal fluid	The output tissue class can be choose to be one of three options or none
Bias corrected	Saving the bias corrected image
Clean up any partitions	Automated brain extraction with three options
Tissue probability maps	Modified versions of the ICBM Tissue Probabilistic Atlases which comprises GM, WM and CSF with 2mm resolution
Gaussians per class	The ability to change the number of Gaussians per each tissue class
Affine regularization	Lead to a more robust segmentation due to an affine registration of images to tissue probability maps
Warping regularization	Regulates the registration procedure when the images being aligned with the tissue probability maps
Warp frequency cutoff	Lead to more detailed deformation in the images by decreasing
Bias regularization	possibility to change the intensity of bias field estimation procedure
Bias FWHM	If the intensities in the image are very smooth, the segmentation tool needs a high cutoff for FWHM of Gaussian smoothness of bias
Sampling distance	Specifies the relative distance between two consecutive sampled voxels
Masking image	to mask the segmentation and avoiding the blank voxels without any data in the output

Table 5, SPM8 Coregister tool option descriptions summary [31]

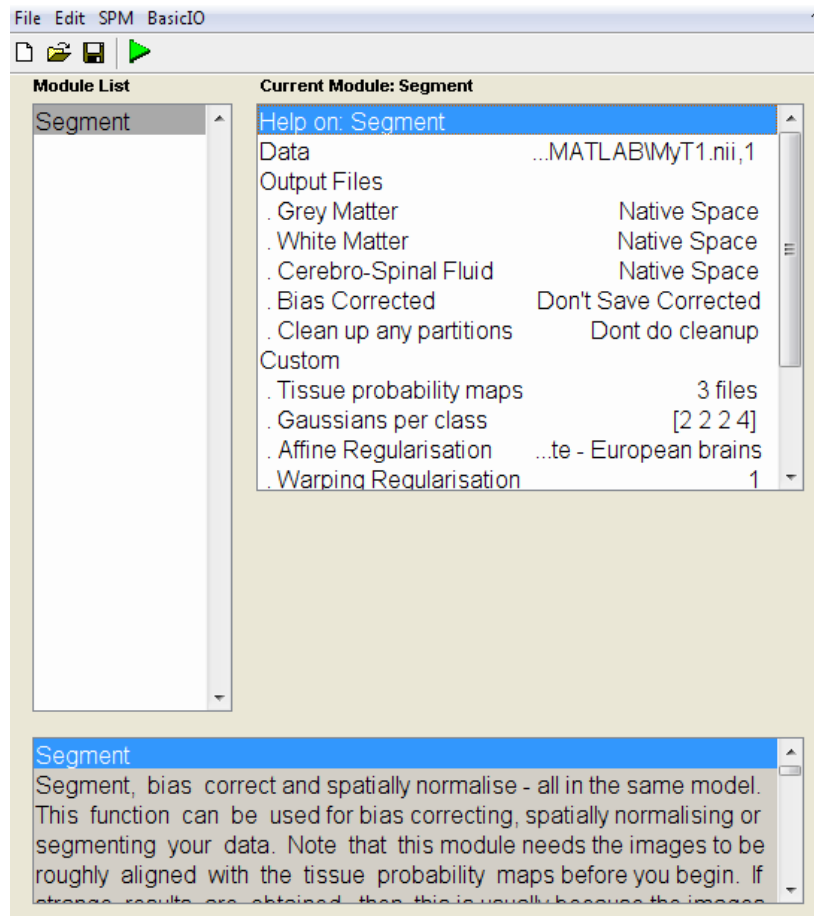


Figure 26, SPM8 segment menu

3.3. Tissue segmentation using FSL 4.1.5 [38]

For running FSL there are two choices. It is possible to use either Graphical User Interface (GUI) or command line in Linux terminal. First step for tissue segmentation with FSL software package is to extract the brain using BET.

3.3.1. Brain Extraction Tool (BET)

For brain extraction, choose the “BET brain extraction” in the GUI, or write “bet <input> <output> [options]” in command line. Pick the input image and specify a name and path for the output image. FSL uses two main programs for brain extraction. “bet2” is the main brain extraction algorithm in FSL and “betsurf” makes it possible to extract scalp and skull (inner and outer). In graphical user interface, there are several options which illustrated in figure 27. In each option of GUI different combinations of these two algorithms has been used. However, one can get better results by choosing manual combinations in the command line. Therefore, it is better to focus on command line instead of explaining the graphical user interface.

For choosing options the most important choice is “-f” which is fractional intensity threshold has a value between 0-1. By increasing its value the extracted brain will get smaller. This option can be combined with “-g” which is vertical gradient in fractional intensity ranging between -1to1. By increasing its value from zero the extracted brain will become larger at the bottom and smaller at top and by using negative values the extracted brain will become smaller at the bottom and larger at top.

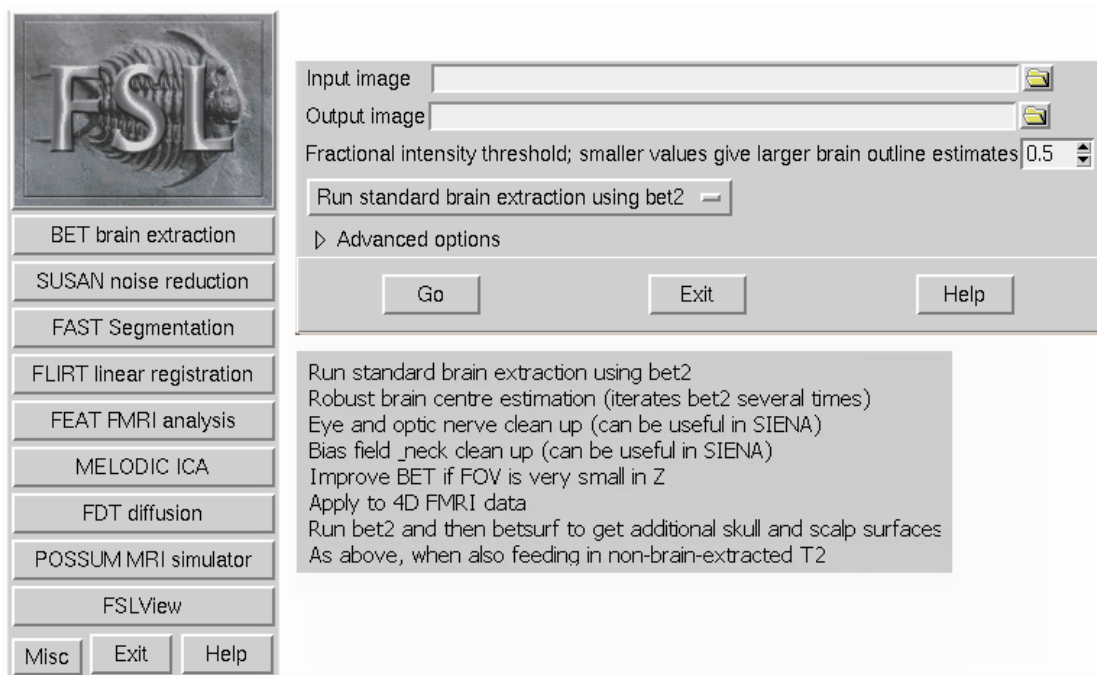


Figure 27, FSL 4.1.5 graphical user interface for BET (Brain Extraction Tool)

Figure 28 shows an illustrative example of how these two options are working for brain extraction. The reason for this example is to show that choosing these two values are crucial for brain extraction results. It is possible to use either T1 or T2 image to extract the brain. However, by running BET the extracted brain will normally contain parts of mouth and neck. To overcome this problem we need an estimation of center of gravity of the brain. It can be done using two options: “-R” and “-c”. The “R” stands for robust estimation for center of gravity which is an iterative method to find the best possible estimation while for using “-c” option user must provide the coordinates of the center of gravity. It can be done by using “FSLview”.

Although, using robust brain extraction will generate a very good result but it is not possible to use this option with “bet surf”. It is possible to produce a skull image using “-s” option together with “-R” however this image is not comparable with “bet surf” results. Thus, for using T₂ weighted image to generate skull and scalp images we need to have a good estimation of center of gravity of brain for “-c” option. A comparison between these two options illustrated in figure 29.

Figure 28, Left column: shows the extracted brain for Different values of fractional intensity. Right column: shows extracted brain in coronal view for different values of vertical gradient.

aI: -f 0.8	aII: -g 0.4
bI: -f 0.5	bII: -g 0
cI: -f 0.1	cII: -g -0.8

```
bet <input> <output> -f ... -g ...
```

Table 6, Commands for generating images in figure28

```
bet <input> <output> -f 0.5 -g 0 -R
bet <input> <output> -f 0.5 -g 0 -c 81 113 101
```

Table 7, Commands for generating images in figure29

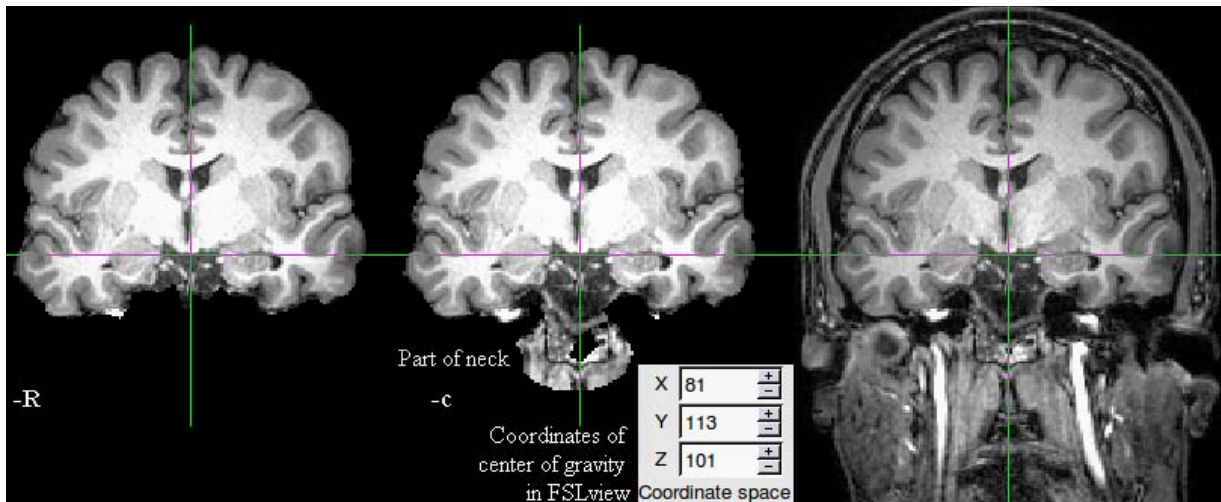
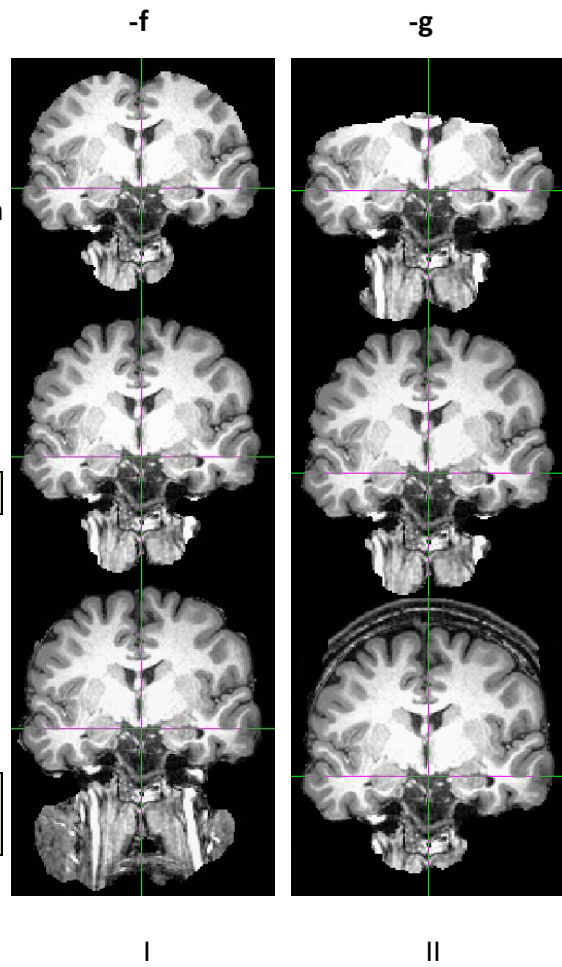


Figure 29, A comparison between the results of “-R” and “-c” for brain extraction, A part of neck remains in generated image using “-c” option but the results of robust brain extraction have no sign of neck (coronal view)

As it is illustrated in figure 29, there is drawback by using “-c” because providing an accurate center of gravity for this option is not easy. Therefore, sometimes parts of neck will be included in output images. However, as I mentioned before for extracting skull and scalp it is unavoidable to use “-c” option.

There are two options to extract skull and scalp: “-A” and “-A2”. Option “-A” doesn’t need a T₂ weighted image for extracting skull and scalp. It can generate these images directly from T₁ image. “-A2” option makes it possible to use an aligned T₂ image together with T₁ to extract skull and scalp. However, if these two images are not registered well it is better to use “-A” option because it can generate more accurate results. Figure 30 shows the results of brain extraction for these two options.

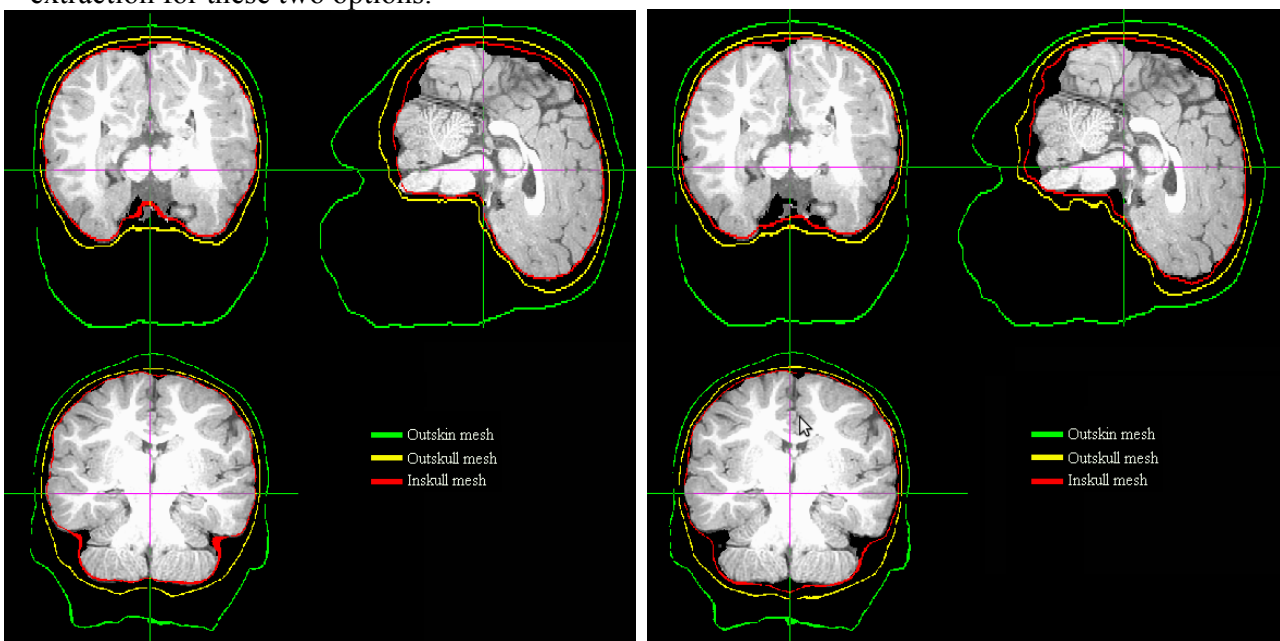


Figure 30, A comparison between the results of “-A” and “-A2” options, left image shows the extracted skull and scalp using “-A” option, right image shows the extracted skull and scalp using “-A2” option, transverse (up left), sagittal (up right), coronal (Bottom)

Left: bet <input> <output> -f 0.6 -g 0 -c <x y z> -A Right: bet <input> <output> -f 0.6 -g 0 -c <x y z> -A2 <input T ₂ >
--

Table 8, Commands for generating images in figure30

The results in figure 30 shows a slightly better extraction of inner skull by using option “-A” comparing to option “-A2”. However, outer skull and scalp for both options showing more or less the same results. It is important to know that mutual use of options with capital letters which are working modes is impossible.

Both of these options will generate volume masks for extracted brain, skull and scalp as well as a surface mask for extracted brain in “vtk” format [33].

A summary of FSL BET (Brain Extraction Tool) shall be found in table 9.

BET	
-f	Fractional intensity threshold has a value between 0-1. By increasing its value the extracted brain will get smaller and vice versa.
-g	Vertical gradient in fractional intensity ranging between -1to1. By increasing its value from zero the extracted brain will become larger at the bottom and smaller at top.
-c	The coordinates of the center of gravity.
-R	Robust estimation for center of gravity which is an iterative method to find the best possible estimation.
-A	Extracting skull and scalp from T ₁ weighted image.
-A2	Extracting skull and scalp from T ₁ weighted image using information from T ₂ weighted image from the same subject with the same alignment.

Table 9, FSL BET option descriptions summary [32]

3.3.2. FAST

FAST or “FMRIB’s Automated Segmentation Tool” is able to classify three tissue types: WM, GM and CSF. It takes brain extracted image as input, does the bias field correction and generates one image or separate images for different tissue classes as output. Similar to other options of FSL it is possible to use this tool either in GUI or command line. The graphical user interface for FAST is illustrated in figure 31.

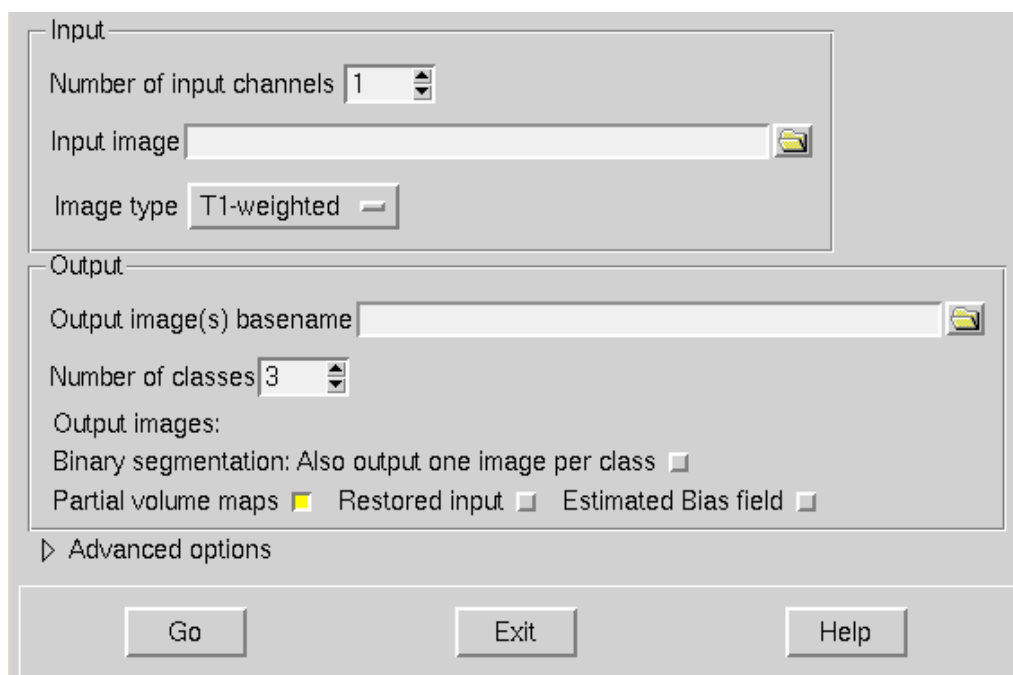


Figure 31, FSL 4.1.5 graphical user interface for FAST (FMRIB’s Automated Segmentation Tool)

As it is shown in figure 31, it is possible to have a number of input images to be segmented. However, it is important to use a brain extracted image and choose the right image type as input

otherwise an odd result will appear in the output. Again, similar to BET it is better to explain everything in command line. The general form of FAST command is “fast [options] -o <output> <input>”.

As it mentioned before, it is important to choose the right value for option “-t” which defines the image type. “-t 1” stands for T_1 weighted images, “-t 2” for T_2 weighted images and “-t 3” means the input image(s) are proton density weighted images (PD). The second important option to in FAST is “-H” which stands for main MRF parameter to determine the spatial smoothness of segmentation. The default value is 0.1 however after different experiments the best results obtained with “-H 0.5”. FAST tool will produce a hard segmented image in the output however by choosing option “-g” separated binary images for each class will be generated. Option “-n” is to determine the number of tissue types to be segmented. Option “-B” stands for correcting bias field and by choosing option “-b” in the command line a bias field corrected version of input image will generate in the output. The results of image segmentation which are illustrated in figure 3.11 shows a better tissue segmentation using T_1 weighted images comparing to segmentation results for T_2 weighted ones.

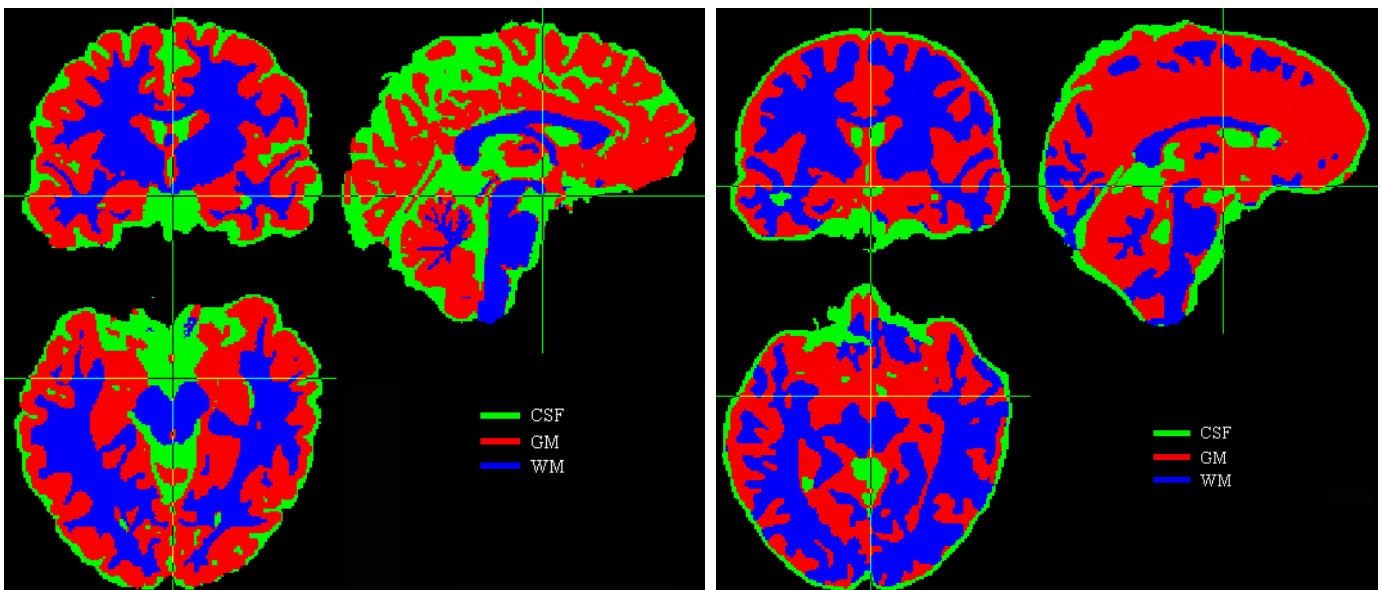


Figure 32, Segmentation results from FAST, T_1 weighted image (left), T_2 weighted image (right), coronal (up left), sagittal (up right), transverse (Bottom row)

<p>Left: fast -t 1 -n 3 -H 0.5 -g -b -B -o <output> <input T_1></p> <p>Right: fast -t 2 -n 3 -H 0.5 -g -b -B -o <output> <input T_2></p>
--

Table 10, Commands for generating images in figure32

However, considering the nature of T_2 weighted images (figure 14), the voxel intensities for white and grey matter are very close. Therefore, the segmentation results for T_2 weighted images as it has shown in figure 32 will be inaccurate. Thus, it is recommended to use T_1 weighted images for tissue segmentation.

A summary of FSL FAST (FMRIB’s Automated Segmentation Tool) shall be found in table 11.

FAST	
-t	Defines the image type. 1 for T ₁ , 2 for T ₂ and 3 for PD (proton density).
-n	Number of tissue types to be segmented.
-H	Stands for main MRF parameter to determine the spatial smoothness of segmentation.
-g	Generating separated binary images for each class.
-b	A bias corrected version of input image will generate in the output.
-B	Stands for bias field correction.
-o	Specifying the output path.

Table 11, FSL FAST option descriptions summary [32]

3.3.3. FLIRT

Similar to SMP8 in the case of using unaligned images as input in BET or FAST, odd results will appear in the output. To solve this problem, FSL uses FLIRT (FMRIB’s Linear Image Registration Tool). It uses the same tissue atlases as SPM8 (MNI152 tissue templates) which are provided by Montreal Neurological Institute and Hospital [14]. Normally when one download FSL software package, these tissue atlases must be included in the software library. However, if the software package doesn’t include these atlases, one can find them in Debian Neuroscience Repository [24]. FLIRT menu in GUI is illustrated in figure 33.

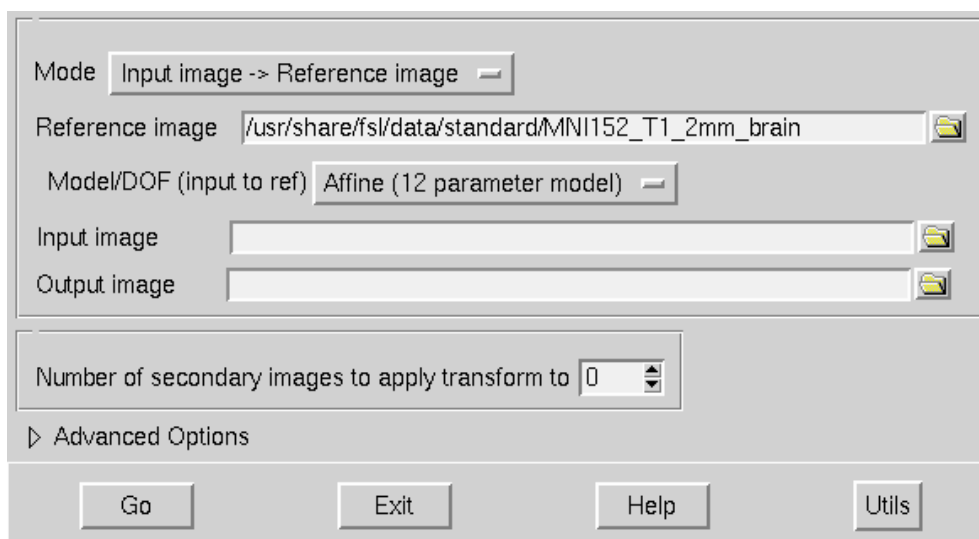


Figure 33, FSL 4.1.5 graphical user interface for FLIRT (FMRIB’s Linear Image Registration Tool)

The graphical user interface for FLIRT is very user friendly and easy to use. “Reference image” should normally choose from MNI152 atlases and “Input image” is the image to be aligned. However, it is good to first align T₁ image with MNI152 atlases then for aligning T₂ and T₁

weighted images for “-A2” option in FAST, one should choose this T₁ image as reference and T₂ as “Input image”.

The path and filename for “Output image” should be manually assigned. Finally number of secondary images can be used to be aligned with the reference.

It is possible to choose 2D to 2D registration for 2D images and 3D to 3D registration for volumes. The degrees of freedom (DOF) may be assigned to 3 (Translation only), 6(Rigid body), 7(Global rescale), 9(Traditional) or 12 parameter model (Affine registration). For 2D to 2D registration only 3 parameter model (Rigid body) registration is available to choose.

3.3.4. FIRST

FIRST (FMRIB’s Integrated Registration and Segmentation Tool) is a tool for subcortical segmentation which is only available on command line. . The general form of FIRST command is “run_first_all -i <input> -o <output> [options]”.

It is important to notice that Input image must be a T₁ weighted image. FIRST needs model data in its library to perform subcortical segmentation. This model data can be downloaded and be installed from Debian Neuroscience Repository [25].

The first option is “-b” to specify that the input image is brain extracted. FIRST is able to perform subcortical segmentation on both original and brain extracted version of T₁ weighted images. Thus, in the case of having a brain extracted image as input it is necessary to use this option in the command line. Option “-m” choose the boundary correction method. Without using this option, the software package will choose the automatic boundary correction. However, it can be changed by choosing “FAST” which based on tissue classification, or “thresh” which uses a Gaussian intensity model to perform thresholding, and finally “none” to avoid boundary correction. Option “-s” will restrict the segmentation results. It makes it possible to select desirable subcortical structures to be segmented. A comma without space should be used to divide between selected structures. Name codes for different possible subcortical structures to choose are:

L_Accu	Left Accumbens area	R_Accu	Right Accumbens area
L_Amyg	Left Amygdala	R_Amyg	Right Amygdala
L_Caud	Left Caudate	R_Caud	Right Caudate
L_Hipp	Left Hippocampus	R_Hipp	Right Hippocampus
L_Late	Left Lateral ventricle	R_Late	Right Lateral ventricle
L_Pall	Left Pallidum	R_Pall	Right Pallidum
L_Puta	Left Putamen	R_Puta	Right Putamen
L_Thal	Left Thalamus	R_Thal	Right Thalamus
BrStem	Brainstem		

Table 12, Name codes for different possible subcortical structures in FIRST [32]

FIRST generates a volumetric image in NIFTI format “outputname_all_fast_firstseg.nii.gz” which shows the volumes of different subcortical structures (figure 3.13). It also produces a series of mesh images in “vtk” format (figure 3.14).

```
Run_first_all -i <input T1> -o <output> -b
```

Table 13, Command for generating images in FIRST

Figure 34, Volumes of different subcortical structures →

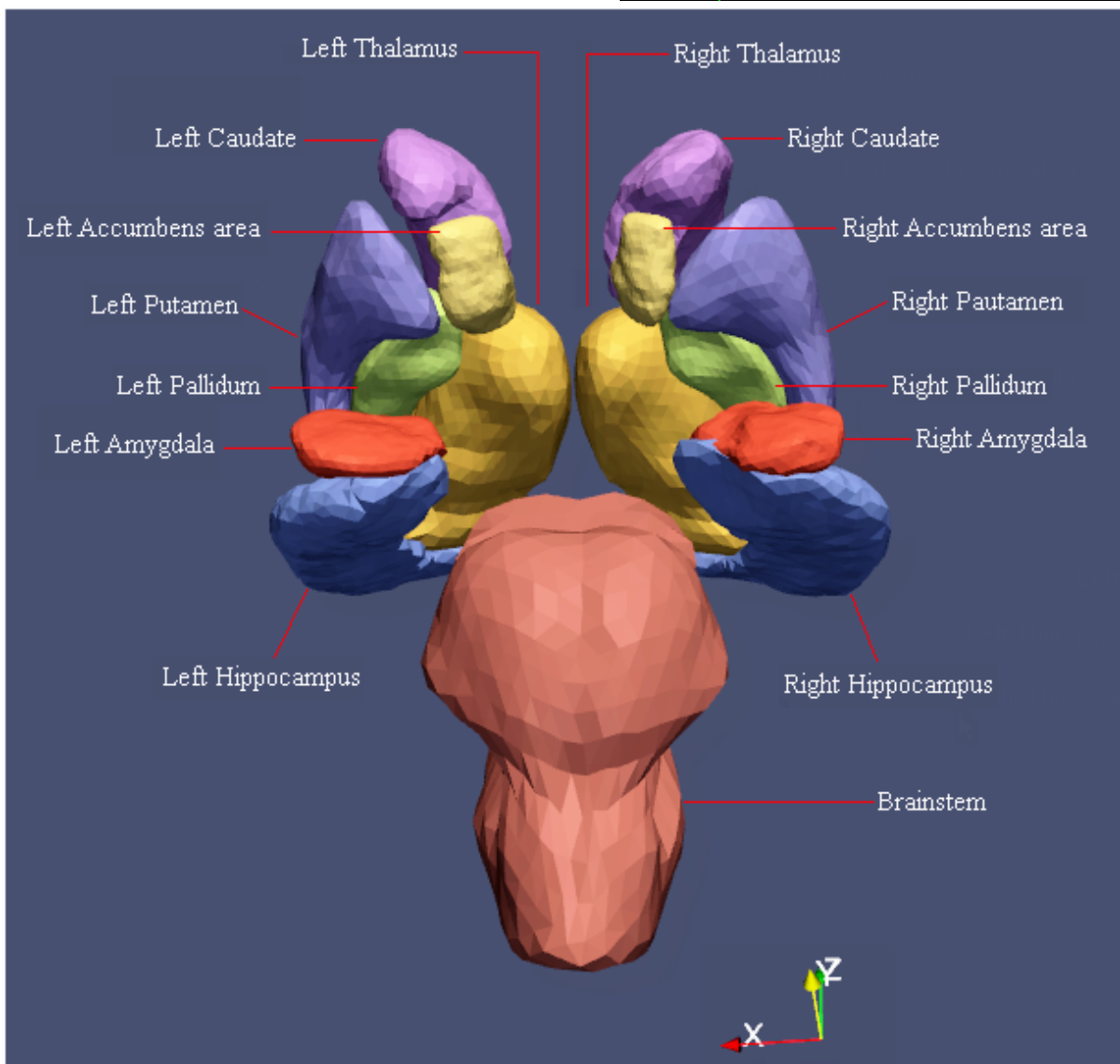
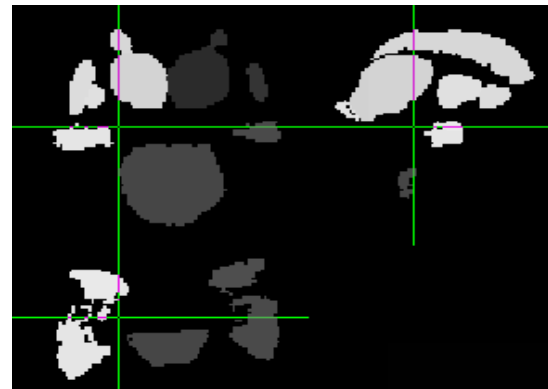


Figure 35, Surface meshes of different subcortical structures (this image created by Paraview [26] in coronal view)

A summary of FSL FIRST (FMRIB’s Integrated Registration and Segmentation Tool) shall be found in table 14.

FIRST	
-i	Input file must be a T ₁ weighted image.
-o	General name for all output files.
-b	Specifies that the input is a brain extracted image.
-m	For selecting the boundary correction method.
-s	Restricts the segmentation results.

Table 14, FSL FIRST option descriptions summary [32]

3.4. Tissue segmentation using FreeSurfer [28]

For running FreeSurfer one can use both graphical user interface and command line. However, using command line in Linux terminal is more recommended. “recon-all” can be used for the whole brain segmentation which comprises volume based and surface based segmentations. It is important to use T₁ weighted image as input for “recon-all” command. It has 31 stages which Started with motion correction, non uniform intensity normalization, an affine registration to Talairach atlases [27], another intensity normalization and finally brain extraction. These 5 steps can be separated from the rest of stages by adding “autorecon1” at the end of command line.

```
recon-all -subject <specify an name> -i <a T1 weighted image > -atuorecon1
```

Table 15, Command for generating registration and brain extraction in FreeSurfer

“autorecon2” will continue until 23th stage which illustrated in table 16. It will perform the whole brain segmentation in both volume based and surface based and will extract all the structures inside the brain. However, the difference between FreeSurfer and two other studied software packages is that it will create a set of folders in “Subject” with the same name that user specified. All the results for volumetric based segmentation are collected in “mri” folder in “aseg.mgz” file which contains all the structures. “autorecon2” also creates a text file “aseg.auto_noCCseg.label_intensities.txt” consist of intensities for all structures in “aseg.mgz” (Table 16). By using this table one can extract different structures from “aseg.mgz”. Although there are individual images for white matter “wm.mgz”, bias corrected T₁ weighted image, brain extracted image in “norm.mgz”, brain mask in “brainmask.mgz” and etc. but it is recommended to use “aseg.mgz” and extracting all desired tissues considering different intensities in table 17. Because other images are not binary and for instance there is a wide intensity variation in “wm.mgz”.

The “aseg.mgz” image is illustrated in figure 36.

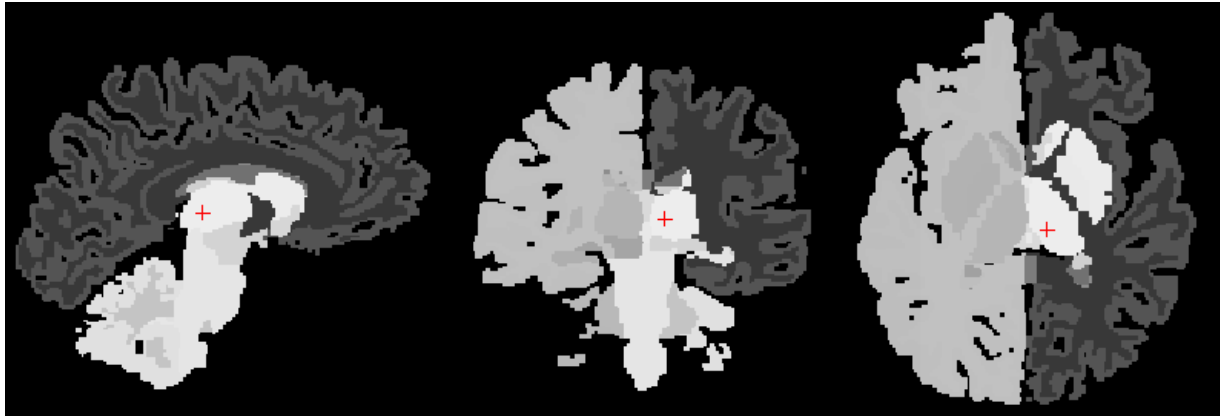


Figure 36, Different extracted tissues and structures in “aseg.mgz”, planes: sagittal (left), coronal (middle), transverse (right)

```
recon-all -subject <specify an name> -i <a T1 weighted image > -atuocon1 -autorecon2
```

Table 16, Command for generating “aseg.mgz”

Intensity	Extracted tissue name	Intensity	Extracted tissue name
1	Left_Cerebral_Exterior	42	Right_Cerebral_Cortex
2	Left_Cerebral_White_Matter	43	Right_Lateral_Ventricle
3	Left_Cerebral_Cortex	44	Right_Inf_Lat_Vent
4	Left_Lateral_Ventricle	46	Right_Cerebellum_White_Matter
5	Left_Inf_Lat_Vent	47	Right_Cerebellum_Cortex
7	Left_Cerebellum_White_Matter	48	Right_Thalamus
8	Left_Cerebellum_Cortex	49	Right_Thalamus_Proper
9	Left_Thalamus	50	Right_Caudate
10	Left_Thalamus_Proper	51	Right_Putamen
11	Left_Cerebral_White_Matter	52	Right_Pallidum
12	Left_Putamen	53	Right_Hippocampus
13	Left_Pallidum	54	Right_Amygdala
14	Third_Ventricle	58	Right_Accumbens_area
15	Fourth_Ventricle	60	Right_VentralDC
16	Brain_Stem	72	Fifth_Ventricle
17	Left_Hippocampus	75	Left_Lateral_Ventricles
18	Left_Amygdala	76	Right_Lateral_Ventricles
24	CSF	77	WM_hypointensities
26	Left_Accumbens_area	78	Left_WM_hypointensities
28	Left_VentralDC	79	Right_WM_hypointensities
40	Right_Cerebral_Exterior	80	non_WM_hypointensities
41	Right_Cerebral_White_Matter	81	Left_non_WM_hypointensities
		82	Right_non_WM_hypointensitie

Table 17, Name codes and intensities for different possible extracted structures using FreeSurfer

As it mentioned before FreeSurfer also performs surface based segmentation. It can generate the white matter surface and pial surface and the thickness of these two surfaces which is the cerebral cortex made of gery matter. The results of surface based segmentation are in the surf folder. Right and left white matter surfaces and pial surfaces can be found. The resulted image is illustrated in figure 37.

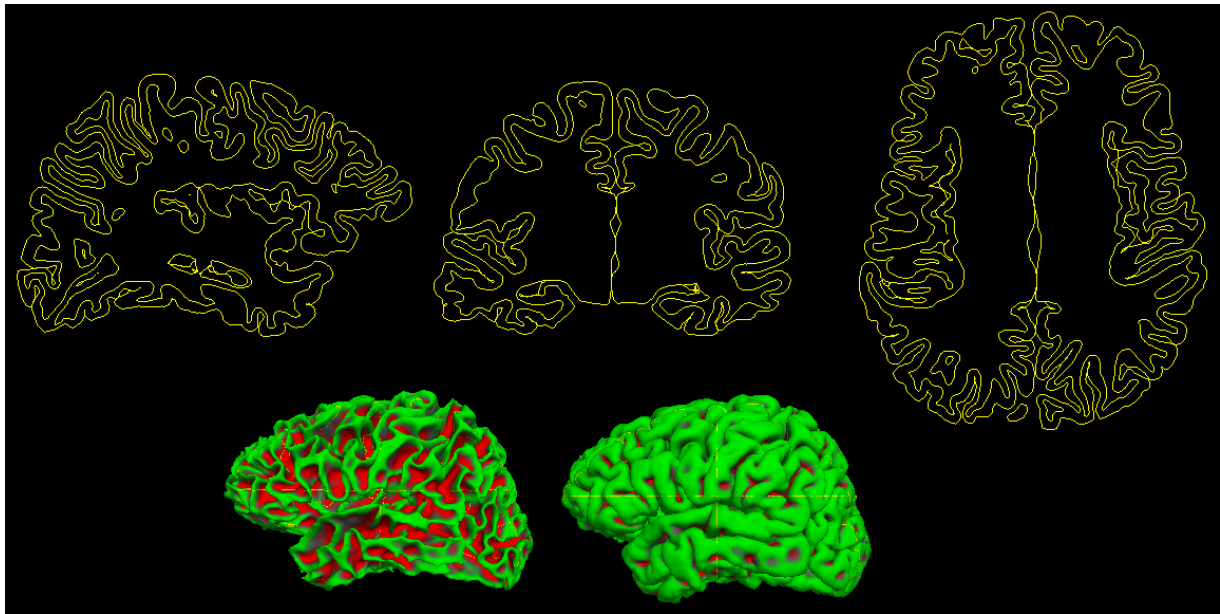


Figure 37, White matter and pial surfaces, planes: sagittal (up left), coronal (up middle), transverse (up right) white matter surface (bottom left), pial surface (bottom right)

Acquiring these results may take around 9 hours using “-autorecon1” and “-autorecon2”. However, as it mentioned before, there are 31 stages with option “-all”. It may take 20-40 hours to finish the whole brain tissue segmentation. It can extract more individual images like “ribbon.mgz” which contains binary information of just white and grey matter. There is also an image of just grey matter in “aparc.a2009s+aseg.mgz” but it is not a binary image. However, for acquiring “aseg.mgz” it is enough to just use “-autorecon1” and “-autorecon2” options. List of all 31 stages for “recon-all” using option “-all” can be found in table 18.



Figure 38, White matter in “wm.mgz” (a), planes: sagittal (left), coronal (middle), transverse (right), grey matter in “aparc.a2009s+aseg.mgz” (b), planes: sagittal (left), coronal (middle), transverse (right)

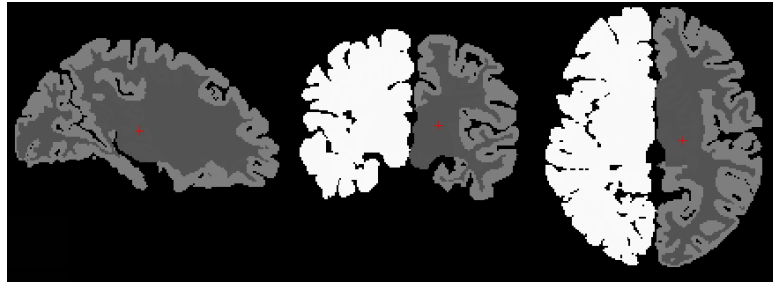


Figure 39, White and grey matter in “ribbon.mgz”, planes: sagittal (left), coronal (middle), transverse (right)

	No.	Stage
-autorecon1	1	Motion Correction and Conform
	2	NU (Non-Uniform intensity normalization)
	3	Talairach transform computation
	4	Intensity Normalization 1
	5	Skull Strip
-autorecon2	6	EM Register (linear volumetric registration)
	7	CA Intensity Normalization
	8	CA Non-linear Volumetric Registration
	9	Remove Neck
	10	LTA with Skull
	11	CA Label (Volumetric Labeling, ie Aseg) and Statistics
	12	Intensity Normalization 2 (start here for control points)
	13	White matter segmentation
	14	Edit WM With ASeg
	15	Fill (start here for wm edits)
	16	Tessellation (begins per-hemisphere operations)
	17	Smooth1
	18	Inflate1
	19	QSphere
	20	Automatic Topology Fixer
	21	Final Surfs (start here for brain edits for pial surf)
	22	Smooth2
	23	Inflate2
-autorecon3	24	Spherical Mapping
	25	Spherical Registration
	26	Spherical Registration, Contralateral hemisphere
	27	Map average curvature to subject
	28	Cortical Parcellation - Desikan_Killiany and Christophe (Labeling)
	29	Cortical Parcellation Statistics
	30	Cortical Ribbon Mask
	31	Cortical Parcellation mapping to Aseg

Table 18, Different stages of tissue segmentation in FreeSurfer [28]

As it has showed in figure 36, segmentation method in FreeSurfer is different from FSL and SPM. Especially for subcortical structures it won't produce individual images like FSL. However, as it mentioned before by using the intensities for different structures in table 17, one can extract different tissues and structures from "aseg.mgz".

One of useful tools in FreeSurfer is "mri_convert" that can be used for image conversion. During the work with MR images, it is very relevant to be forced to convert between different formats. The reason is different software packages work with different image formats. For instance when I got my own MR images from my brain using "PHILIPS" scanner in Sahlgrenska Hospital, they were in "DICOM" [29] format. None of these software packages work with "DICOM" format.

The general format of command line for image conversion in FreeSurfer is "mri_convert [options] <input image> <output image>".

The list of options can be found in FreeSurfer wiki [30]. However, different possible image format conversions are listed in table 19.

Format	Description	Format	Description
cor	MGH-NMR COR format (deprecated)	dicom	generic DICOM Format (input only)
mgh	MGH-NMR format	siemens_dicom	Siemens DICOM Format (input only)
mgz	MGH-NMR gzipped (compressed) mgh format	afni	AFNI format
minc	MNI's Medical Imaging NetCDF format (output may not work)	brik	same as afni
analyze	3D analyze (same as spm)	bshort	MGH-NMR bshort format
analyze4d	4D analyze	bfloat	MGH-NMR bfloat format
spm	SPM Analyze format (same as analyze and analyze3d)	sdt	Varian
ge	GE Genesis format (input only)	outline	MGH-NMR Outline format
gelx	GE LX (input only)	otl	same as outline
lx	same as gelx	gdf	GDF volume (requires image stem for output; use -gis)
ximg	GE XIMG variant (input only)	nifti1	NIfTI-1 volume (separate image and header files)
siemens	Siemens IMA (input only)	nii	NIfTI-1 volume (single file), if input/output has extension .nii.gz, then compressed is used

Table 19, Different possible image formats conversion using FreeSurfer [30]

Although "mri_convert" in FreeSurfer is a sophisticated tool for image conversion but it is not useful for some of formats. For instance, FreeSurfer cannot convert "DICOM2" [29] too "nii" [31]. For this conversion "MRICron" [32] software package can be used.

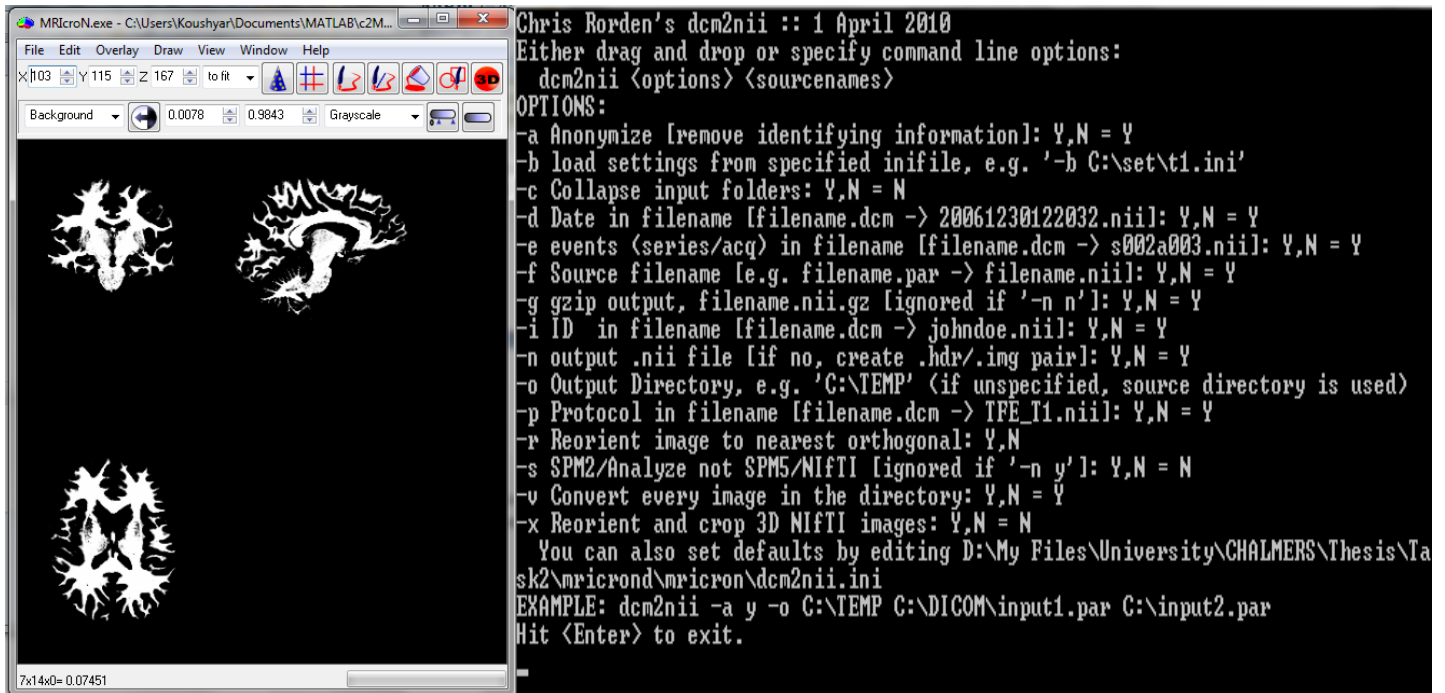


Figure 40, Screen snapshot: MRIcron viewer user interface (left), MRIcron converter user interface (right)

The other important image format can be “vtk” [33]. Again FreeSurfer is not going to be useful for conversion to this image format. “ITKsnap” [34] is a useful software package for converting from “nii” to “vtk”.

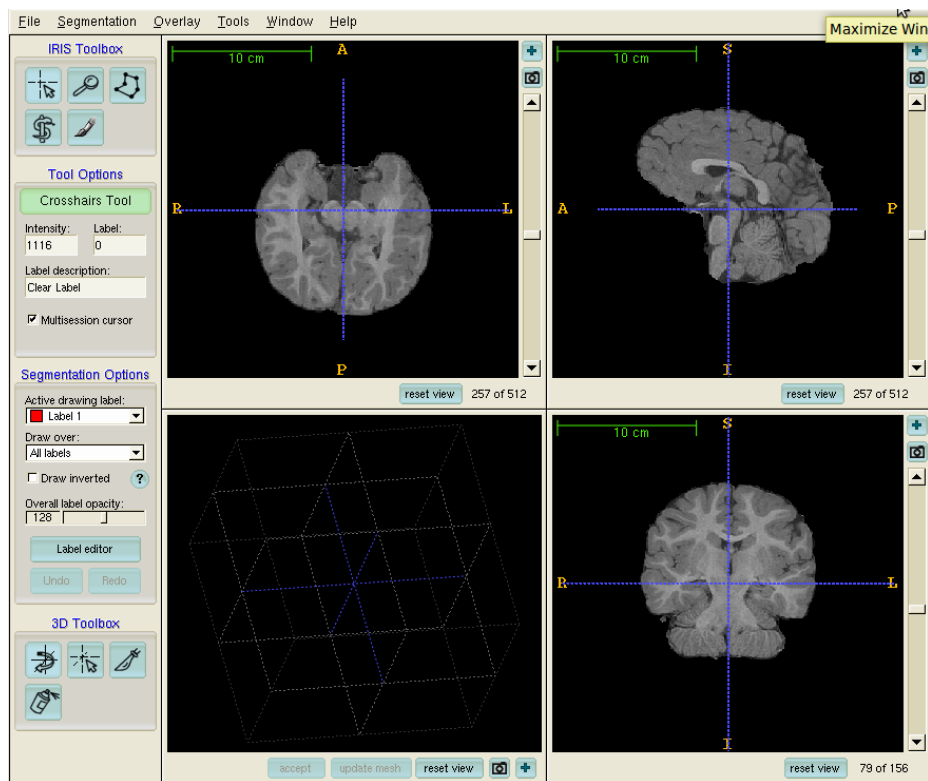


Figure 41, Screen snapshot from ITKsnap user interface

Chapter 4

4. Evaluation and Comparison between performances of three software packages

This chapter explains the evaluation method which used for evaluating the results of these three software packages and then using these evaluations to perform a comparison between them. Finally it will represent the results of this comparison.

4.1. Evaluation method

To evaluate the performances of these three software packages a data set consists of 18 Brainweb [35] T_1 weighted phantoms were used. These phantoms were generated with slice thickness of 1mm ($1\text{mm} \times 1\text{mm} \times 1\text{mm}$) and echo time of 10ms. Six different noise levels (0%, 1%, 3%, 5%, 7% and 9%) were used and for each noise level three various RF inhomogeneity values (0%, 20%, 40%) were employed. The ground truth of white matter, grey matter and cerebrospinal fluid for these phantoms were provided from Brainweb. However, the ground truth for subcortical structures was inaccessible. Therefore, there is no evaluation of subcortical structures in this chapter.

All 18 phantoms were used in all three software packages to obtain the segmentation results for three tissue classes (WM, GM and CSF) using the methods that explained in previous chapter. To evaluate the segmentation a voxel by voxel comparison between segmented images and the ground truth performed using 3dOverlap command line from AFNI software package [41] and MATLAB together with Jimmy Shen's library [36]. This comparison showed the number of voxels as true positives, false positives, true negatives and false negatives.

True positive	Classification of a voxel as tissue when it is tissue
False positive	Classification of a voxel as tissue when it is background
True negative	Classification of a voxel as background when it is background
False negative	Classification of a voxel as background when it is tissue

Table 20, Definition of true and false classification

It is possible to calculate the sensitivity and specificity of the segmentation performance from these classification parameters. Sensitivity or recall rate shows the rate of true classification. Regarding to this definition by increasing the sensitivity the number of missed true tissue voxels will decrease. However, the drawback is there will be more voxels classified as tissue when they were actually background. High sensitivity is considered good when it is important to preserve all tissue pixels. Sensitivity can be calculated as follow:

$$sensitivity = \frac{\text{number of true positives}}{\text{number of true positives} + \text{number of false negatives}}$$

Specificity or precision on the other hand is a measure of background voxels where correctly identified as background. Thus, by increasing the specificity the number of false positive (which means classification of a voxel as tissue when it is background) will decrease but the drawback is there some tissue voxels will wrongly classified as background. However, specificity is important to preserve the background pixels. Specificity can be calculated as follow:

$$specificity = \frac{\text{number of true negatives}}{\text{number of true negatives} + \text{number of false positives}}$$

Sensitivity and specificity were calculated for all three software packages for every noise level and RF inhomogeneity value. However, to evaluate the performance of the software packages it is important to have a single measure. Misclassification rate (MCR) [40], [61] can be calculated from sensitivity and specificity using priori probabilities of voxels. In this problem there are two cases: tissue or background. Sensitivity is representing true classification rate of tissue voxels and specificity represents the rate of true classification for background voxels. A random choice of a voxel can have two outcomes: tissue or background. Thus misclassification rate can be calculated using this formula:

$$MCR = P_1 \times (1 - sensitivity) + P_2 \times (1 - specificity),$$

where P_1 is the priori probability of a voxel to be background and P_2 is the priori probability of a voxel to be tissue. P_1 is the weight for $(1 - sensitivity)$ which means whatever is not the true classification rate of tissue voxels and P_2 is the weight for $(1 - specificity)$ which means whatever is not the true classification rate of background voxels. MCR were calculated for all three software packages for every noise level and RF inhomogeneity value. Finally the average value of sensitivity, specificity and MCR in each tissue class will represent the performance of each software package for segmenting each of these three tissue classes (WM, GM, CSF).

4.1.1. Results

To compare the performance of different software packages, segmentation of three tissue classes (WM, GM and CSF) performed over all 18 phantoms then for each tissue type sensitivity, specificity and MCR calculated. The results are illustrated in a graphical format to show the quality of segmentation for various amounts of noise and RF inhomogeneity.

4.1.1.1. SPM8

4.1.1.1.1. White matter

As it mentioned before sensitivity shows the rate of true classification. Thus, it is good to start with this measure. The results of sensitivity for white matter is getting better (closer to 1) for more noise and less RF inhomogeneity. However, as it has shown in figure 42, the difference between various RF inhomogeneity values is negligible. Normally one expects better results from less noise level but reviewing table 21 shows that the best outcome were from 9% noise level. The same performance for SPM5 noticed in Ferreira da Silva [39] publication and another review [40] as well. The reason is this software package is designed to work with noisy images as long as practical images from patients are always along with noise.

Sensitivity – white matter							
SPM8		Noise (%)					
		0	1	3	5	7	9
RF	0	0.7120	0.8996	0.9661	0.9596	0.9836	0.9910
	20	0.7105	0.8992	0.9564	0.9537	0.9820	0.9885
	40	0.7133	0.8874	0.9606	0.9496	0.9745	0.9851

Table 21, Sensitivity of segmentation for white matter in SPM8

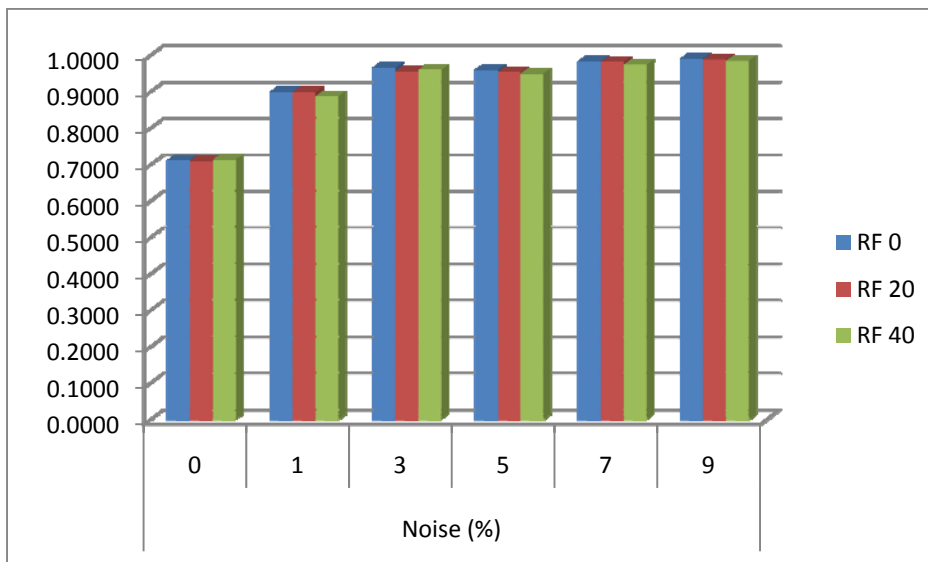


Figure 42, Sensitivity of segmentation for white matter in SPM8

Regarding to specificity definition in section 4.1, high values for this measure gives better classification rate of background voxels. The results of specificity for white matter shows high value of specificity (close to 1) for less noise level, and low value for high noise level can be observed. The difference between RF inhomogeneity values is more dominant in specificity. Classification rate is slightly better for lower values of RF inhomogeneity. The results are illustrated in table 22 and figure 43.

Specificity – white matter							
SPM8		Noise (%)					
		0	1	3	5	7	9
RF	0	0.99981	0.99958	0.98581	0.97307	0.93947	0.91752
	20	0.99982	0.99959	0.98995	0.97701	0.94220	0.92270
	40	0.99981	0.99963	0.98844	0.97890	0.95019	0.92797

Table 22, Specificity of segmentation for white matter in SPM8

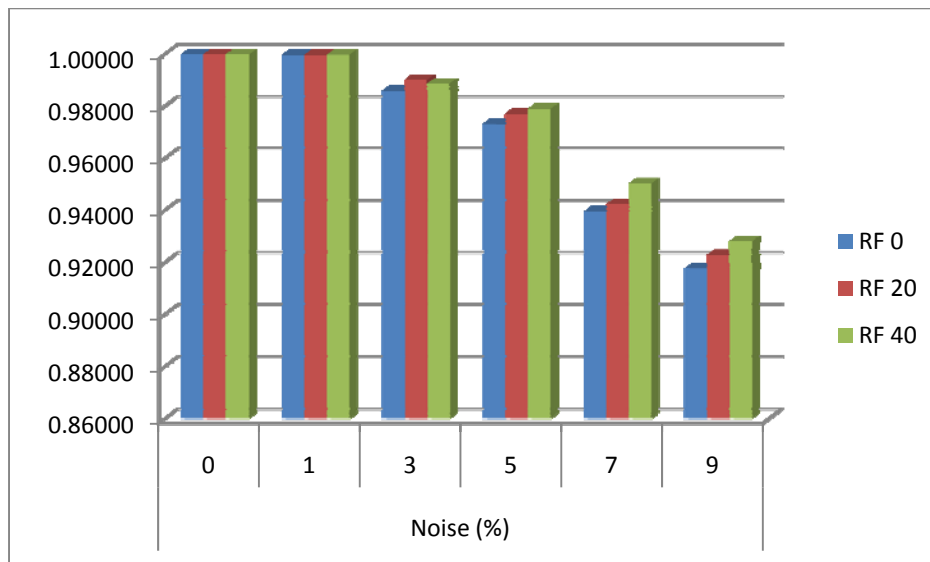


Figure 43, Specificity of segmentation for white matter in SPM8

MCR shows the highest error rate without any noise. As it is illustrated in figure 44 the misclassification rate is around 26% for zero noise and by increasing noise level the error rate will become lower and reach to the lowest MCR (around 2%) for 9% of noise and RF inhomogeneity of zero. However, RF inhomogeneity value doesn't have a significant influence.

MCR – white matter							
SPM8		Noise (%)					
		0	1	3	5	7	9
RF	0	0.2631	0.0895	0.0313	0.0385	0.0240	0.0232
	20	0.2645	0.0898	0.0394	0.0432	0.0248	0.0239
	40	0.2619	0.1005	0.0359	0.0465	0.0295	0.0254

Table 23, Misclassification rate of segmentation for white matter in SPM8

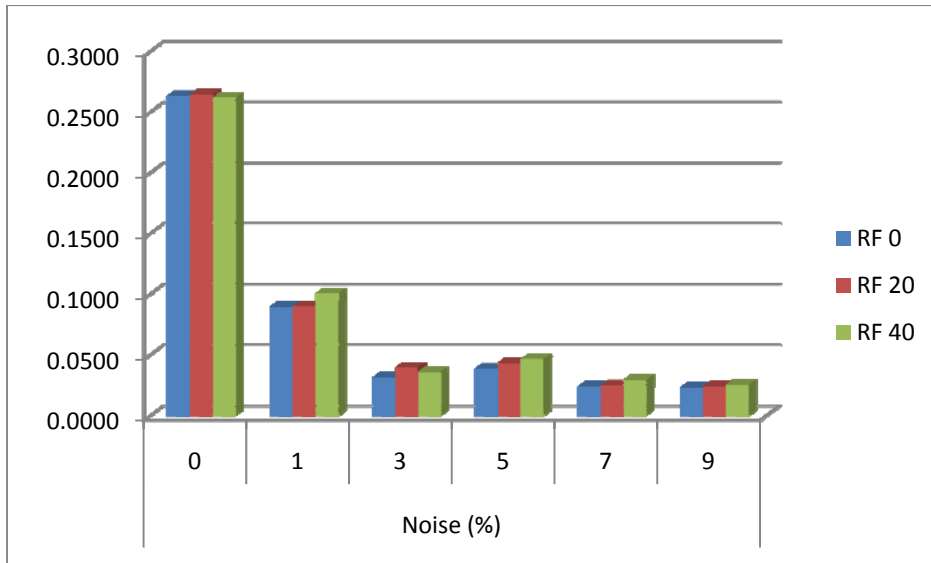


Figure 44, Misclassification rate of segmentation for white matter in SPM8

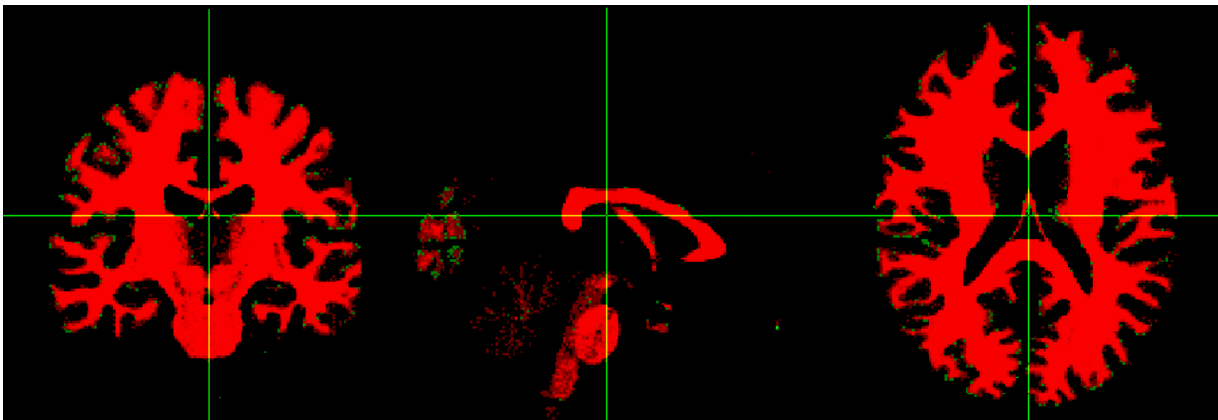


Figure 45, Segmented white matter using SPM8 (red), Brainweb phantom ground truth (green), planes: sagittal (left), coronal (middle), transverse (right)

4.1.1.1.2. Grey matter

The results of sensitivity for grey matter surprisingly showed better results for no noise. Although finally by reaching to 9% of noise level the sensitivity starts to get better but the results with no noise still had the best sensitivity. The RF inhomogeneity had not a noticeable effect.

Sensitivity – grey matter							
SPM8		Noise (%)					
		0	1	3	5	7	9
RF	0	0.9623	0.9420	0.9434	0.9278	0.9301	0.9382
	20	0.9602	0.9400	0.9345	0.9215	0.9313	0.9390
	40	0.9586	0.9416	0.9373	0.9179	0.9235	0.9340

Table 24, Sensitivity of segmentation for grey matter in SPM8

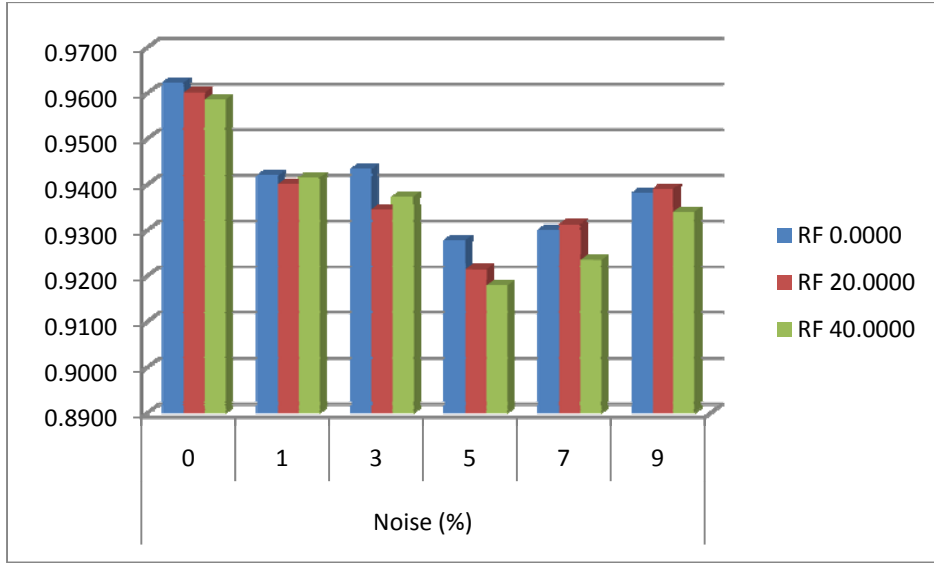


Figure 46, Sensitivity of segmentation for grey matter in SPM8

The results of specificity, again, showed higher values for less noise levels and lower values for more noise levels. The RF inhomogeneity values still had not a significant influence at the results. The best specificity is for 5% of noise level. However, the overall results showed a good specificity for grey matter.

Specificity – grey matter							
SPM8	Noise (%)						
	0	1	3	5	7	9	
RF	0	0.9600	0.9612	0.9599	0.9664	0.9541	0.9423
	20	0.9601	0.9623	0.9579	0.9686	0.9549	0.9427
	40	0.9605	0.9612	0.9579	0.9693	0.9587	0.9462

Table 25, Specificity of segmentation for grey matter in SPM8

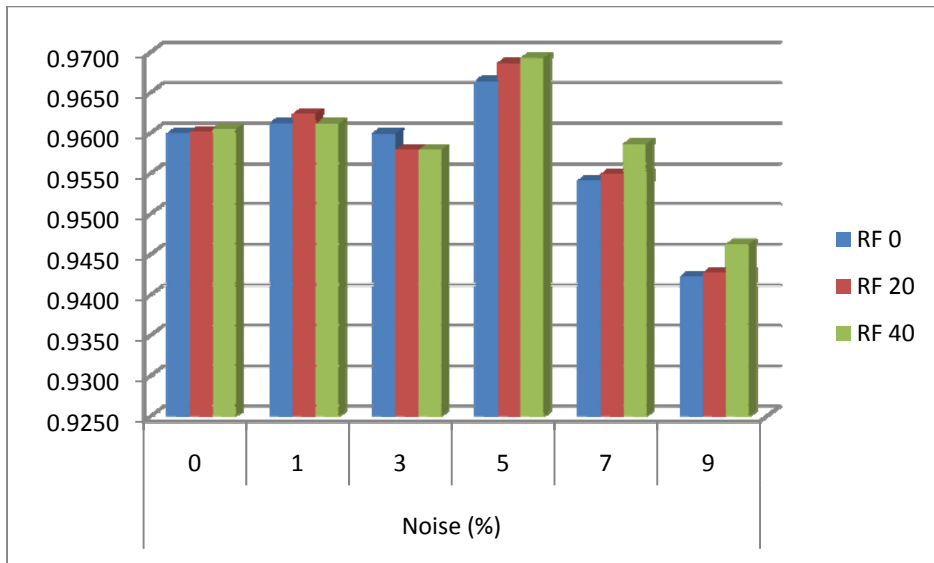


Figure 47, Specificity of segmentation for grey matter in SPM8

Misclassification rate for grey matter showed the lowest error around 3% for 0% of noise level and 0% of RF inhomogeneity value. The results are illustrated in table 26 and figure 48.

MCR – grey matter							
SPM8		Noise (%)					
		0	1	3	5	7	9
RF	0	0.0382	0.0541	0.0532	0.0646	0.0649	0.0609
	20	0.0398	0.0555	0.0607	0.0695	0.0638	0.0602
	40	0.0410	0.0544	0.0585	0.0722	0.0694	0.0634

Table 26, Misclassification rate of segmentation for grey matter in SPM8

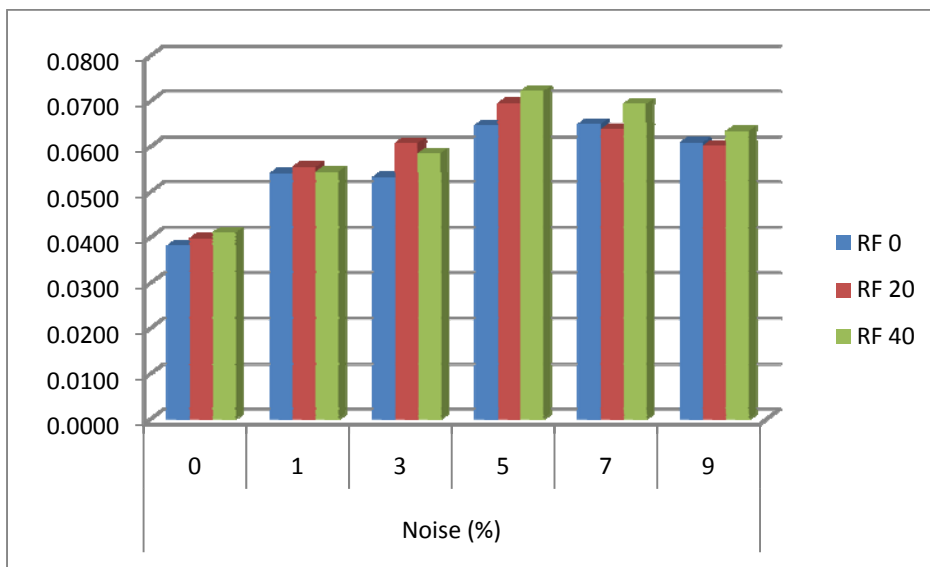


Figure 48, Misclassification rate of segmentation for grey matter in SPM8

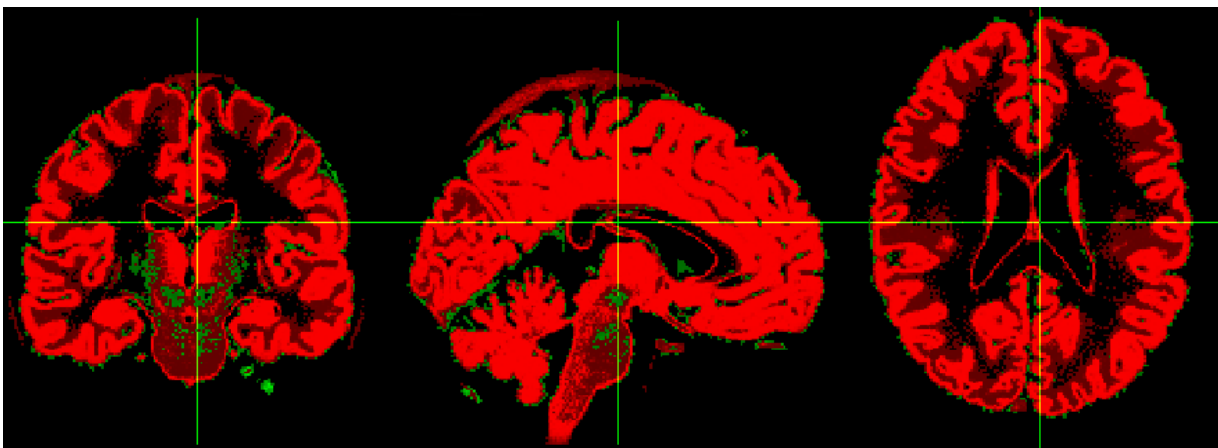


Figure 49, Segmented grey matter using SPM8 (red), Brainweb phantom ground truth (green), planes: sagittal (left), coronal (middle), transverse (right)

4.1.1.1.3. CSF

The sensitivity for CSF had its best result (97%) for 1% of noise level and the worst result (85%) for 9% of noise level. Thus, as it has illustrated in table 27 and figure 50 the best results are in lower noise levels and it is getting worse with increasing noise level. RF inhomogeneity effect is not significant.

Sensitivity – CSF							
SPM8		Noise (%)					
		0	1	3	5	7	9
RF	0	0.9383	0.9761	0.9591	0.9187	0.8875	0.8585
	20	0.9528	0.9784	0.9644	0.9320	0.8961	0.8586
	40	0.9633	0.9772	0.9625	0.9401	0.8852	0.8655

Table 27, Sensitivity of segmentation for CSF in SPM8

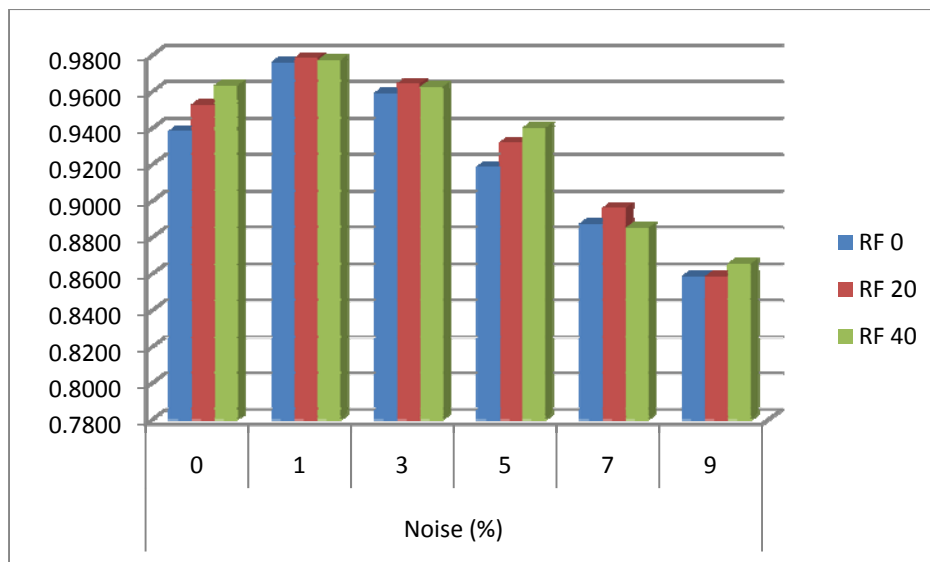


Figure 50, Sensitivity of segmentation for CSF in SPM8

Specificity on the other hand showed the highest values for no noise and lowest values for 9% of noise level. It means the background voxels were better classified by SPM8 when there was no noise. As it is shown in figure 51, changes in RF inhomogeneity values in specificity were more effective than they were for sensitivity.

Specificity – CSF							
SPM8		Noise (%)					
		0	1	3	5	7	9
RF	0	0.9355	0.9181	0.9182	0.9198	0.9067	0.8985
	20	0.9332	0.9158	0.9143	0.9185	0.9052	0.8990
	40	0.9321	0.9186	0.9154	0.9183	0.9156	0.8992

Table 28, Specificity of segmentation for CSF in SPM8

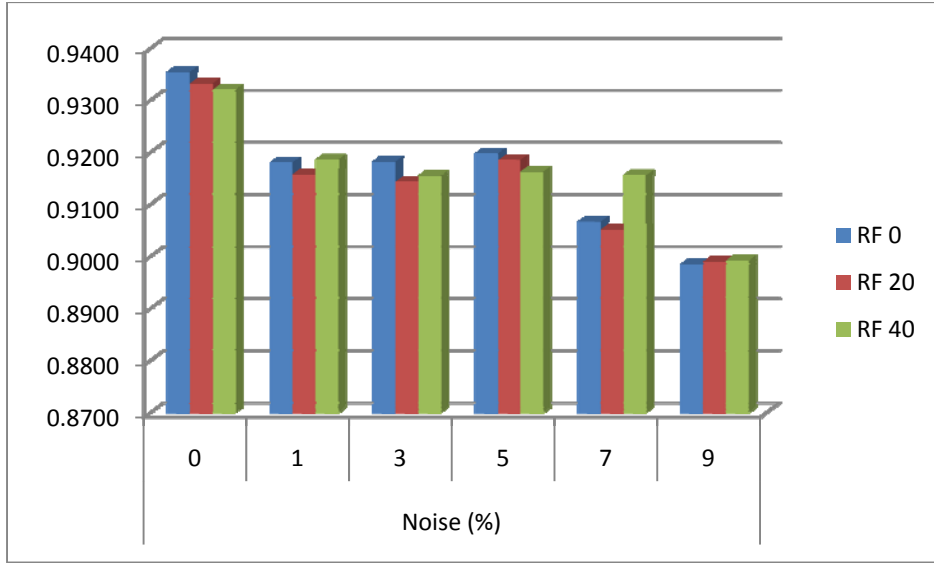


Figure 51, Specificity of segmentation for CSF in SPM8

Misclassification rate for CSF showed the lowest error around 3% for 1% of noise level and 20% of RF inhomogeneity. By increasing noise level the error rate will become larger around 13%. The results are illustrated in table 29 and figure 51.

MCR – CSF							
SPM8	Noise (%)						
	0	1	3	5	7	9	
RF	0	0.0621	0.0331	0.0474	0.0811	0.1094	0.1348
	20	0.0500	0.0317	0.0437	0.0699	0.1024	0.1347
	40	0.0412	0.0321	0.0451	0.0637	0.1101	0.1289

Table 29, Misclassification rate of segmentation for CSF in SPM8

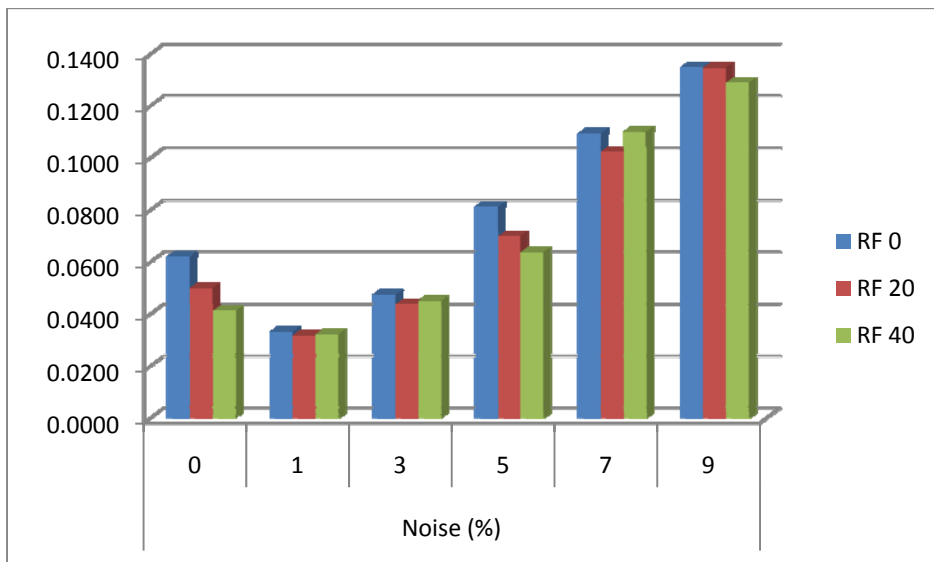


Figure 52, Misclassification rate of segmentation for CSF in SPM8

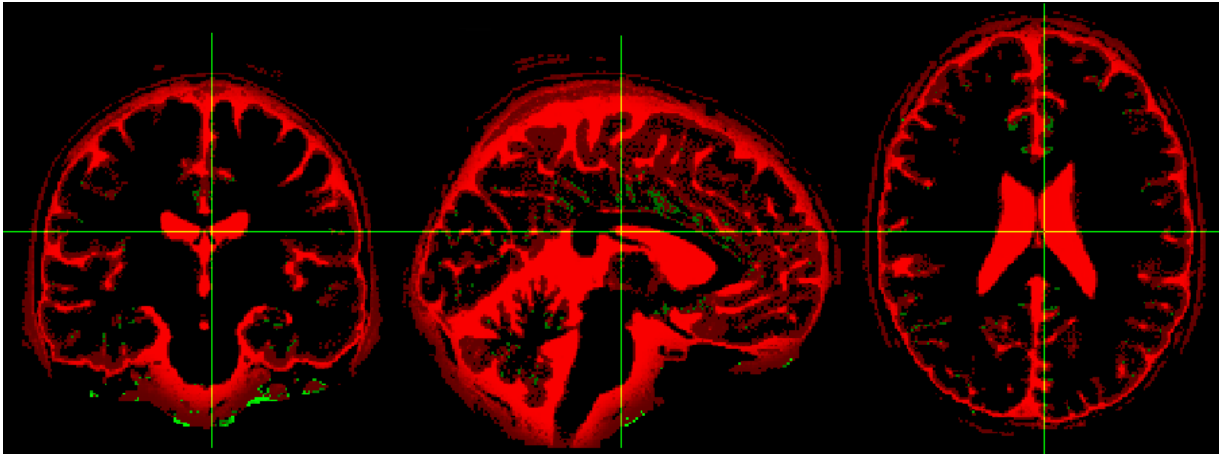


Figure 53, Segmented CSF using SPM8 (red), Brainweb phantom ground truth (green), planes: sagittal (left), coronal (middle), transverse (right)

The average values of sensitivity, specificity and MCR for each tissue type used for an overall evaluation of SPM8 performance for tissue segmentation. The results for all tissue types are very good and the misclassification rate for each tissue type shows a low value (less than 10% of error).

SPM8	Sensitivity	Specificity	MCR
WM	0.91515	0.97175	0.0808
GM	0.93794	0.95801	0.0580
CSF	0.92857	0.91555	0.0734

Table 30, Overall evaluation of tissue segmentation using SPM8

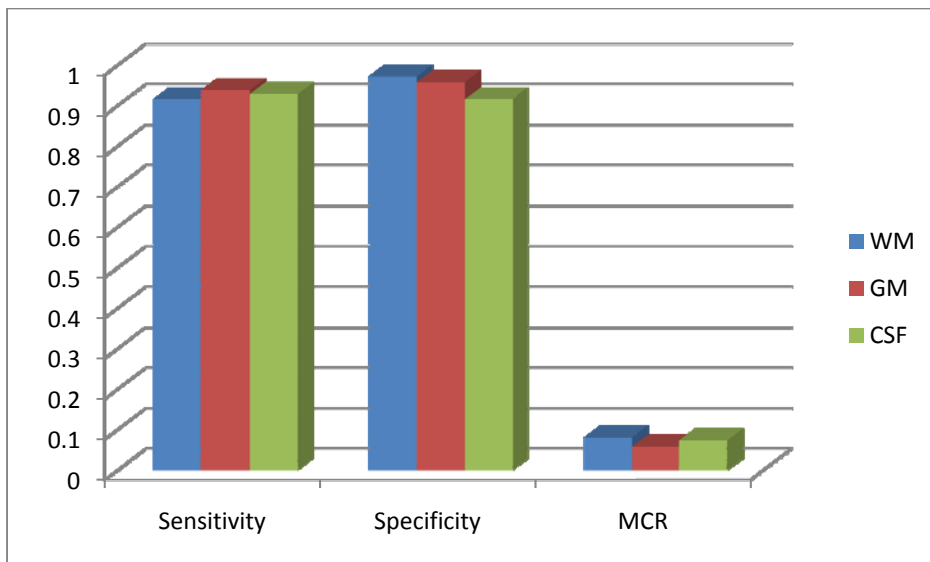


Figure 54, Overall evaluation of tissue segmentation using SPM8

4.1.1.2. FSL

4.1.1.2.1. White matter

The sensitivity of tissue classification for white matter in FSL is getting better (around 77%) by increasing noise level. However, the value of RF inhomogeneity does not have a significant effect on sensitivity.

Sensitivity – white matter							
FSL		Noise (%)					
		0	1	3	5	7	9
RF	0	0.47736	0.62513	0.73657	0.76508	0.77815	0.78137
	20	0.62901	0.65702	0.73080	0.76104	0.77437	0.77532
	40	0.63143	0.65243	0.71857	0.75030	0.76752	0.77205

Table 31, Sensitivity of segmentation for white matter in FSL

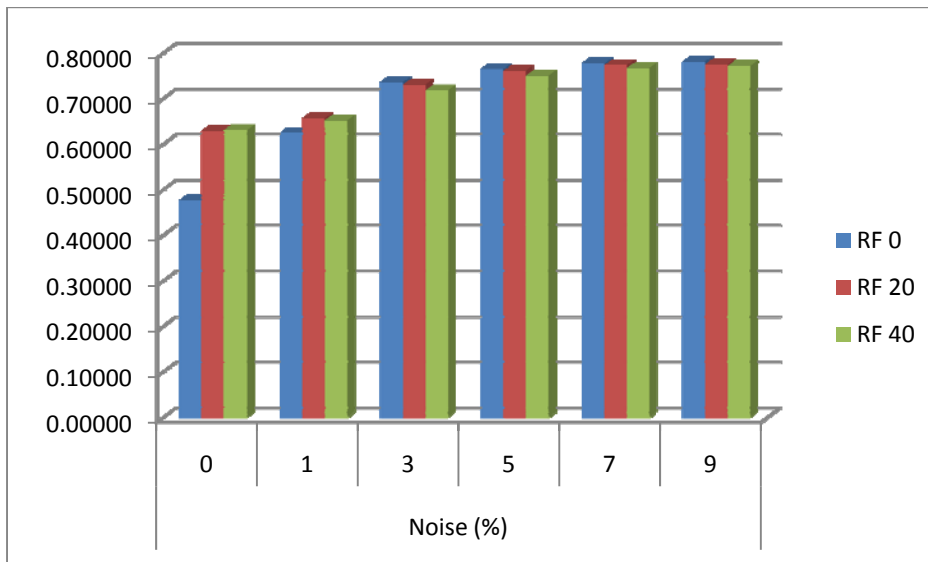


Figure 55, Sensitivity of segmentation for white matter in FSL

On the other hand, specificity shows a very good background classification with less noise level. By increasing noise level, specificity will decrease. RF inhomogeneity just has a small influence on specificity on 9% of noise level.

Specificity – white matter							
FSL		Noise (%)					
		0	1	3	5	7	9
RF	0	1.00000	1.00000	1.00000	0.99993	0.99958	0.99885
	20	1.00000	1.00000	1.00000	0.99995	0.99967	0.99914
	40	1.00000	1.00000	1.00000	0.99996	0.99972	0.99924

Table 32, Specificity of segmentation for white matter in FSL

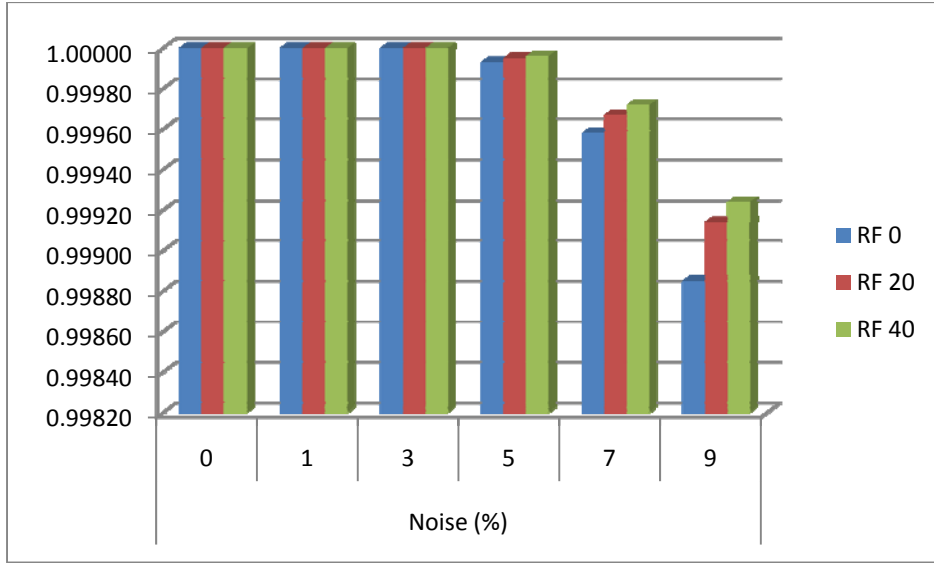


Figure 56, Specificity of segmentation for white matter in FSL

Misclassification rate for white matter showed the lowest error around 19% for 9% of noise level and RF inhomogeneity value of zero. By decreasing noise level the error rate will become larger around 34%. However, the worst error rate is from 0% of noise level and RF inhomogeneity value of zero. Results are illustrated in table 33 and figure 57.

MCR – white matter							
FSL	Noise (%)						
	0	1	3	5	7	9	
RF	0	0.49241	0.34647	0.23992	0.21313	0.20089	0.19782
	20	0.34271	0.31567	0.24536	0.21692	0.20442	0.20348
	40	0.34037	0.32009	0.25693	0.22699	0.21083	0.20654

Table 33, Misclassification rate of segmentation for white matter in FSL

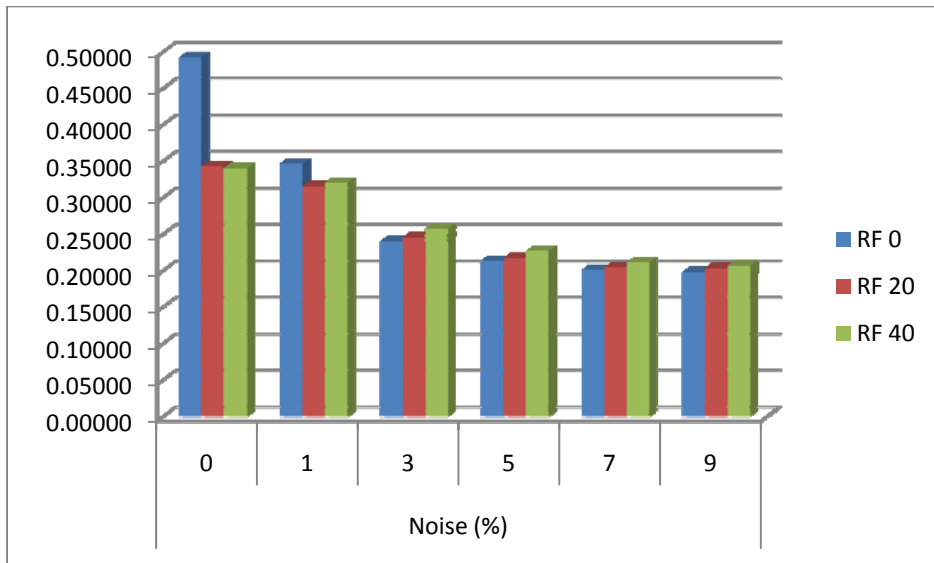


Figure 57, Misclassification rate of segmentation for white matter in FSL

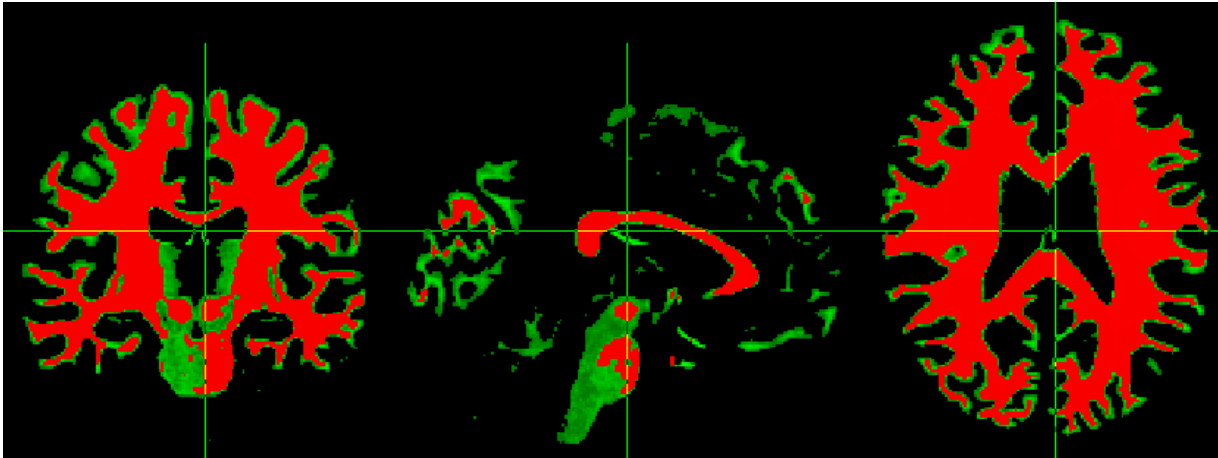


Figure 58, Segmented white matter using FSL (red), Brainweb phantom ground truth (green), planes: sagittal (left), coronal (middle), transverse (right)

4.1.1.2.2. Grey matter

The sensitivity value for classification of grey matter using FSL is the opposite of white matter. Therefore, by increasing noise level the sensitivity will decrease. However, changes in RF inhomogeneity had not a significant effect.

Sensitivity – grey matter							
FSL	Noise (%)						
	0	1	3	5	7	9	
RF	0	0.83261	0.76266	0.68421	0.67745	0.68375	0.69301
	20	0.75447	0.73547	0.68632	0.67839	0.68546	0.69652
	40	0.75089	0.73619	0.69193	0.67311	0.68099	0.68931

Table 34, Sensitivity of segmentation for grey matter in FSL

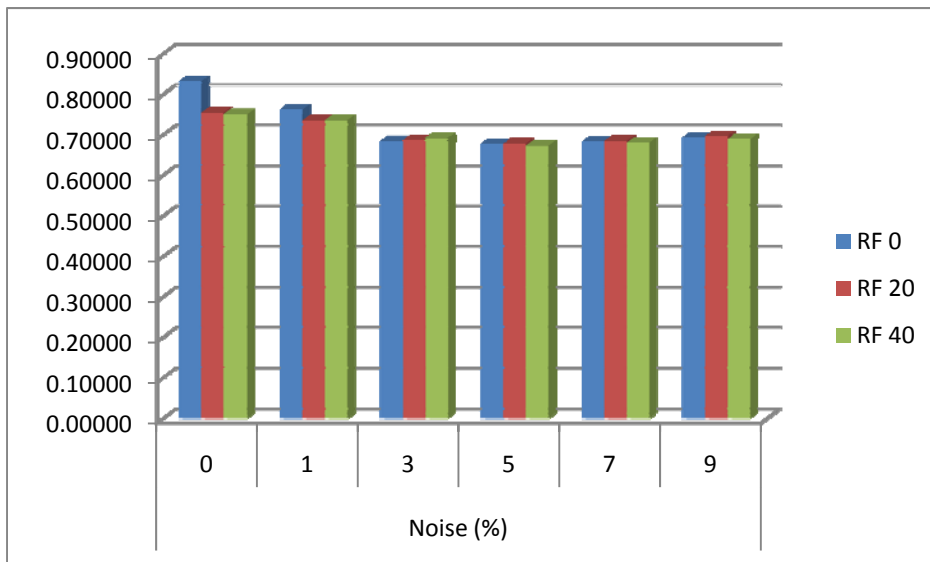


Figure 59, Sensitivity of segmentation for grey matter in FSL

The specificity of grey matter segmentation is almost the same and close to one for all noise levels and RF inhomogeneity values except for zero noise and zero RF which has slightly lower value of specificity.

Specificity – grey matter							
FSL		Noise (%)					
		0	1	3	5	7	9
RF	0	0.9903	0.9981	0.9988	0.9988	0.9987	0.9985
	20	0.9983	0.9985	0.9988	0.9989	0.9988	0.9986
	40	0.9984	0.9985	0.9988	0.9990	0.9990	0.9987

Table 35, Specificity of segmentation for grey matter in FSL

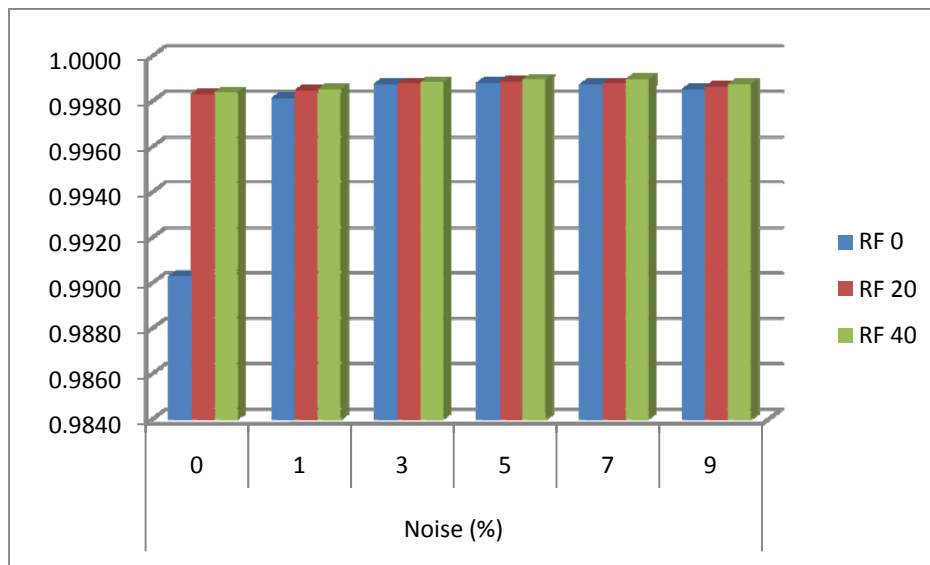


Figure 60, Specificity of segmentation for grey matter in FSL

Misclassification rate for grey matter showed the lowest error around 14% for zero noise level and RF inhomogeneity value of zero. The error rate has its largest value around 27% for moderate amount of noise (3%, 5% and 7% of noise). However, the worst error rate is from 5% of noise level and RF inhomogeneity value of 40%. Results are illustrated in table 36 and figure 61.

MCR – grey matter							
FSL		Noise (%)					
		0	1	3	5	7	9
RF	0	0.14231	0.20442	0.27644	0.28276	0.27688	0.26823
	20	0.21184	0.22912	0.27448	0.28189	0.27528	0.26499
	40	0.21508	0.22848	0.26928	0.28684	0.27947	0.27170

Table 36, Misclassification rate of segmentation for grey matter in FSL

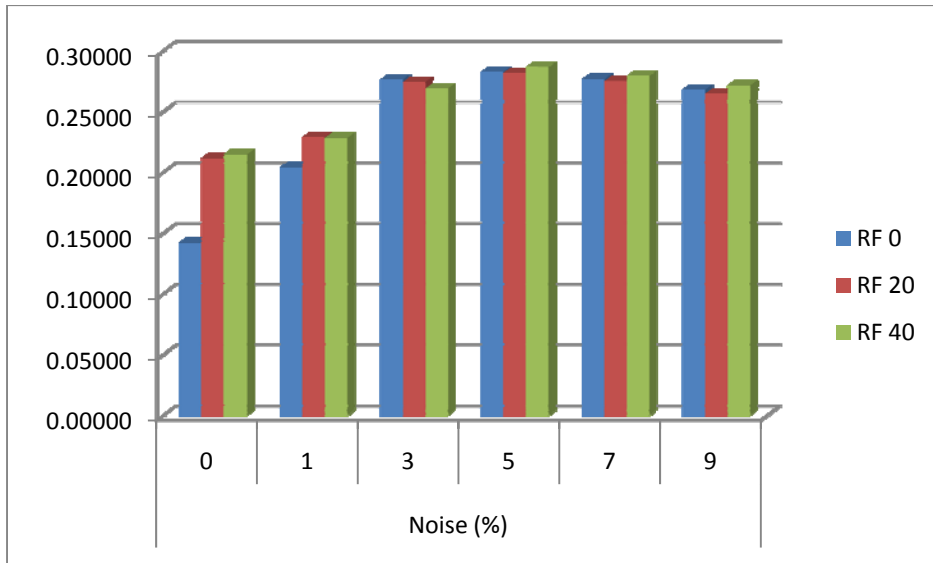


Figure 61, Misclassification rate of segmentation for grey matter in FSL

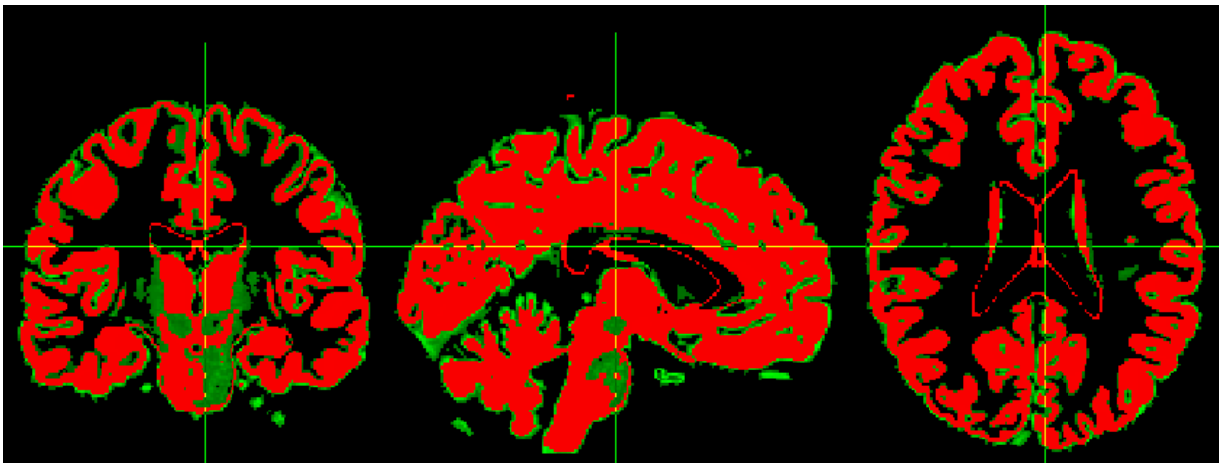


Figure 62, Segmented grey matter using FSL (red), Brainweb phantom ground truth (green), planes: sagittal (left), coronal (middle), transverse (right)

4.1.1.2.3. CSF

The sensitivity for classification of CSF is decreasing by increasing noise but the effect of RF inhomogeneity value is negligible. Therefore, the best value of sensitivity is around 55% for less noise values.

		Sensitivity – CSF					
FSL		Noise (%)					
		0	1	3	5	7	9
RF	0	0.53593	0.55470	0.53489	0.50119	0.47922	0.46354
	20	0.55528	0.55862	0.53260	0.49707	0.48366	0.46761
	40	0.55502	0.55593	0.52753	0.48678	0.47066	0.45418

Table 37, Sensitivity of segmentation for CSF in FSL

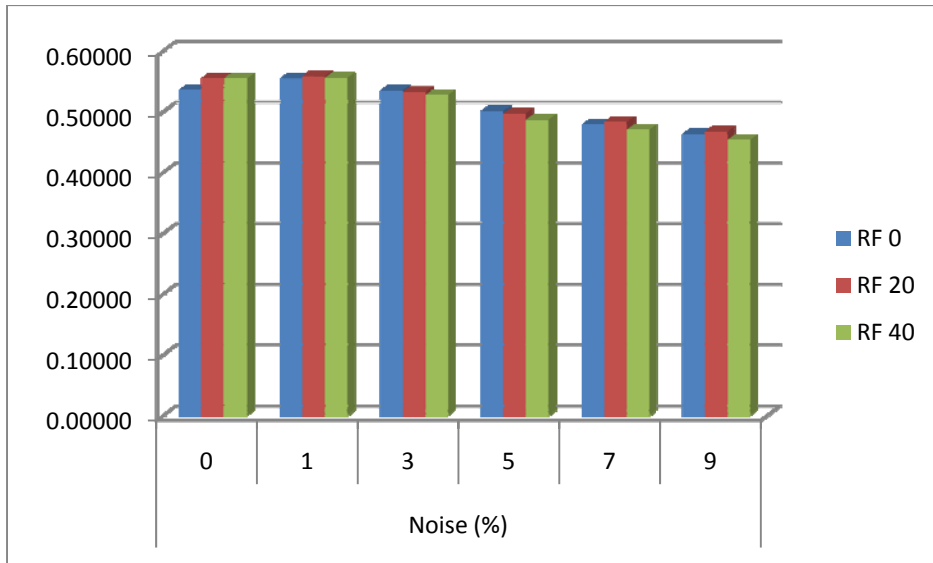


Figure 63, Sensitivity of segmentation for CSF in FSL

The specificity of CSF tissue class is close to one and will slightly decrease by increasing noise level. RF inhomogeneity changes had not significant effect on the results.

Specificity – CSF							
FSL		Noise (%)					
		0	1	3	5	7	9
RF	0	0.9971	0.9969	0.9971	0.9971	0.9962	0.9958
	20	0.9973	0.9971	0.9973	0.9972	0.9965	0.9958
	40	0.9971	0.9971	0.9972	0.9972	0.9967	0.9960

Table 38, Specificity of segmentation for CSF in FSL

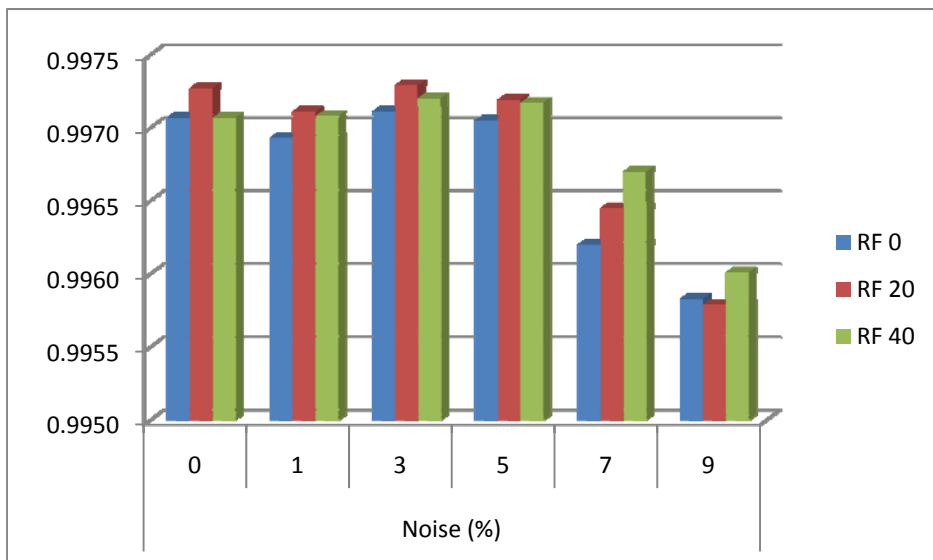


Figure 64, Specificity of segmentation for CSF in FSL

Misclassification rate for CSF showed the lowest error around 42% for 1% noise level and RF inhomogeneity value of 20%. The error rate has its largest value around 52% for 9% noise level and RF inhomogeneity value of 40%. However, by looking at the images in figure 66 it can be seen that there is a part of ground truth that didn't overlap with segmented tissue. Results are illustrated in table 36 and figure 61.

MCR – CSF							
FSL		Noise (%)					
		0	1	3	5	7	9
RF	0	0.44177	0.42316	0.44282	0.47629	0.49786	0.51339
	20	0.42269	0.41935	0.44516	0.48046	0.49353	0.50929
	40	0.42289	0.42199	0.45016	0.49072	0.50665	0.52286

Table 39, Misclassification rate of segmentation for CSF in FSL

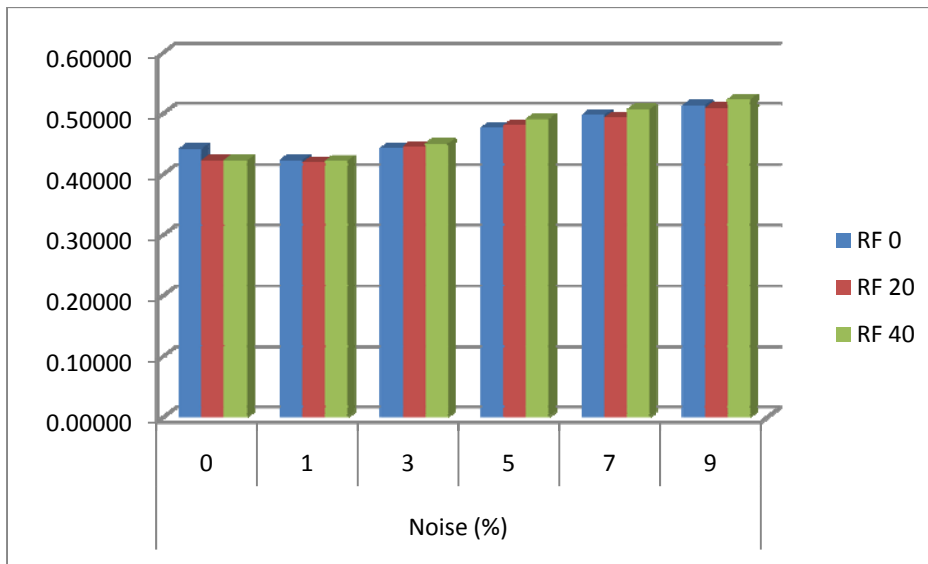


Figure 65, Misclassification rate of segmentation for CSF in FSL

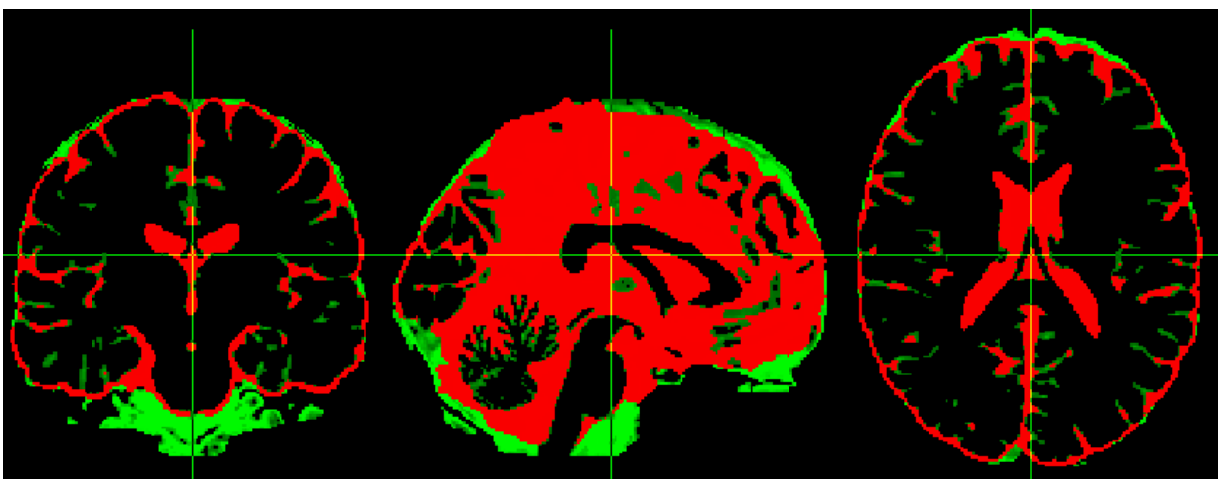


Figure 66, Segmented CSF using FSL (red), Brainweb phantom ground truth (green), planes: sagittal (left), coronal (middle), transverse (right)

Again an average of sensitivity, specificity and MCR from each issue class is used to obtain an overall evaluation of FSL performance for tissue segmentation. The lowest error rate with 25% and 26% of error calculated for grey matter and white matter respectively and the highest error rate is from CSF with 46% of error. The overall results are illustrated in table 40 and figure 67.

FSL	Sensitivity	Specificity	MCR
WM	0.7102	0.99978	0.2656
GM	0.71071	0.99819	0.2522
CSF	0.51191	0.99681	0.4656

Table 40, Overall evaluation of tissue segmentation using FSL

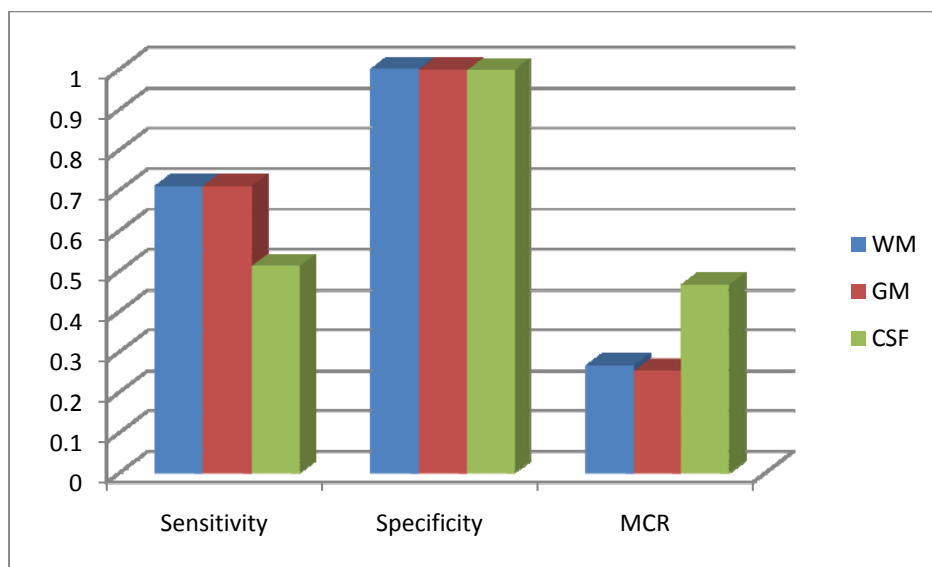


Figure 67, Overall evaluation of tissue segmentation using FSL

4.1.1.3. FreeSurfer

As it mentioned in section 3.4, FreeSurfer performs the tissue segmentation in a different way. The output of FreeSurfer is an image (aseg.mgz) with different intensities for each structure inside the brain. There is also a list of different structures with their intensity levels in a text file (aseg.auto_noCCseg.label_intensities.txt) together with “aseg.mgz” image in the output of FreeSurfer segmentation which has been shown in section 3.4 table 17.

For evaluating tissue segmentation using FreeSurfer, first step was extracting different tissue types from the “aseg.mgz” image and creating new separated images to represent white matter, grey matter and cerebrospinal fluid. Thus, I used table 17 which came from “aseg.auto_noCCseg.label_intensities.txt” file and consulted with Anders Hedström [42] to extract different tissue types from “aseg.mgz” image. The resulted classification of different structures in “aseg.mgz” is illustrated in table 41.

Intensity	Tissue type	Extracted tissue name	Intensity	Tissue type	Extracted tissue name
1	CSF	Left_Cerebral_Exterior	42	GM	Right_Cerebral_Cortex
2	WM	Left_Cerebral_White_Matter	43	CSF	Right_Lateral_Ventricle
3	GM	Left_Cerebral_Cortex	44	CSF	Right_Inf_Lat_Vent
4	CSF	Left_Lateral_Ventricle	46	WM	Right_Cerebellum_White_Matter
5	CSF	Left_Inf_Lat_Vent	47	GM	Right_Cerebellum_Cortex
7	WM	Left_Cerebellum_White_Matter	48	GM	Right_Thalamus
8	GM	Left_Cerebellum_Cortex	49	GM	Right_Thalamus_Proper
9	GM	Left_Thalamus	50	GM	Right_Caudate
10	GM	Left_Thalamus_Proper	51	GM	Right_Putamen
11	WM	Left_Cerebral_White_Matter	52	GM	Right_Pallidum
12	GM	Left_Putamen	53	GM	Right_Hippocampus
13	GM	Left_Pallidum	54	GM	Right_Amygdala
14	CSF	Third_Ventricle	58	GM	Right_Accumbens_area
15	CSF	Fourth_Ventricle	60	GM	Right_VentralDC
16	W+GM	Brain_Stem	72	CSF	Fifth_Ventricle
17	GM	Left_Hippocampus	75	CSF	Left_Lateral_Ventricles
18	GM	Left_Amygdala	76	CSF	Right_Lateral_Ventricles
24	CSF	CSF	77	WM	WM_hypointensities
26	GM	Left_Accumbens_area	78	WM	Left_WM_hypointensities
28	GM	Left_VentralDC	79	WM	Right_WM_hypointensities
40	CSF	Right_Cerebral_Exterior	80	CSF	non_WM_hypointensities
41	WM	Right_Cerebral_White_Matter	81	CSF	Left_non_WM_hypointensities
			82	CSF	Right_non_WM_hypointensitie

Table 41, Name codes, intensities and tissue types for different possible extracted structures using FreeSurfer

4.1.1.3.1. White matter

Sensitivity of the classified white matter using FreeSurfer in the best case is 75% which is for noise level of 3% for zero RF inhomogeneity and noise level of 5% for 40% RF inhomogeneity. However, unlike two other software packages, FreeSurfer could not perform the segmentation over 9% of noise level and 40% of RF inhomogeneity.

Sensitivity – white matter							
FreeSurfer		Noise (%)					
		0	1	3	5	7	9
RF	0	0.73200	0.73670	0.75060	0.73860	0.73640	0.73510
	20	0.74120	0.73730	0.74480	0.73910	0.73610	0.74070
	40	0.73870	0.73870	0.74660	0.74980	0.73120	-

Table 42, Sensitivity of segmentation for white matter in FreeSurfer

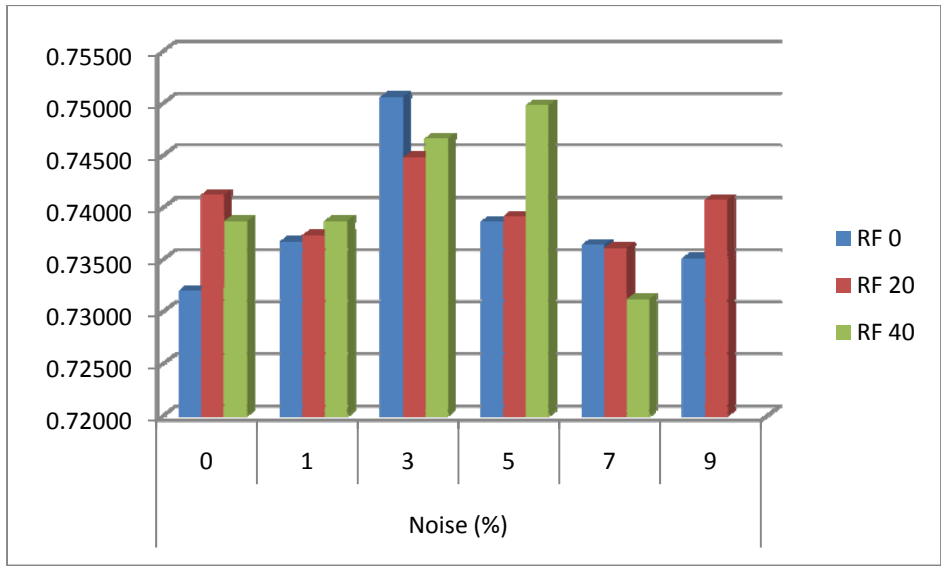


Figure 68, Sensitivity of segmentation for white matter in FreeSurfer

Segmented white matter using FreeSurfer shows specificity of 98% almost for all conditions. However, a closer look shows a slightly higher specificity in zero noise level and zero RF inhomogeneity. The lowest specificities are calculated for moderate noise levels (3% and 5%) but as it is illustrated in table 43 and figure 69 the difference is not significant.

Specificity – white matter							
FreeSurfer	Noise (%)						
	0	1	3	5	7	9	
RF	0	0.98520	0.98490	0.98380	0.98450	0.98470	0.98480
	20	0.98460	0.98490	0.98450	0.98440	0.98460	0.98440
	40	0.98450	0.98490	0.98400	0.98360	0.98510	-

Table 43, Specificity of segmentation for white matter in FreeSurfer

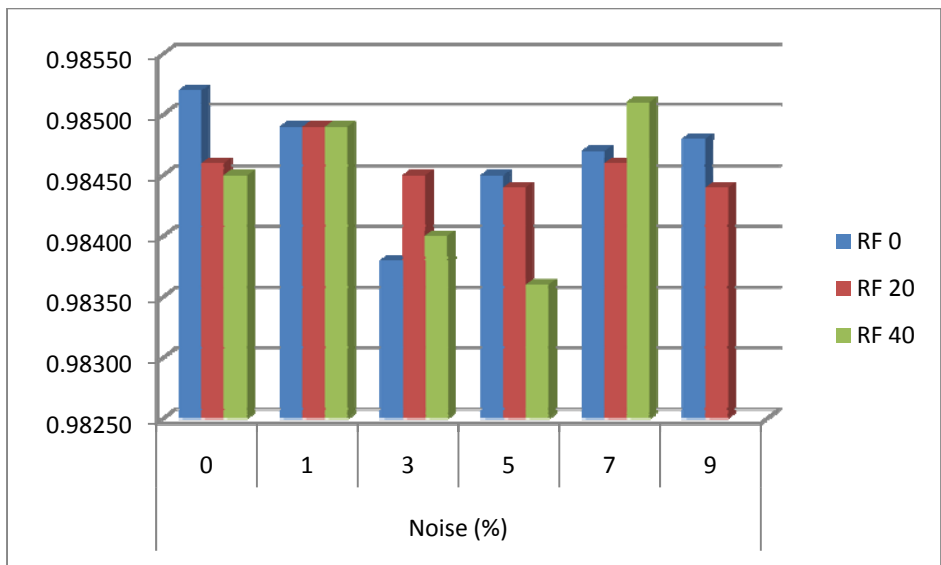


Figure 69, Specificity of segmentation for white matter in FreeSurfer

Misclassification rate for white matter showed the lowest error around 22% for noise level of 3% and RF inhomogeneity value of zero. However, the error rate at its highest value is around 24% which indicates that there is not a large gap between different noise levels for FreeSurfer performance. Results are illustrated in table 44 and figure 70.

MCR – white matter							
FreeSurfer		Noise (%)					
		0	1	3	5	7	9
RF	0	0.24337	0.23895	0.22594	0.23715	0.23922	0.24046
	20	0.23473	0.23895	0.23138	0.23668	0.23949	0.23519
	40	0.23705	0.23710	0.22965	0.22665	0.24411	-

Table 44, Misclassification rate of segmentation for white matter in FreeSurfer

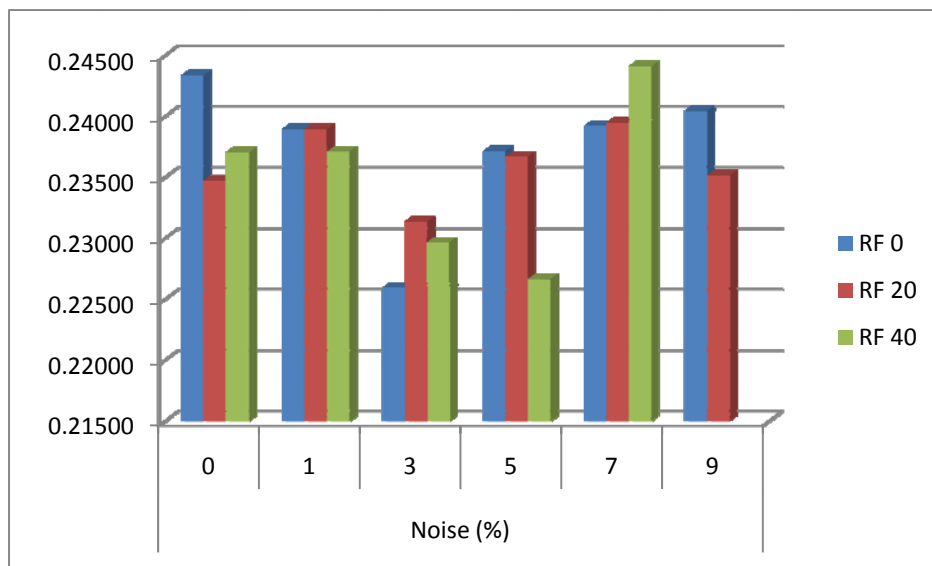


Figure 70, Misclassification rate of segmentation for white matter in FreeSurfer

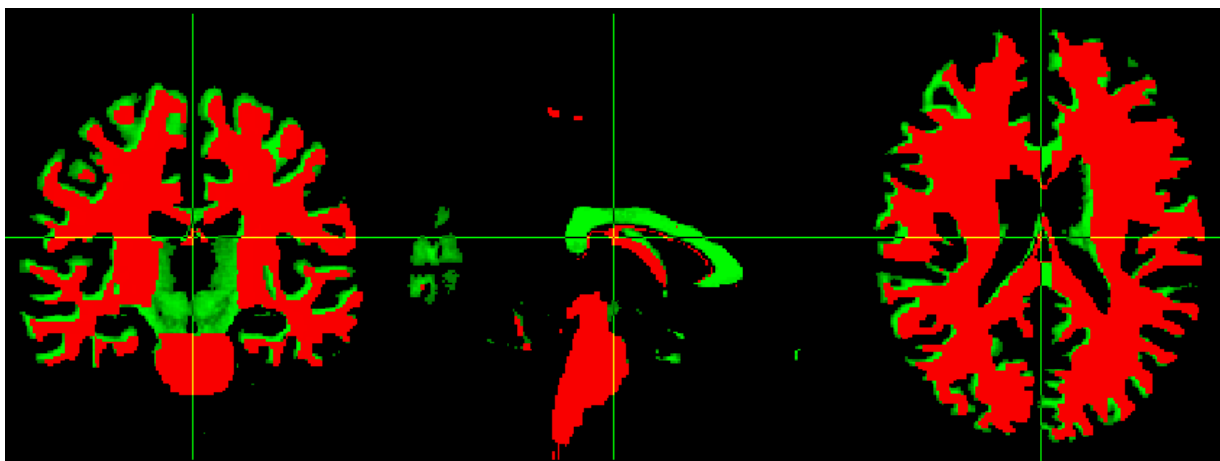


Figure 71, Segmented white matter using FreeSurfer (red), Brainweb phantom ground truth (green), planes: sagittal (left), coronal (middle), transverse (right)

4.1.1.3.2. Grey matter

Sensitivity of segmented grey matter using FreeSurfer is around 67% and has its best value in 7% of noise and 40% of RF inhomogeneity (68%). Again FreeSurfer was unable to perform segmentation over the phantom with noise level of 9% and RF inhomogeneity value of 40%. The results are illustrated in table 45 and figure 72.

Sensitivity – grey matter							
FreeSurfer		Noise (%)					
		0	1	3	5	7	9
RF	0	0.67570	0.67420	0.66880	0.67400	0.67430	0.68040
	20	0.67270	0.67390	0.67030	0.67190	0.67850	0.67730
	40	0.67420	0.67450	0.66870	0.66530	0.68160	-

Table 45, Sensitivity of segmentation for grey matter in FreeSurfer

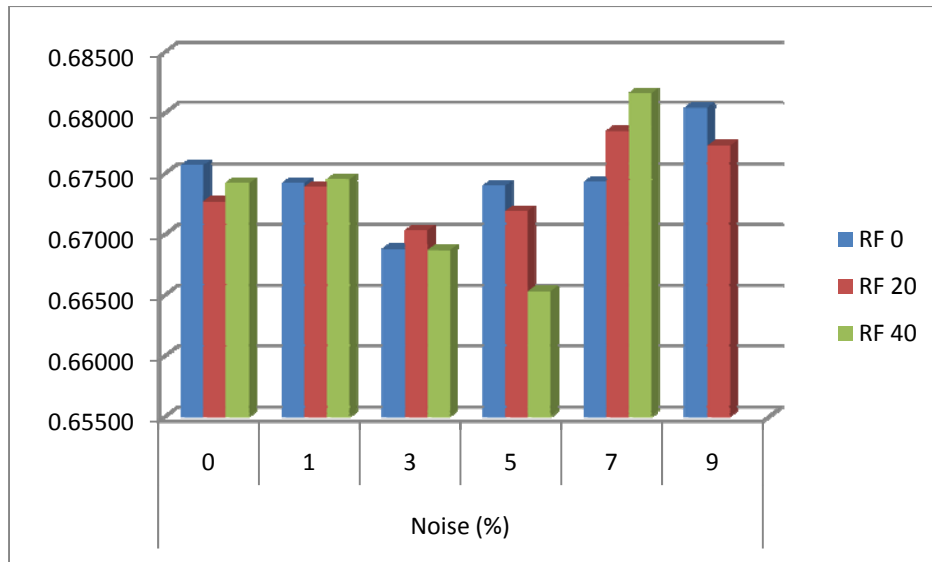


Figure 72, Sensitivity of segmentation for grey matter in FreeSurfer

Similar to white matter classification the results of specificity for grey matter are around 98% for all conditions for noise and RF inhomogeneity levels. However, closer look shows slightly higher specificity values for moderate noise levels (3% and 5%).

Specificity – grey matter							
FreeSurfer		Noise (%)					
		0	1	3	5	7	9
RF	0	0.98480	0.98480	0.98540	0.98470	0.98470	0.98410
	20	0.98500	0.98500	0.98520	0.98490	0.98450	0.98460
	40	0.98510	0.98530	0.98530	0.98550	0.98440	-

Table 46, Specificity of segmentation for grey matter in FreeSurfer

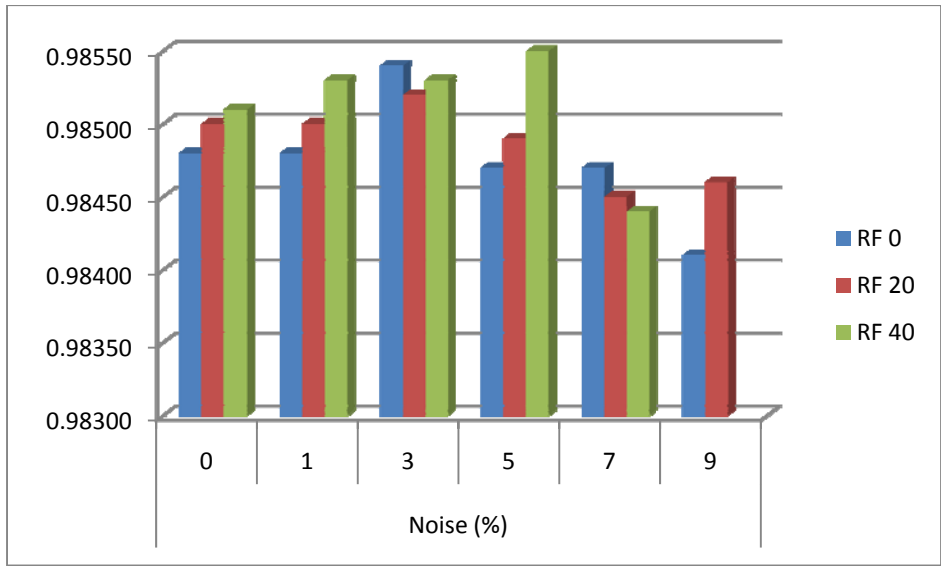


Figure 73 , Specificity of segmentation for grey matter in FreeSurfer

Misclassification rate for grey matter showed the lowest error around 28% for noise level of 7% and RF inhomogeneity value of 40%. However, the error rate at its highest value is around 29% which again similar to white matter indicates that there is not a big difference between different noise levels for FreeSurfer performance. Results are illustrated in table 47 and figure 74.

MCR – grey matter							
FreeSurfer	Noise (%)						
	0	1	3	5	7	9	
RF	0	0.28515	0.28652	0.29167	0.28673	0.28647	0.28077
	20	0.28797	0.28686	0.29021	0.28874	0.28257	0.28371
	40	0.28661	0.28635	0.29175	0.29493	0.27971	-

Table 47, Misclassification rate of segmentation for grey matter in FreeSurfer

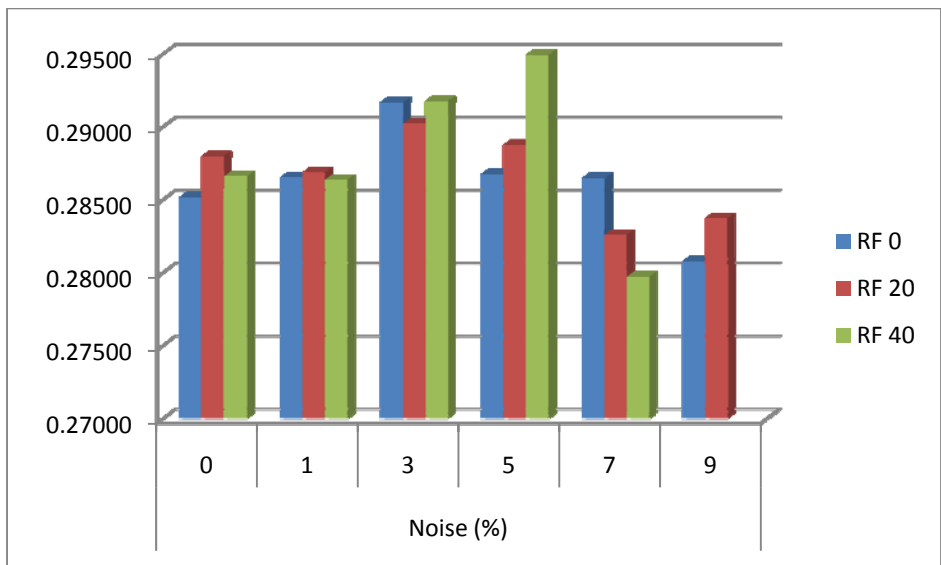


Figure 74, Misclassification rate of segmentation for grey matter in FreeSurfer

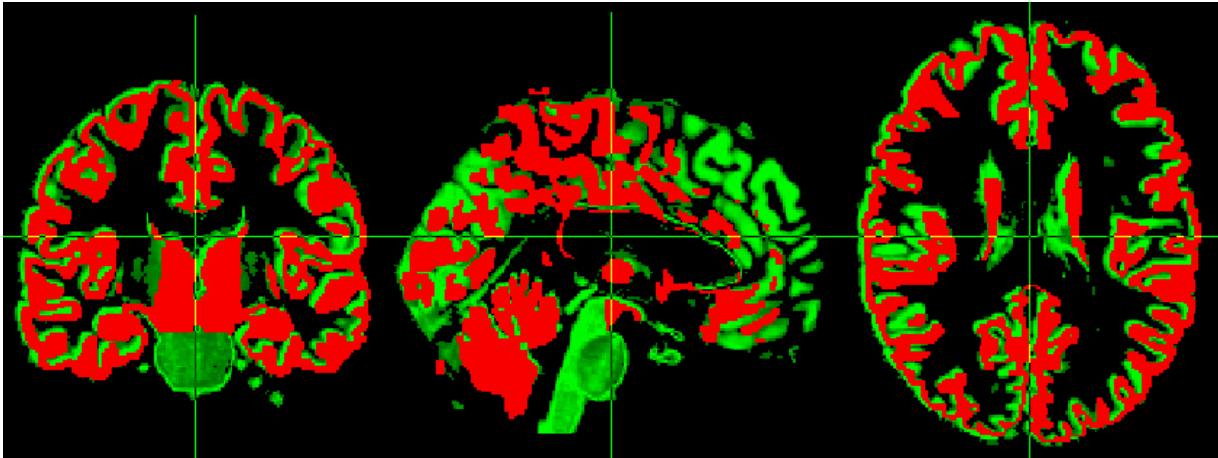


Figure 75, Segmented grey matter using FreeSurfer (red), Brainweb phantom ground truth (green), planes: sagittal (left), coronal (middle), transverse (right)

4.1.1.3.3. CSF

The rate of true classification which is sensitivity for classification of CSF using FreeSurfer showed a result close to zero. Figure 79 shows very small amount of extracted CSF using FreeSurfer. The results are listed in table 48.

		Sensitivity – CSF					
FreeSurfer		Noise (%)					
		0	1	3	5	7	9
RF	0	0.04170	0.04200	0.04210	0.04170	0.04210	0.04210
	20	0.04190	0.04200	0.04190	0.04200	0.04220	0.04240
	40	0.04210	0.04170	0.04190	0.04210	0.04220	-

Table 48, Sensitivity of segmentation for CSF in FreeSurfer

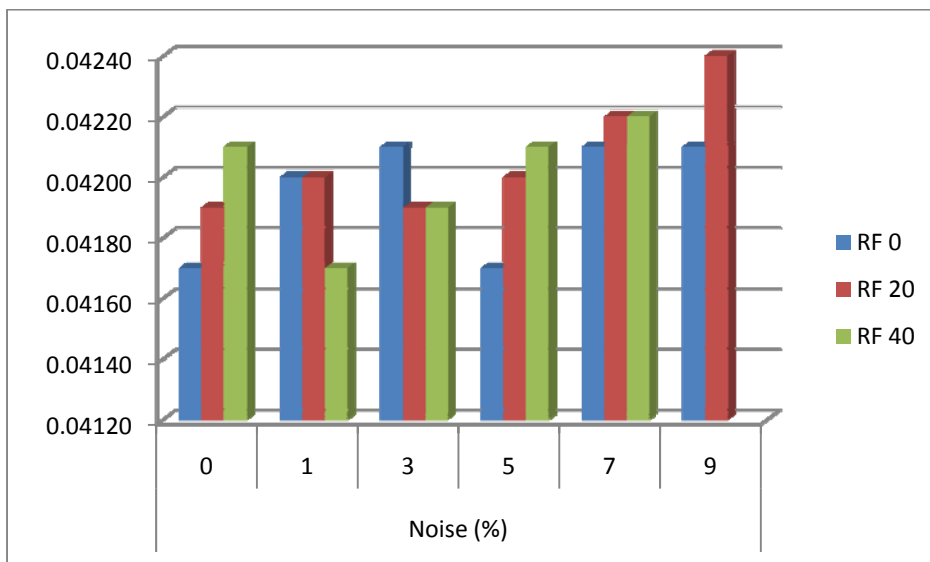


Figure 76, Sensitivity of segmentation for CSF in FreeSurfer

On the other hand, specificity of CSF is very high which is reasonable. Because the number of tissue voxels is really low, therefore the rest of voxels in the image will classify as background.

Specificity – CSF							
FreeSurfer	Noise (%)						
	0	1	3	5	7	9	
RF	0	0.99993	0.99994	0.99990	0.99990	0.99990	0.99988
	20	0.99993	0.99994	0.99994	0.99989	0.99987	0.99989
	40	0.99990	0.99991	0.99990	0.99989	0.99989	-

Table 49, Specificity of segmentation for CSF in FreeSurfer

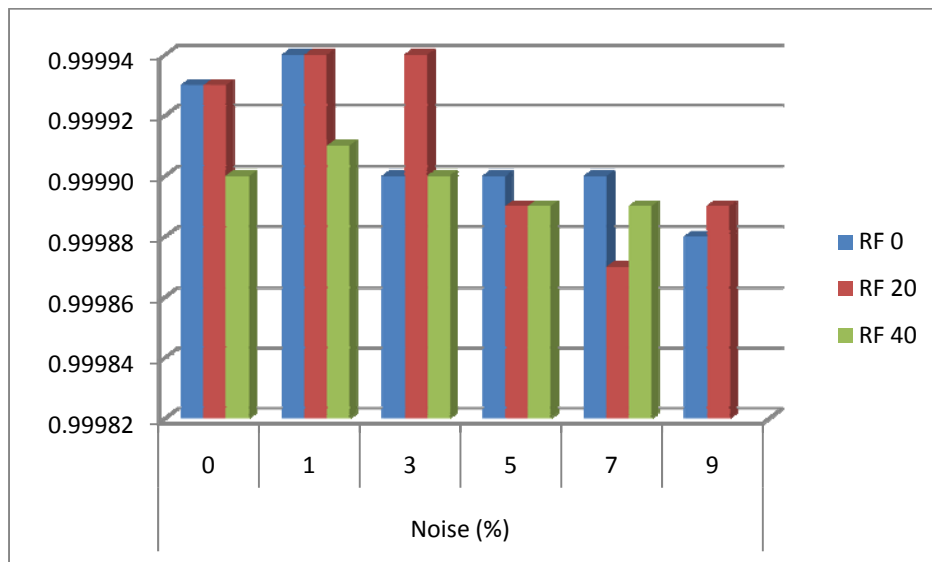


Figure 77, Specificity of segmentation for CSF in FreeSurfer

Finally misclassification rate for CSF did not show a good classification. It can be seen in figure 79 that there is a large difference between the ground truth and segmented image for CSF. The error rate is around 95% for all noise levels and RF inhomogeneity values. However, again performance of FreeSurfer is not influenced by noise or RF inhomogeneity. The results are illustrated in table 50 and figure 78.

MCR – CSF							
FreeSurfer	Noise (%)						
	0	1	3	5	7	9	
RF	0	0.95401	0.95369	0.95354	0.95399	0.95354	0.95352
	20	0.95380	0.95368	0.95378	0.95363	0.95340	0.95319
	40	0.95354	0.95399	0.95377	0.95353	0.95342	-

Table 50, Misclassification rate of segmentation for CSF in FreeSurfer

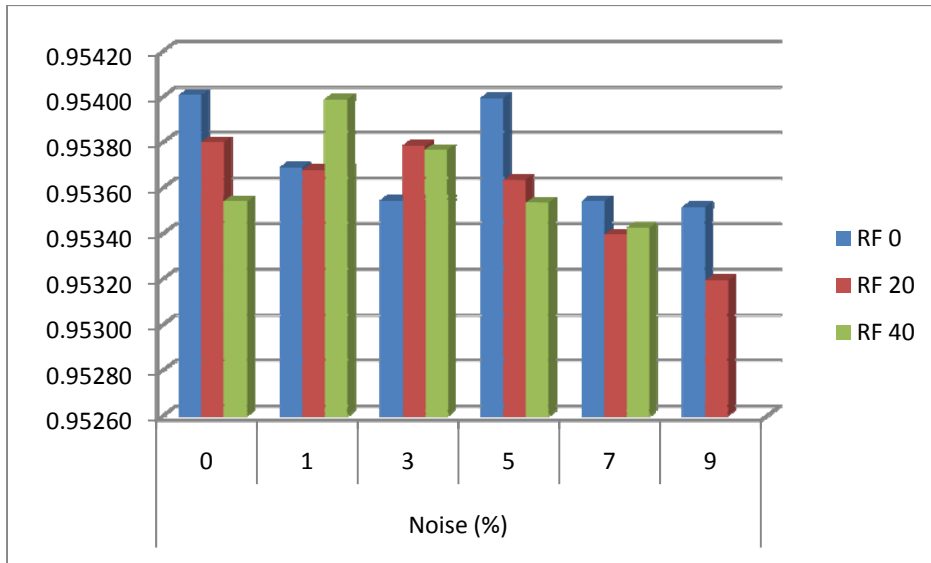


Figure 78, Misclassification rate of segmentation for CSF in FreeSurfer

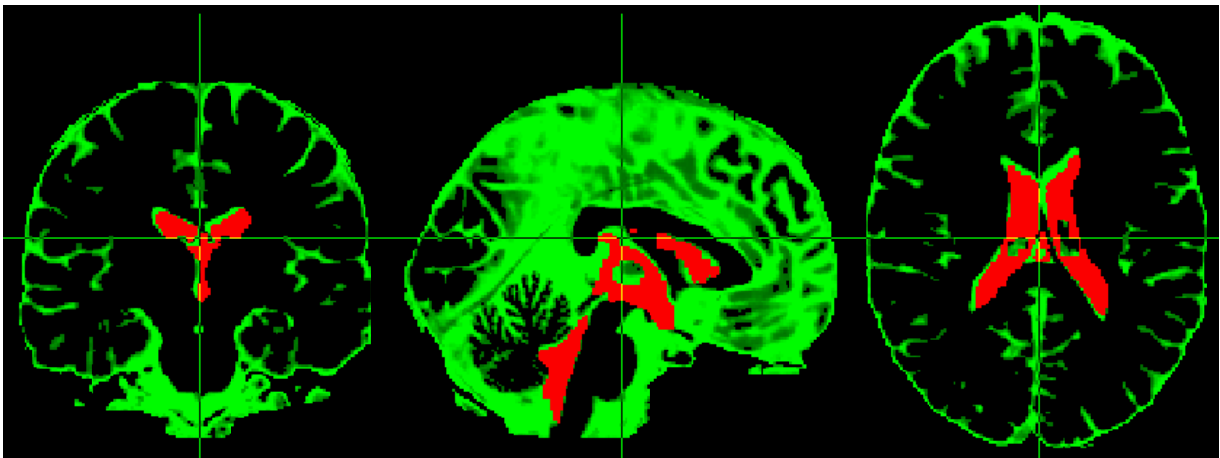


Figure 79, Segmented CSF using FreeSurfer (red), Brainweb phantom ground truth (green), planes: sagittal (left), coronal (middle), transverse (right)

Again an average of sensitivity, specificity and MCR from each tissue class is used to obtain an overall evaluation of FreeSurfer performance for tissue segmentation. The lowest error rate with 23% and 28% of error calculated for white matter and grey matter respectively and the highest error rate is for CSF with 95% of error. The overall results are illustrated in table 51 and figure 80.

FreeSurfer	Sensitivity	Specificity	MCR
WM	0.73962	0.98455	0.23624
GM	0.6739	0.9849	0.28687
CSF	0.04201	0.9998	0.95365

Table 51, Overall evaluation of tissue segmentation using FreeSurfer

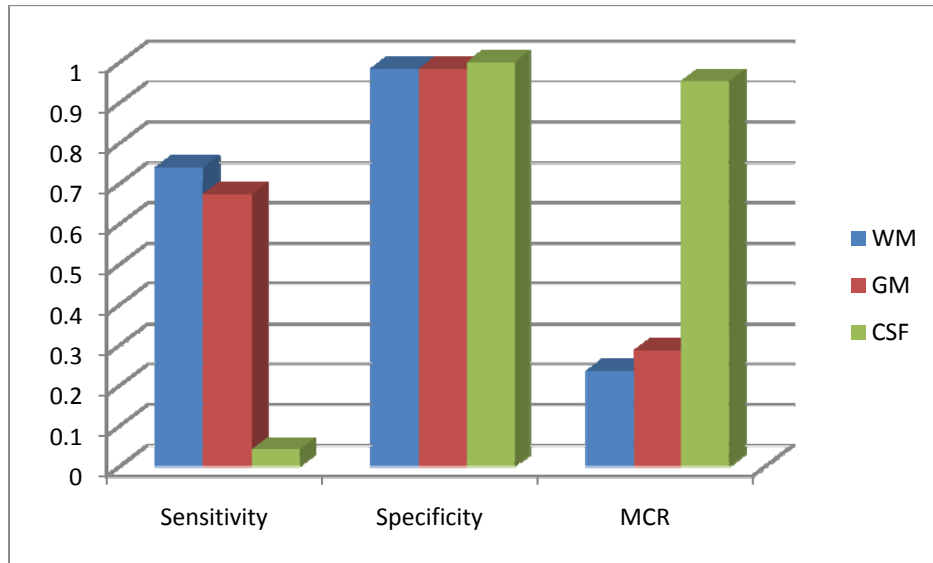


Figure 80, Overall evaluation of tissue segmentation using FreeSurfer

4.2. Conclusion and discussion

The misclassification rate of tissue segmentation shows the amount of error in tissue classification. By reviewing this feature for all three software packages, SPM8 shows 8% error in classification of white matter while misclassification rate for this tissue type in FreeSurfer is 23% and in FSL is 26%. The error in classification of grey matter for SPM8 shows even better output with misclassification rate of 5% which is much better comparing to FreeSurfer with error rate of 28% and FSL with error rate of 25%. Finally misclassification rate of cerebrospinal fluid in SPM8 shows 7% of error while the other two couldn't manage to obtain good classification for this tissue type at all. The error rate for FSL is 46% and FreeSurfer shows a high error rate of 95%. The reason of bad classification of CSF in FSL can be solve by decreasing the amount of erosion in brain extraction step using BET, however, it will cause more errors in other tissue types. The reason is by reducing erosion in BET some parts of skull and neck will be included as brain and subsequently will be classified as brain tissues. Thus, the problem with FSL is initiating from the first step which is BET. Regarding to FreeSurfer, as it mentioned before every voxel which was considered CSF in the "aseg.auto_noCCseg.label_intensities.txt" file were used to create the CSF image. But, the resulted image (figure 79) showed a significant lack of CSF. By considering the misclassification rate, SPM8 has the best output among these three tools. Table 52 and figure 81 show the misclassification rates for three tissue classes in each software package.

Software package	Tissue type	MCR
FreeSurfer	WM	0.23624
	GM	0.28687
	CSF	0.95365
FSL	WM	0.26561
	GM	0.25219
	CSF	0.46561
SPM8	WM	0.08084
	GM	0.05802
	CSF	0.07341

Table 52, Comparison of misclassification rates between three software packages

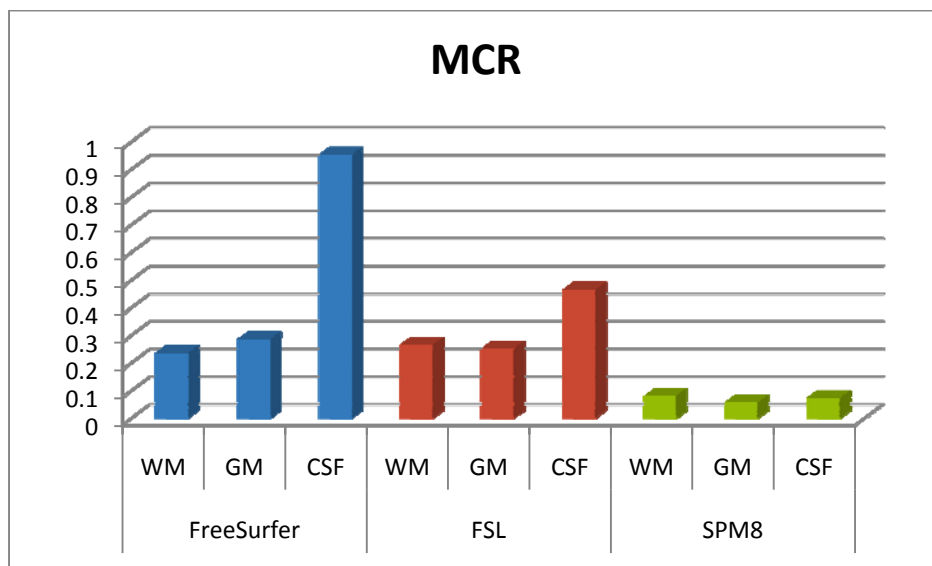


Figure 81, Comparison of misclassification rates between three software packages

Although SPM8 has the lowest error rate among three evaluated software packages but considering the capabilities of SPM8 it is not going to be a good choice for developing a head model. The reason is obvious! As it mentioned before SPM8 is just able to extract three tissue classes (WM, GM and CSF) which means subcortical segmentation and extracting skull and scalp cannot be carried out using SPM8 while for creating a head model for EEG source localization scalp and skull are crucial components.

FSL and FreeSurfer are able to do subcortical segmentation. However, lack of ground truth for subcortical structures didn't allow evaluation of their performance. Although, FreeSurfer can extract more subcortical structures comparing to FSL and it shows better results in white matter segmentation but it doesn't have any tool for extracting skull and scalp. Moreover, the results of grey matter are not as good as FSL and the error rate for CSF is very high. Thus, after all despite of very good results of segmentation in SPM8 and high number of subcortical structures extracted by FreeSurfer, they are not the best choice for creating a head model. Although, FSL is not as good as SPM8 in segmenting three tissue classes (WM, GM, CSF), but it is much more

sophisticated. It can extract subcortical structures, inner skull, outer skull and scalp which are important for developing a head model. And comparing to FreeSurfer it is much faster in every possible way. Using FreeSurfer for a normal segmentation takes at least 8 hours with a good computer while this time for the same results in FSL is around 30 minutes.

A question that may come into mind is, can we use these results together? The answer is yes! But there are a lot overlaps between voxels from different tissue types which will decrease the accuracy of the model. For instance figure 82 shows a combination of tissue segmentation from SPM8 together with skull and scalp extraction using FSL. By a comparison to the original image in figure 83 which only uses FSL results, it can be see that there are a lot of overlaps between CSF voxels and skull in figure 82. Although, regarding to ground truth the error must be in skull and scalp extraction in FSL.

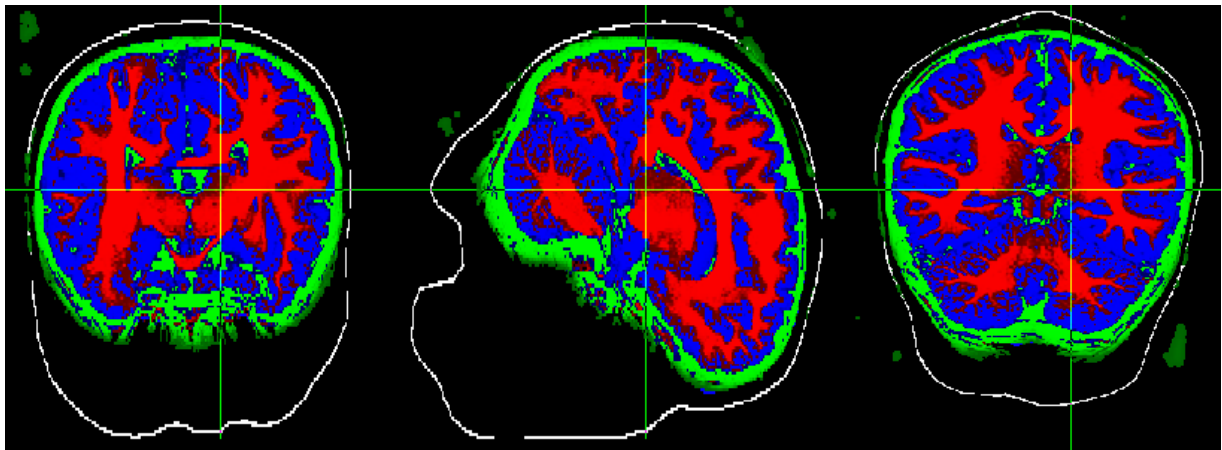


Figure 82, Segmented tissues by SPM8 together with extracted skull and scalp by FSL, planes: sagittal (left), coronal (middle), transverse (right)

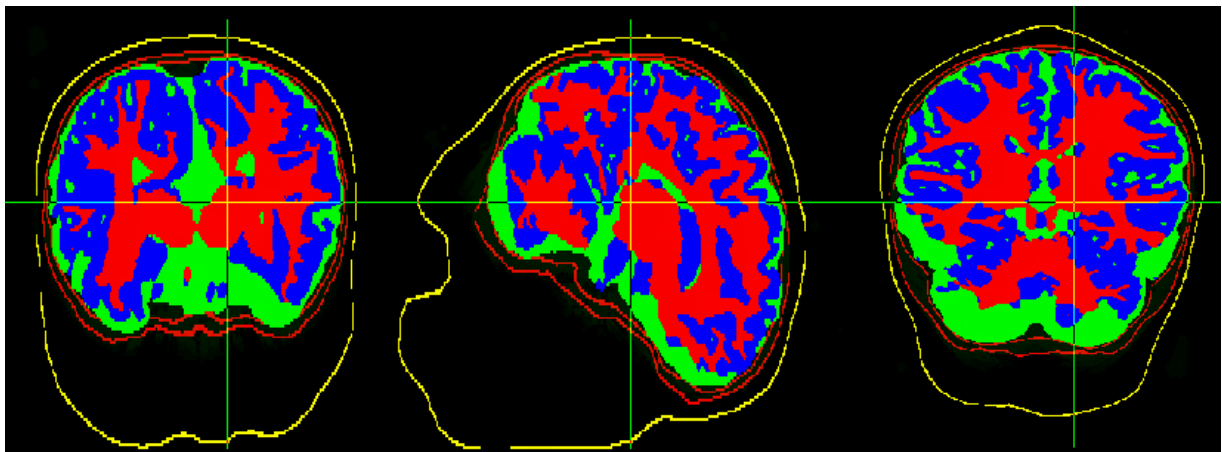


Figure 83, Segmented tissues and extracted skull and scalp by FSL, planes: sagittal (left), coronal (middle), transverse (right)

A future work in this area can be done by using new features which will be included in all three software packages and evaluating the results of them. For example SPM will include subcortical

segmentation in newer versions which makes it a very sophisticated tool for brain tissue segmentation. However, considering the state of art FSL can be considered the most sophisticated tool for the sake of developing the head model but of course SPM8 is the best software package for tissue classification between all three. FreeSurfer is able to extract many structures inside the brain. However, lack of ground truth for subcortical structures didn't allow a good evaluation for FreeSurfer after all.

5. Terminology

1. Alzheimer disease is the most common form of dementia, which cause lapses of memory in early stages and with progress of the disease patients will have severe communication problems. However, Alzheimer disease is unique for every patient and different people may experience it in different ways. [43]
2. By increasing the firing rate of neurons in the brain they need more oxygen and nutrients. As a result the circulatory system will increase the amount of oxygenated blood on that area. The oxygenated blood has different magnetic signature comparing to deoxygenated blood which is due to magnetic characteristics of hemoglobin. fMRI uses this characteristic of blood oxygen level to capture the activities in the brain. This signal is called blood oxygen level dependent (BOLD). [44]
3. Dura mater is the outermost membrane of meninges and the thickest one. It is close to the skull and consists of two layers: periosteal and meningeal. Its main function is to preserve CSF inside the meninges sac. [45]
4. Arachnoid mater is between two other layers of meninges and sometimes considered as a single structure with pia mater. [45]
5. Pia mater is the innermost layer of meninges which is in contact with surface of brain and its function is to supply blood for the superficial areas of the cortex. [45]
6. Striatum (neostriatum or strate nucleus) is a subcortical structure and part of the basal nuclei. its functions are mostly modulating and planning for movements in the body. However, recent studies showed activation of striatum with respect to stimuli such as reward. It has two subdivision nuclei: Caudate and Putamen. Caudate nucleus is mainly responsible for learning and memory and putamen is responsible for learning and movement regulation. Striatum contains a collection of neurons called Accumbens which are responsible for different functions such as addiction, pleasure, fear, reward, aggression, laughter. [46] , [47]
7. Pallidum (paleostriatum) is a subcortical structure and part of the basal nuclei. It is mostly responsible for controlling motor functions. [48]
8. Substantia nigra is a subcortical structure and part of the basal nuclei. It is responsible for eye movement, motor planning, reward, learning and addiction. [49]

9. subthalamic nucleus is a subcortical structure and a part of basal nuclei. Its function is unknown. However, studies have shown an increase in its activities in response to a rewarding stimuli. [50]
10. Pituitary gland (also known as hypophysis) is an important endocrine structure attached to the bottom of hypothalamus via a stalk. It has several functions such as preservation of growth, blood pressure, some aspects of pregnancy, production of breast milk, sex organ functions, thyroid gland functions, metabolism, osmolarity regulation, water absorption in kidneys and temperature regulation. [4] [51]
11. Hippocampus is a large structure in the brain which is part of limbic system and responsible for long term memory and spatial navigation. [52]
12. Amygdala is a small almond-shaped structure inside the mid-brain and part of the limbic system and responsible for processing and memory of emotional reactions. [53]
13. Anterior thalamic nuclei are a group of nuclei in front of the thalamus and part of limbic system. Their function is not precisely known, however, studies have shown that they are responsible for learning, memory and modulation of alertness. [54]
14. Limbic cortex is fraction of cerebral cortex and part of limbic system and responsible for emotional reactions. [55]
15. Midbrain (or Mesencephalon) is the starting part of brainstem and consists of several nuclei. Midbrain's function is mostly related to coordinating motor system pathways. [56]
16. Pons is a part of brainstem and in the middle of two other structures of brainstem (see figure 4). pons comprises two nuclei, one of them is responsible for conducting signals from cerebrum to cerebellum. The other one is responsible for a number of functions such as posture, swallowing, taste, facial sensation and expressions, hearing, eye movement, respiration, sleep, equilibrium and bladder control. [57]
17. Medulla oblongata is a part of brainstem responsible for vital functions such as heart rate, breathing, blood pressure, cardiac and respiratory systems. [56]
18. Angular momentum is a physical property of a particle which defined as a vector quantity to describe the position of particles in a physical system. [58]
19. Magnetic moment is a physical property of a particle to describe its tendency to align with a magnetic field. [59]

20. Rotating about the vertical axis of the nucleus. Precession always occurs opposite the direction of static magnetic field. [6]
21. MR images are inhomogeneous in terms of voxel intensities. Bias field correction creates a version of the image with uniform voxel intensities for all types of tissues which is important for subsequent usages such as tissue classification based on voxel intensities. [37]

6. References

[1] J. D. E. Gabrieli, J. B. Brewer, J. E. Desmond, G. H. Glover, "Separate neural bases of two fundamental memory processes in the human medial temporal lobe," *Science*, Vol. 276, pp. 264–266 1997.

[2] Tissue segmentation of the brain in Alzheimer disease, JL Tanabe, D Amend, N Schuff, V DiSclafani, F Ezekiel, D Norman, G Fein and MW Weiner, Department of Radiology, University of California at San Francisco Medical Center 94121, USA, *American Journal of Neuroradiology*, Vol 18, Issue 1 115-123, Copyright © 1997 by American Society of Neuroradiology.

[3] Ary JP, Klein SA, Fender DH. Location of sources of evoked scalp potentials: Corrections for skull and scalp thickness. *IEEE Trans Biomed Eng* 1981;28:447±452.

[4] VANDERS'S HUMAN PHYSIOLOGY: THE MECHANISMS OF BODY FUNCTION, ELEVENTH EDITION. Published by McGraw-Hill, Copyright © 2008 by The McGraw-Hill. ISBN 978-0-07-128366-3. MHID 0-07-128366-8.

[5] Copyright © 2001 Benjamin Cummings, an imprint of Addison Wesley Longman, Inc.

[6] *Medical Imaging Signals and Systems*, Jerry L. Prince, Jonathan M. Links. ISBN 0-13-065353-5.

[7] *Statistical Parametric Mapping (SPM)*, The Wellcome Trust Centre for Neuroimaging at University College of London, John Ashburner, Gareth Barnes, Chun-Chuan Chen, Jean Daunizeau, Guillaume Flandin, Karl Friston, Stefan Kiebel, James Kilner, Vladimir Litvak, Rosalyn Moran, Will Penny, Klaas Stephan, Rik Henson, Chloe Hutton, Volkmar Glauche, Jeremie Mattout, Christophe Phillips <http://www.fil.ion.ucl.ac.uk/spm/>

[8] FMRIB Analysis Group & MGH, Boston.

Bannister, M. De Luca, I. Drobnyak, D.E. Flitney, R. Niazy, J. Saunders, J. Vickers, Y. Zhang, N. De Stefano, J.M. Brady, and P.M. Matthews. Advances in functional and structural MR image analysis and implementation as FSL. *NeuroImage*, 23(S1):208-219, 2004.

M.W. Woolrich, S. Jbabdi, B. Patenaude, M. Chappell, S. Makni, T. Behrens, C. Beckmann, M. Jenkinson, S.M. Smith. Bayesian analysis of neuroimaging data in FSL. *NeuroImage*, 45:S173-186,2009.

S.M. Smith, M. Jenkinson, M.W. Woolrich, C.F. Beckmann, T.E.J. Behrens, H. Johansen-Berg, P.R. <http://www.fmrib.ox.ac.uk/fslcourse/>

[9] Athinoula A. Martinos Center for Biomedical Imaging. <http://surfer.nmr.mgh.harvard.edu/>

[10] Bioimage suite developed in Yale University, Bioimage Suite User's manual, X. Papademetris, M. Jackowski, N. Rajeevan, R.T. Constable, and L.H Staib, Section of Bioimaging Sciences, Dept. of Diagnostic Radiology, Yale School of Medicine. <http://www.bioimagesuite.org/index.html>

[11] BrainSuite was written by Dr. David W. Shattuck and is produced and distributed as a collaborative project between the Laboratory of Neuro Imaging at the University of California Los Angeles (Director: Dr. Arthur W. Toga) and the Biomedical Imaging Research Group at the University of Southern California (Director: Dr. Richard M. Leahy). The work is supported by grants from the National Institute of Biomedical Imaging and Bioengineering (R01 EB002010, PI: R.M. Leahy) and from the National Center for Research Resources (P41 RR013642, PI: A.W. Toga). <http://www.loni.ucla.edu/Software/BrainSuite>

[12] © 1994-2010 The MathWorks, Inc. <http://www.mathworks.com/>

[13] the International Consortium for Brain Mapping, John C. Mazziotta and Arthur W. Toga. http://www.loni.ucla.edu/ICBM/ICBM_TissueProb.html

[14] Montreal Neurological Institute and Hospital, <http://www.mni.mcgill.ca/>

[15] Martinos Center for Biomedical Imaging
<http://www.nmr.mgh.harvard.edu/martinos/noFlashHome.php>

[16] Talairach anatomical atlases <http://www.talairach.org/>

[17] A.Collignon, F.Maes, D. Delaere, D.Vandermeulen, P.Suetens, and G. Marchal. Automated multi-modality image registration based on information theory. In Y. Bizais, C. Barillot, and R. Di Paola, editors, Proc. Information Processing in Medical Imaging, pages 263-274, Dordrecht, The Netherlands, 1995. Kluwer Academic Publishers.

[18] W. M. Wells III, P. Viola, H. Atsumi, S. Nakajima, and R. Kikinis. Multi-modal volume registration by maximisation of mutual information. *Medical Image Analysis*, 1(1):35-51,1996.

[19] C. Studholme, D. L. G. Hill, and D. J. Hawkes. An overlap invariant entropy measure of 3D medical image alignment. *Pattern Recognition*, 32:71-86, 1999.

[20] F. Maes, A. Collignon, D. Vandermeulen, G. Marchal, and P. Seutens. Multimodality image registration by maximisation of mutual information. *IEEE Transactions on Medical Imaging*, 16:187-197, 1997.

[21] P. Th_{even}az, T. Blu, and M. Unser. Interpolation revisited. *IEEE Transactions on Medical Imaging*, 19(7):739-758, 2000.

- [22] M. Unser, A. Aldroubi, and M. Eden. B-spline signal processing: Part I - theory. IEEE Transactions on Signal Processing, 41(2):821-833, 1993.
- [23] M. Unser, A. Aldroubi, and M. Eden. B-spline signal processing: Part II - efficient design and applications. IEEE Transactions on Signal Processing, 41(2):834-848, 1993.
- [24] <http://neuro.debian.net/pkgs/fsl-atlases.html#pkg-fsl-atlases>
- [25] <http://neuro.debian.net/pkgs/fsl-first-data.html#pkg-fsl-first-data>
- [26] open-source, multi-platform data analysis and visualization application
<http://www.paraview.org/>
- [27] Talairach brain atlas http://www.neurovia.umn.edu/webservice/tal_atlas.html
- [28] FreeSurfer wiki, tools and commands, recon-all,
<http://surfer.nmr.mgh.harvard.edu/fswiki/recon-all>
- [29] DICOM is managed by the Medical Imaging & Technology Alliance, a division of NEMA,
<http://medical.nema.org/>
- [30] FreeSurfer wiki, tools and commands, mri_convert,
http://surfer.nmr.mgh.harvard.edu/fswiki/mri_convert
- [31] NIFTI, Neuroimaging Informatics Technology Initiative,
<http://nifti.nih.gov/board/read.php?f=1&i=402&t=402>
- [32] Chris Rorden, Principal Investigator, Neuropsychology Lab, Atlanta GA, USA
Professor, Georgia Institute of Technology, Atlanta GA, USA
Director, GSU/GT Center for Advanced Brain Imaging, Atlanta GA, USA,
<http://www.cabiatl.com/mricro/>
- [33] Kitware, VTK file format, www.vtk.org/VTK/img/file-formats.pdf
- [34] Paul A. Yushkevich (University of Pennsylvania) - Lead Developer, Hui Zhang (University of Pennsylvania) Developer, Casey Goodlett (University of Utah) Contributor, Timothy Burke Contributor, Nicholas Tustison Contributor, Supported by the U.S. National Institute of Biomedical Imaging and BioEngineering and the NIH Blueprint for Neuroscience through grant 1 R03 EB008200-01, <http://www.itksnap.org/pmwiki/pmwiki.php>
- [35] *BrainWeb*: Simulated Brain Database, <http://mouldy.bic.mni.mcgill.ca/brainweb/>
- [36] Shen, Jimmy. Tools for NIfTI and ANALYZE image. [Online] April 13, 2010. [Cited: May 3, 2010.] <http://www.mathworks.com/matlabcentral/fileexchange/8797-tools-for-nifti-and-analyze-image>

- [37] SPM8 Manual The FIL Methods Group (and honorary members), John Ashburner, Gareth Barnes, Chun-Chuan Chen, Jean Daunizeau, Guillaume Flandin, Karl Friston, Stefan Kiebel, James Kilner, Vladimir Litvak, Rosalyn Moran, Will Penny, Klaas Stephan, Darren Gitelman, Rik Henson, Chloe Hutton, Volkmar Glauche, J_er_emie Mattout, Christophe Phillips, <http://www.fil.ion.ucl.ac.uk/spm/doc/manual.pdf>
- [38] FSL, list of tools, <http://www.fmrib.ox.ac.uk/fsl/fsl/list.html>
- [39] Ferreira da Silva, A.R., "A Dirichlet Process Mixture Model for Brain MRI Tissue Classification", *Medical Image Analysis*, vol. 11(2), pp. 169-182, 2007.
- [40] On Tsang, Ali Gholipour, Nasser Kehtarnavaz, Senior Member, IEEE, Kaundinya Gopinath, Richard Briggs, and Issa Panahi, Senior Member, IEEE, "COMPARISON OF TISSUE SEGMENTATION ALGORITHMS IN NEUROIMAGE ANALYSIS SOFTWARE TOOLS", 30th Annual International IEEE EMBS Conference Vancouver, British Columbia, Canada, August 20-24, 2008
- [41] Cox, R.W., "AFNI: Software for Analysis and Visualization of Functional Magnetic Resonance Neuroimages," *Comp & Biomedical Research*, vol. 29, pp.162-173, 1996.
- [42] Anders Hedström, MD, Senior Consultant CNS-Diagnostics, Department of clinical neurophysiology, Sahlgrenska University Hospital, Göteborg, Sweden.
- [43] "What is Alzheimer's disease?", Alzheimers.org.uk. August 2007. Retrieved 2008-02-21.
- [44] Haller, S., Bartsch, A. (2009). Pitfalls in fMRI. *European Radiology*. 19, 2689-2706.
- [45] Orlando Regional Healthcare, Education and Development. 2004. "Overview of Adult Traumatic Brain Injuries." Retrieved on January 16, 2008.
- [46] Pieter Voorn, Louk J. M. J. Vanderschuren, Henk J. Groenewegen, Trevor W. Robbins and Cyriel M. A. Pennartz, Putting a spin on the dorsal-ventral divide of the striatum, *Trends in Neurosciences*, Volume 27, Issue 8, 1 August 2004, Pages 468-474.
- [47] Schwienbacher I, Fendt M, Richardson R, Schnitzler HU (2004). "Temporary inactivation of the nucleus accumbens disrupts acquisition and expression of fear-potentiated startle in rats". *Brain Res*. 1027 (1-2): 87-93. doi:10.1016/j.brainres.2004.08.037. PMID 15494160.
- [48] di Figlia, M., Pasik, P., Pasik, T. (1982) A Golgi and ultrastructural study of the monkey globus pallidus. *J. Comp. Neurol*. 212: 53-75.
- [49] Nicola, S M; Surmeier, J; Malenka, R C (2000). "Dopaminergic modulation of neuronal excitability in the striatum and nucleus accumbens". *Annu Rev Neurosci* 23: 185-215. doi:10.1146/annurev.neuro.23.1.185. PMID 10845063.

- [50] Frank, M.; Samanta, J.; Moustafa, A.; Sherman, S. (2007). "Hold Your Horses: Impulsivity, Deep Brain Stimulation, and Medication in Parkinsonism". *Science* 318 (5854): 1309–12. doi:10.1126/science.1146157. PMID 17962524.
- [51] Gibo H, Hokama M, Kyoshima K, Kobayashi S (1993). "[Arteries to the pituitary]". *Nippon Rinsho* 51 (10): 2550–4. PMID 8254920.
- [52] Amaral, D; Lavenex P (2006). "Ch 3. Hippocampal Neuroanatomy". in Andersen P, Morris R, Amaral D, Bliss T, O'Keefe J. *The Hippocampus Book*. Oxford University Press. ISBN 9780195100273.
- [53] Amunts K, Kedo O, Kindler M, Pieperhoff P, Mohlberg H, Shah N, Habel U, Schneider F, Zilles K (2005). "Cytoarchitectonic mapping of the human amygdala, hippocampal region and entorhinal cortex: intersubject variability and probability maps". *Anat Embryol (Berl)* 210 (5-6): 343–52. doi:10.1007/s00429-005-0025-5. PMID 16208455.
- [54] <http://www.nlm.nih.gov/medlineplus/ency/imagepages/19244.htm>
- [55] Pandya, DN; Yeterian, EH (2001). "The role of the cerebral cortex". in Gainotti, G. *Handbook of neuropsychology, Vol. 5, Emotional behavior and its disorders* (second ed.). Amsterdam: Elsevier Science BV. p. 68. ISBN 0444503625.
- [56] *brainstem* at Dorland's Medical Dictionary.
- [57] Saladin Kenneth S.(2007) *Anatomy & physiology the unity of form and function*. Dubuque, IA: McGraw-Hill
- [58] E. U. Condon and G. H. Shortley (1935) *The Theory of Atomic Spectra*. Cambridge University Press, ISBN 0-521-09209-4. Esp. chpt. 3.
- [59] B. D. Cullity, C. D. Graham (2008). *Introduction to Magnetic Materials* (2 ed.). Wiley-IEEE. p. 103. ISBN 0471477419.
- [60] Göran Starck, Sahlgrenska University Hospital, Göteborg, Sweden.
- [61] Song, T., Jamshidi, M.M., Lee, R.R., Huang, M., "A Modified Probabilistic Neural Network for Partial Volume Segmentation in Brain MR Image," *IEEE Transactions on Neural Networks*, vol. 18(5), pp. 1424-1432, 2007.